POOL BOILING HEAT TRANSFER CHARACTERISTICS OF STRUCTURED SURFACES

Ph.D. Thesis

By

VISHAL V. NIRGUDE
(Roll No. 1401203005)

DISCIPLINE OF MECHANICAL ENGINEERING
INDIAN INSTITUTE OF TECHNOLOGY INDORE
DECEMBER 2019

POOL BOILING HEAT TRANSFER CHARACTERISTICS OF STRUCTURED SURFACES

A THESIS

Submitted in partial fulfillment of the requirements for the award of the degree
of
DOCTOR OF PHILOSOPHY

by
VISHAL V. NIRGUDE
(Roll No. 1401203005)

DISCIPLINE OF MECHANICAL ENGINEERING
INDIAN INSTITUTE OF TECHNOLOGY INDORE
DECEMBER 2019

INDIAN INSTITUTE OF TECHNOLOGY INDORE

CANDIDATE'S DECLARATION

I hereby certify that the work which is being presented in the thesis entitled **POOL BOILING HEAT TRANSFER CHARACTERISTICS OF STRUCTURED SURFACES** in the partial fulfillment of the requirements for the award of the degree of **DOCTOR OF PHILOSOPHY** and submitted in the **DISCIPLINE OF MECHANICAL ENGINEERING, Indian Institute of Technology Indore**, is an authentic record of my own work carried out during the time period from December 2014 to December 2019 under the supervision of Dr. Santosh Kumar Sahu, Associate Professor, Discipline of Mechanical Engineering, Indian Institute of Technology Indore.

The matter presented in this thesis has not been submitted by me for the award of any other degree of this or any other institute.

Vishal 24/12/2019

Signature of the student with date
(Vishal V. Nirgude)

This is to certify that the above statement made by the candidate is correct to the best of my/our knowledge.

24/12/2019

Signature of Thesis Supervisor with date
(Dr. Santosh Kumar Sahu)

Vishal V. Nirgude has successfully given his/~~her~~ Ph.D. Oral Examination held on **29/05/2020**.

29/05/2020
Signature of Chairperson (OEB)
Date:

Signature of External Examiner
Date: 29-05-2020

29/05/2020
Signature(s) of Thesis Supervisor(s)
Date:

Signature of PSPC Member #1
Date: May 29, 2020

Signature of PSPC Member #2
Date: 29/5/2020

29/05/2020
Signature of Convener, DPGC
Date:

May 29, 2020
Signature of Head of Discipline
Date:

ACKNOWLEDGEMENTS

I would like to express my sincere gratitude to my supervisor, **Dr. Santosh Kumar Sahu**, Discipline of Mechanical Engineering, Indian Institute of Technology Indore, for his valuable guidance, consistent effort and encouragement throughout my research work. I am very grateful to him for his support, patience, motivation and enthusiasm provided to me during the course of this research.

I wish to express my gratitude to **Dr. Shanmugam Dhinakaran,** Discipline of Mechanical Engineering, Indian Institute of Technology Indore, **Dr. Prabhat Kumar Upadhyay,** Discipline of Electrical Engineering, Indian Institute of Technology Indore and **Dr. Anil Kumar Emadabathuni**, Department of Mechanical Engineering, Indian Institute of Technology Tirupati for providing various technical inputs and valuable suggestions, which has greatly helped in shaping this thesis.

My sincere acknowledgement and respect to **Prof. Pradeep Mathur,** Director, Indian Institute of Technology Indore for providing me the opportunity to explore my research capabilities at **Indian Institute of Technology Indore**. I am grateful to him for providing me financial support to present my research work in International conferences within and outside India.

I am thankful to the Council of Scientific and Industrial Research **(CSIR),** India**,** American Society of Mechanical Engineering **(ASME),** USA**,** Japan Society of Mechanical Engineering **(JSME),** Japan and Chinese Nuclear Society (CNS), China for the financial support to present my work in **ICONE25-2017** at **Shanghai, China**.

I am very thankful to **Dr. I. A. Palani, Dr. Akash K., Mr. Mani and Mr. Abhinav** of Mechatronics and Instrumentation Laboratory, Indian Institute of Technology Indore, for their valuable support in the development test surfaces by using laser setup. I am thankful to the all the staff members of Workshop, Advanced Manufacturing Processes lab and Sophisticated Instrument Centre (SIC) for their support during the development of test facility, fabrication of test surfaces and characterization at IIT Indore. Many thanks to **Mr. Arun Kumar Bhagwaniya**, Fluid Mechanics and Machinery Lab for his assistance for the fabrication of test facility.

I would like to appreciate the fine company of my dearest colleagues and friends especially, **Dr. Manish K. Agrawal, Dr. Hari Mohan Kushwaha, Dr. Mayank Modak, Dr. Sandesh Chougule,** Dr. Aniket Kulkarni, Dr. Rakesh Sharma, Dr. Balmukund Dhakar, Dr. Prateek Jain, Dr. Karthik Thirumala, Dr. Mayank Swarnkar, Mr. Navneet Pratap Singh, Mr. Vijay Anand, Mr. Dharmendra Kumar, Mr. Vasudev. Hearty thanks to all my labmates, **Mr. Avadhesh K. Sharma**, **Mr. Saurabh Yadav, Mr. Rohit Kothari, Mr. Pushpanjay Singh, Mr. Anuj Kumar, Mr. Jay Joshi** and **Mr. Jayant** for their cooperation during the course of my research.

I would like to express my heartfelt respect to my **family members** for their love, care and support they have provided to me throughout my life.

Finally, I am thankful to all who directly or indirectly contributed, helped and supported me. To Sign off, I write a quote by Robert Frost:

“In three words I can sum up everything I've learned about life: it goes on.”

Vishal V. Nirgude

Dedicated to all those who stood by me in my difficult times

ABSTRACT

The present dissertation reports experimental investigations pertaining to the pool boiling performance of test surfaces developed by using wire-EDM, nanosecond pulsed laser, continuous wave laser with different pool liquids such as water, isopropyl alcohol and acetone. The objective of the present work is to analyze the effects of variation of laser type, power and wavelength on physical characteristics of the test surface. Also, the pool boing performance of surfaces, developed by wire-EDM method and laser processing technique, are studied for a varied range of input heat fluxes and different pool liquids.

Design and development of a test facility involving various modules such as cylindrical boiling container, heater assembly, condensing coil, power supply system and temperature measurement scheme have been made to study the pool boiling heat transfer characteristics of smooth and different structured surfaces. Initial tests are conducted at atmospheric pressure with saturated condition for a smooth copper surface. The input heat supplied to the test section is calculated by measuring the voltage and current values across the heater. The surface temperature of the boiling surface is calculated by using the measured temperature data of the test section and input heat flux. Subsequently, the heat transfer coefficient is evaluated by using the input heat flux and wall superheat values. Four different structured surfaces with different structured geometries are fabricated by employing wire-EDM machining process and their boiling performance is studied for heat flux input in the range of 0-300 kW/m^2 for water and 0-250kW/m^2 for isopropyl alcohol. The pool boiling performances of structured surfaces are compared with the smooth surface. Also, the mechanisms of boiling phenomena in structured surfaces are discussed.

Next, multiscale functionalized copper surfaces are fabricated by employing nano-second pulsed wave laser for a varied range of laser

power and laser wavelength settings (1064 nm, 532 nm and 355 nm). The pulsed laser is a Nd:YAG (Quanta-Ray, Spectra Physics) that produces 5-8 nanosecond pulses with a wavelength of 1064 nm at a repetition rate of 10 Hz. The physical characteristics of the fabricated test surfaces are studied by using stereomicroscopic images (EZ4HD), scanning electron microscope (SEM) (Supra55, Zeiss) images and 3D profile of the test section. The pool boiling characteristics of nanosecond pulse laser processed surfaces are analyzed for different pool liquids, varied range of wall heat flux values and different laser powers (4.6 W, 4.2 W, 4.0 W, 1.8 W, 1.6 W, 1 W and 0.8 W).

In addition to this, six copper test sections are developed by using continuous wave laser for a varied range of laser power (40-50W). The continuous wave laser used in the present investigation is Ytterbium (Yb)-doped fiber laser (IPG Photonics) and is installed in a laser marking machine (SCANTECH, India). The physical characteristics of the test specimens developed by using continuous wave laser are studied by using SEM images. Also, the pool boiling characteristics of laser processed test surfaces are compared with the smooth surface. The results obtained by the present experimental study are compared with the test results obtained by previous researchers.

Keywords: *heat flux, pool boiling, enhanced surfaces, laser ablation, nucleate boiling, heat transfer coefficient, microstructure, structured geometries*

TABLE OF CONTENTS

ABSTRACT	i
LIST OF FIGURES	vii
LIST OF TABLES	xiii
NOMENCLATURE	xv
Chapter 1	
Introduction and literature survey	1
1.1 General background	1
1.2 Boiling heat transfer	2
1.3 Mechanism of pool boiling heat transfer	7
1.4 Techniques for enhancement in boiling heat transfer	11
1.5 Literature review	13
1.6 Scope and objective of the present investigation	27
Chapter 2	
Enhancement of nucleate pool boiling performance by using structured surfaces	31
2.1 General background	31
2.2 Fabrication of experimental test facility and test surface	33
2.2.1 Experimental test facility	33
2.2.2 Fabrication of the test surfaces	36
2.2.3 Experimental procedure	39
2.2.4 Data reduction	40
2.3 Results and Discussion	42

2.3.1 Effect of surface structure on heat transfer performance 43

2.3.2 Boiling mechanisms 48

2.4 Concluding remarks 51

Chapter 3

Enhancement of nucleate pool boiling heat transfer performance by using a novel nanosecond laser processing fabrication method 53

3.1 General background 53

3.2 Fabrication of experimental test facility and test surface 54

3.2.1 Test surface fabrication by laser processing 54

3.2.2 Laser ablation 55

3.2.3 Characterization of laser processed surface 57

3.3 Results and Discussion 61

3.3.1 Effect of laser processing with 1064nm wavelength on heat transfer performance 61

3.3.2 Effect of laser micro structuring with different wavelength on heat transfer performance 64

3.3.3 Effect of variation in laser wavelength and laser power 66

3.3.4 Comparison of present test data with the results of other laser micro structured surfaces 67

3.3.5 Proposed boiling mechanism responsible for augmentation in heat transfer performance 69

3.4 Concluding remarks 70

Chapter 4

Nucleate boiling performance of continuous wave laser processed surfaces 73

4.1 General background 73

4.2 Development of test facility and fabrication of test surface 74

4.3 Results and Discussion 80

4.3.1 Effect of laser markings on heat transfer performance 80

4.3.2 Effect of variation in laser power and distance between channels/grooves 82

4.3.3 Liquid vapor interaction on test surface 83

4.3.4 Comparison of present study with other test data 84

4.4 Effect of pulsed and continuous wave laser processing on heat transfer performance 86

4.5 Comparison of heat transfer performance different structured surfaces 89

4.6 Concluding remarks 92

Chapter 5

Summary and Conclusions 95

5.1 Conclusions from the present work 95

5.2 Contributions from the present work 99

5.3 Limitations of the present work 100

5.4 Scope for future work 100

References 102

Appendix I	113
Appendix II	119
List of Publications	121
Resume	125

LIST OF FIGURES

Figure 1.1	Typical values of convective heat transfer coefficients in different convection modes	2
Figure 1.2	(**a**) Forced convection boiling or flow boiling	3
	(b) Pool boiling	3
Figure 1.3	Boiling curve for saturated water at atmospheric pressure	4
Figure 1.4	Mechanism of boiling	
	(**a**) Free or Natural convection	5
	(**b**) Nucleate boiling (individual bubble)	5
	(**c**) Nucleate boiling (Jet or columns of vapor)	5
	(**d**) Transition boiling	5
	(**e**) Film boiling.	5
Figure 1.5	Mechanism of bubble dynamics during pool boiling heat transfer	9
Figure 1.6	Boiling mechanism	
	(a) On a porous surface proposed by Wang et al. [13]	11
	(b) On open micro channeled surface proposed by Cooke and Kandlikar [15]	11
Figure 1.7	SEM images of test specimens developed by Kang et al. [20] with different surface roughness	
	(a) Rough surface 60.9 nm	14
	(b) Smooth surface 15.1 nm	14
Figure 1.8	**(a)** Photographic view of helix fin used by Chen et al. [30]	16
	(b) Characteristic dimensions of structured enhanced tubes used by Kim and Choi [39] with pores	16
	(c) With gaps	16
	(d) Pores with connecting gaps	16
Figure 1.9	Structured surfaces developed by Das et al. [43]	

	(a) Schematic view of tunnel geometries	18
	(b) Pictorial view of test surfaces	18
Figure 1.10	**(a)** SEM image showing the diametric view of 0.01" nickel wire with 40 bilayers PAH/SiO_2 Forrest et al [46]	19
	(b) SEM image of type-B MWCNT synthesized on silicon substrate by using chemical vapor deposition (CVD) technique Ahn et al. [48]	19
Figure 1.11	Microfabricated enhanced structures fabricated by Ramaswamy et al. [50] by using	
	(a) Wet-etched method	20
	(b) Wafer-dicing method	20
Figure 1.12	SEM micrographs of the composite porous surface developed by Xu et al. [72]	
	(a) Macroporous	24
	(b) Microporous	24
	(c) Dendritic structure	24
	(d) Side view of the porous surface	24
Figure 1.13	**(a)** SEM photograph of nano-porous surface developed by Vemuri and Kim [75]	25
	(b) FESEM image of nano-porous surface developed by using the anodizing technique by Lee et al. [76]	25
Figure1.14	SEM images of SiNW array with different heights developed by Lu et al. [67]	
	(a) 16 μm	26
	(b) 32 μm	26
	(c) 59 μm	26
	(d) 122 μm	26
Figure 2.1	**(a)** Schematic diagram of the experimental setup	34
	(b) Photographic view of the experimental set up	34
	(c) Location of thermocouple in test specimen to	34

	measure temperature	
Figure 2.2	Schematic diagram of wire-EDM process	37
Figure 2.3	Schematic and photographic view of test surfaces	38
Figure 2.4	**(a)**Comparison of experimental heat transfer coefficient with correlation	41
	(b) Test Run on smooth surface	41
Figure 2.5	**(a)** Comparison boiling curve for a smooth surface and T-0.725-0.5-0.9	44
	(b) Comparison heat transfer coefficient for a smooth surface and T-0.725-0.5-0.9	44
Figure 2.6	**(a)** Comparison of heat flux versus wall superheat with water as pool liquid	45
	(b) Comparison of heat transfer coefficient versus heat flux with water as pool liquid	45
Figure 2.7	**(a)** Comparison of heat flux versus wall superheat with isopropyl alcohol as pool liquid	46
	(b) Comparison of heat transfer coefficient versus heat flux with isopropyl alcohol as pool liquid	46
Figure 2.8	Comparisons of heat transfer coefficient of the structured surface with	
	(a) Water	48
	(b) Isopropyl alcohol	48
Figure 2.9	**(a)** Boiling mechanism over structured surface	49
	(b) Representation of bubble growth on the surface with 0.725 mm width	49
	(c) Representation of bubble growth on the surface with 0.61 mm width	49
	(d, e) Representation of bubble growth on the surface with 0.5 mm and 1 mm depth	49
Figure 3.1	**(a)** Schematic diagram of nanosecond laser surface processing (NLSP) setup used in the present	56

	investigation	
	(b) Schematic of laser ablation process	56
Figure 3.2	**(a)** Microscopic and SEM images of laser processed test sections	58
	(b) Topography images (3D) of laser processed test sections	59
Figure 3.3	**(a)** Variation of heat flux with wall superheat for laser processed and smooth surface with water as pool liquid	62
	(b) Variation of heat transfer coefficient with heat flux for laser processed and smooth surface with water as pool liquid	62
Figure 3.4	**(a)** Variation of heat flux with wall superheat for laser processed and smooth surface with acetone as pool liquid	63
	(b) Variation of heat transfer coefficient with heat flux for laser processed and copper surface with acetone as pool liquid	63
Figure 3.5	**(a)** Comparison of heat flux versus wall superheat with water as pool liquid	65
	(b) Comparison of heat transfer coefficient versus heat flux with water as pool liquid	65
Figure 3.6	Comparison of heat transfer coefficient with different laser wavelength and laser power	67
Figure 3.7	Comparison of present test data with other test results [21, 98-99, 104]	68
Figure 3.8	**(a)**Graphical representation of multiscale functionalized surfaces	70
	(b) Proposed boiling mechanism	70
Figure 4.1	**(a)** Schematic diagram of laser marking machine	75
	(b) Schematic representation of laser processing	75
	(c) Representation of nanosecond and continuous laser	75

	wave	
Figure 4.2	Photographic view of test surfaces.	76
Figure 4.3	SEM and Microscopic images of test sections	77
Figure 4.4	SEM images of microcavities	78
Figure 4.5	**(a)** Comparison of heat flux versus wall superheat with water as pool liquid	81
	(b) Comparison of heat transfer coefficient versus heat flux with water as pool liquid	81
Figure 4.6	Comparison of heat transfer coefficient with laser power and 1 mm and 0.5 mm laser channel/groove distance	83
Figure 4.7	(**a**) Graphical representation of microscope images	84
	(b) Graphical representation of liquid vapor interaction on the test surface	84
	(c) Photographic view of bubble generation	84
Figure 4.8	Comparison of present result with test data of Dehghani-Ashkezari and Salimpour [107], Jones et al. [21], Kathiravan et al. [108] and Kim et al. [104]	85
Figure 4.9	(**a**) Variation of heat flux with wall superheat	88
	(**b**) Variation of heat transfer coefficient with heat flux for both laser processed and smooth copper surface with water as pool liquid	88
	(**c**) Comparison of percentage enhancement in HTC at various heat flux input compared to smooth surface for FS1 and LM-1-50-1064	88
Figure 4.10	(a) Comparison of heat flux versus wall superheat with water as pool liquid	90
	(b) Comparison of heat transfer coefficient versus heat flux with water as pool liquid	90

LIST OF TABLES

Table 1.1	Different studies on microstructured surfaces	21
Table 2.1	Summary of surfaces used in the present investigation	38
Table 3.1	Surface characteristics of test sections	60
Table 4.1	Surface characteristics of test sections	79

NOMENCLATURE

English Symbols

C_{pl}	Specific heat of liquid, J/kg-K
C_{sf}	Surface liquid parameter used in Rohsenow correlation
d_{cyl}	Diameter of copper block, m
g	Acceleration due to gravity, m/s^2
h	Heat transfer coefficient, W/m^2-K
h_{lg}	Latent heat of vaporization, J/Kg
I	Corresponding current value across heater terminals, amp
k	Thermal conductivity of copper, W/m-K
k_l	Thermal conductivity of liquid, W/m-K
m,n	Empirical constants used in Rohsenow correlation
q''	Heat flux, W/m^2
T	Temperature recorded by thermocouple in test surface, K
T_s	Surface temperature, K
T_{sat}	Saturation temperature, K
V	Voltage applied across heater terminals, volt
ΔT	Wall superheat, K
Δx	Distance of thermocouple hole in test surface from top, m

Greek Symbols

μ_l	Liquid dynamic viscosity, Pa-s
ρ_g	Density of vapor, kg/m^3
ρ_l	Density of liquid, kg/m^3
σ	Surface tension, N/m

Subscripts

sat	Saturation
l	Liquid

g	Gas
cyl	Cylinder
lg	Latent heat
sf	Surface parameter

Chapter 1

Introduction and literature survey

1.1 General background

Heat transfer, that deals with mechanism and rate of energy transfer because of temperature difference, is widely used in various scientific and industrial applications. The mechanism of heat transfer is broadly classified into three categories such as conduction, convection and radiation. The heat transfer mechanism because of the temperature gradient in a stationary medium is termed as conduction. Convection takes place between the surface and flowing fluid, while radiation heat transfer takes place in the absence of a medium. Convection heat transfer mechanism is widely used in various heating and cooling applications due to higher thermal performance that enables compactness of thermal systems. This mode of heat transfer is further classified into two categories, namely, single phase and two phase heat transfer. In general, single phase heat transfer takes place through the change in the sensible energy and two phase heat transfer occurs through latent heat transfer that induces the change of phase (boiling/condensation) of working fluid.

The rate of heat transfer during convection is expressed as:

$$q" = h\ (T_s - T_\infty) \tag{1.1}$$

where, q'', HTC, T_s and T_∞ denote the heat flux, convective heat transfer coefficient, surface and fluid temperature, respectively. The ranges of variation in HTC for different mechanism of heat transfer are summarized in Fig. 1.1.

Convection heat transfer, that involves the change of phase from liquid to vapor (boiling) or vapor to liquid (condensation), exhibits a higher value of HTC due to additional heat transfer equal to the latent heat of the fluid.

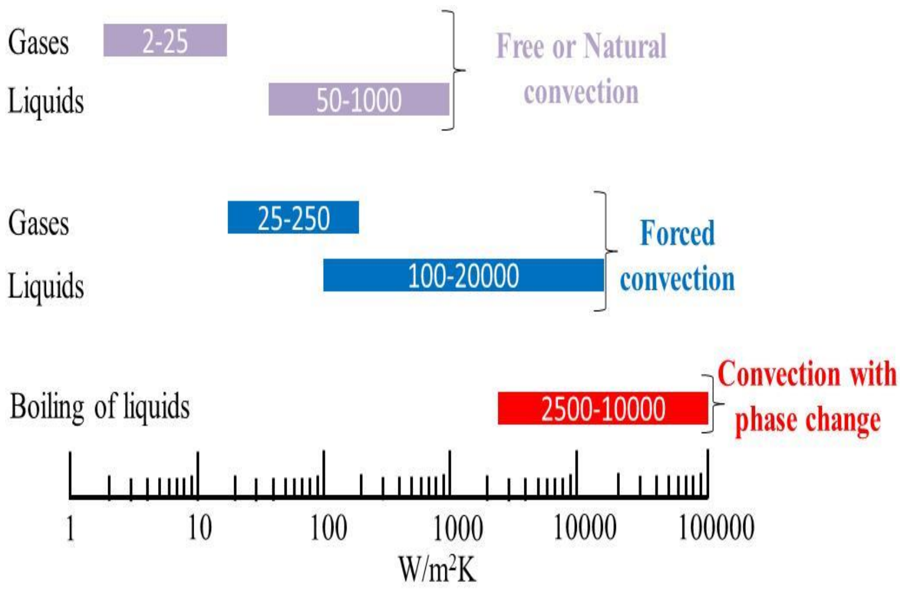

Figure 1.1: Typical values of convective heat transfer coefficients in different convection modes

1.2 Boiling heat transfer

Boiling is the phase change process in which vapor bubbles are formed either on the heated surface or inside the superheated liquid layer adjacent to the heated surface. It can be classified as forced convection boiling or flow boiling (Fig. 1.2 a) and pool boiling (Fig. 1.2 b). In forced convection, boiling the liquid in contact of a hot surface is moved due to externally applied force and the fluid mixing occurs due to the bubble growth and departure. On the contrary, in case of pool boiling, the movement and mixing of liquid adjacent to the hot surface is mainly due to the growth and departure of bubbles. Because of the higher value of heat transfer coefficient, heat transfer during the boiling process is preferred in thermal systems that generate a larger value of heat energy over a smaller surface area. Although the flow boiling process exhibits higher heat transfer coefficient, this process is difficult in certain applications due to various issues such as flow instabilities and large pumping power requirements (higher pressure drop). Therefore, pool boiling offers a great alternative to develop compact high heat removal system and finds application in boilers, heat exchangers, electronics cooling and nuclear reactor core cooling systems.

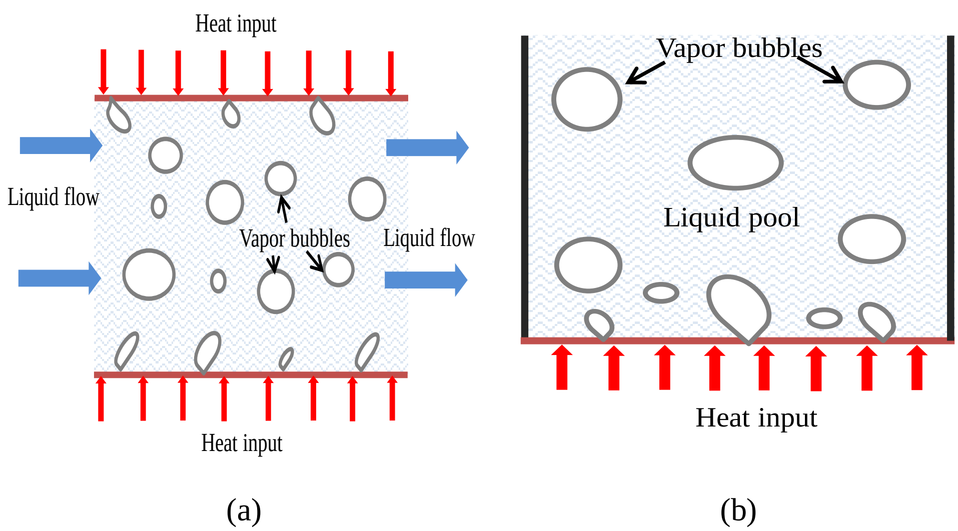

Figure 1.2: (a) Forced convection boiling or flow boiling (b) Pool boiling

Pool boiling

When the hot surface is submerged below the free surface of a quiescent liquid, the boiling process is termed as pool boiling. In such a case, the formation of bubbles takes place at the hot surface, they grow while moving up and collapse at the free surface. Pool boiling can be of two types such as subcooled boiling and saturated boiling. In the case of subcooled boiling, the bulk liquid temperature is kept below the saturation temperature of the liquid. While, in case of saturated pool boiling, the bulk temperature of the liquid is maintained at the saturation temperature. The pool boiling heat transfer mechanisms can be explained by using a boiling curve. The boiling curve with its different boiling regimes is elaborated below.

Nukiyama [1] was the first to introduce the boiling curve (Fig. 1.3) and its different regimes during pool boiling with saturated liquid. The boiling curve, used to quantify the heat dissipation capacity of surface in the boiling process, defines the dependence of the wall heat flux with wall superheat (the difference between surface temperature and saturation temperature of liquid). Fig. 1.3 shows the pool boiling curve for a flat plate or horizontal wire to which the heat input is controlled. Based on his work [1], four different regimes such as free convection boiling, nucleate boiling, transition boiling and film boiling are identified.

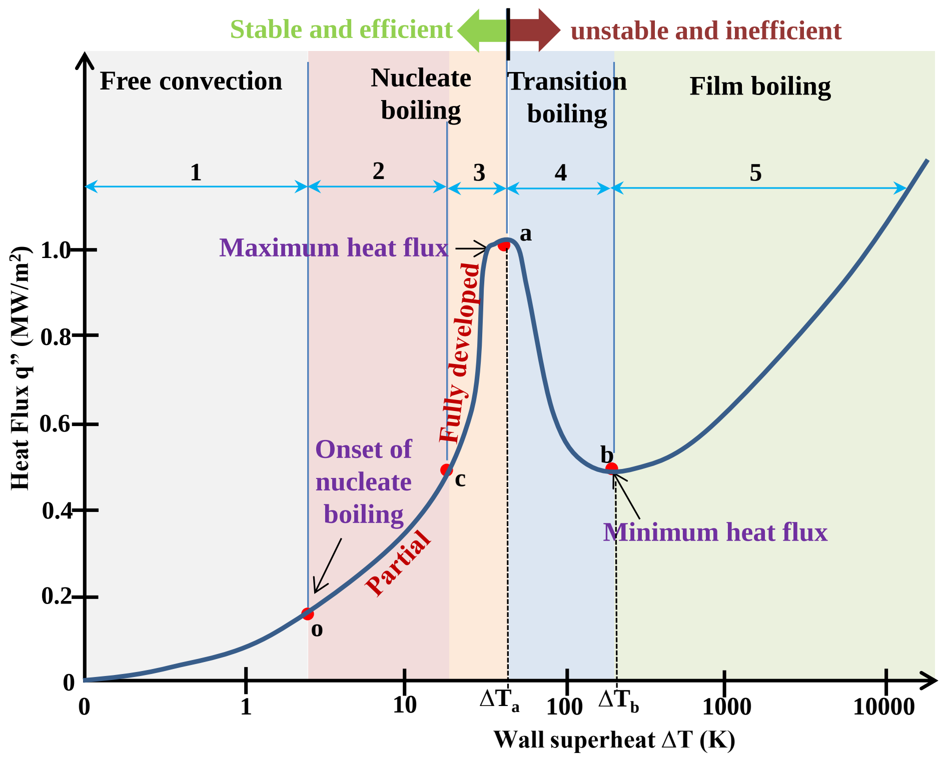

Figure 1.3: Boiling curve for saturated water at atmospheric pressure

Free convection

As the heat input is increased the surface temperature of the hot surface (T_w) becomes higher than the saturation temperature of water (T_s). In such a case, a density gradient is generated where the hot fluid moves up and cold fluid moves toward the hot surface (Fig. 1.4 a). This mode of heat transfer is termed as free or natural convection. The free or natural convection is the first regime in the boiling curve and denoted as region 1 in Fig. 1.3. The wall superheat in this region is insufficient to initiate nucleation, hence, no bubble growth and departure is observed in this region.

Further increase in heat input raises the wall superheat, which initiates bubble nucleation on the surface. This condition, at which the bubble nucleation starts, is termed as the onset of nucleate boiling (ONB), shown in Fig. 1.3.

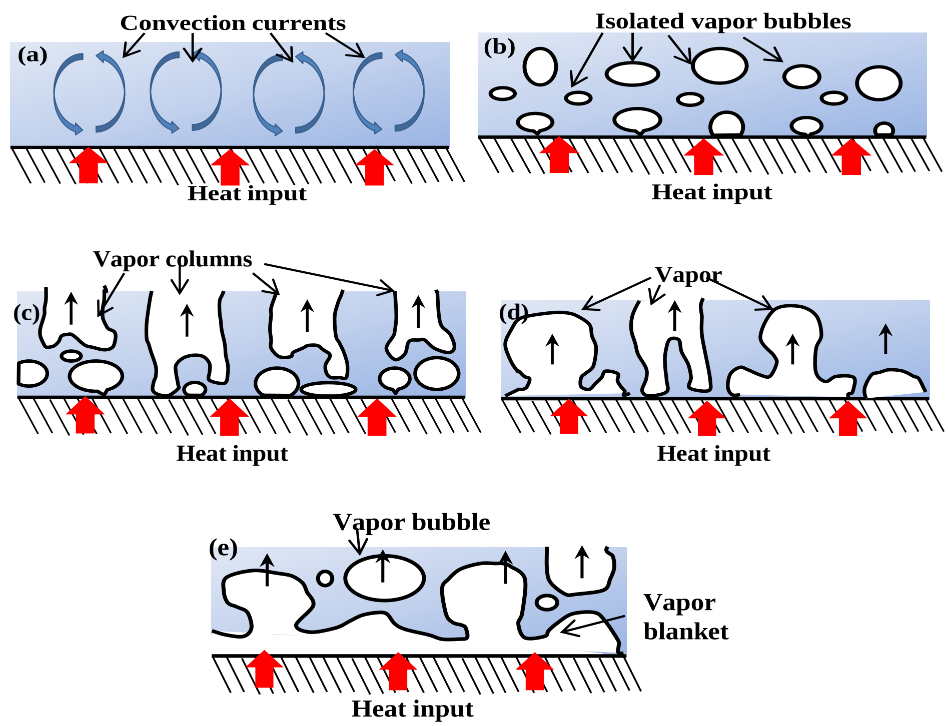

Figure 1.4: Mechanism of boiling (a) Free or Natural convection (b) Nucleate boiling (Individual bubble) (c) Nucleate boiling (Jet or columns of vapor) (d) Transition boiling (e) Film boiling

Nucleate boiling

With further increase in wall heat flux, the wall superheat value increases. At a certain value of wall superheat, the bubbles are observed on the heater surface. This is termed as the onset of nucleate boiling (Point o, Fig. 1.3). After this, a sharp increase in the slope of the boiling curve is observed. Two different regimes such as partial (oc) and fully developed (ca) nucleate boiling are observed in this region. In the partial nucleate boiling regime, discrete bubbles are generated at the selected sites of the heater surface. With further increase in wall heat flux value, the wall superheat value increases and transition from an isolated bubble to fully developed nucleate boiling takes place (ca). in this region, the bubble growth and departure frequency increases. The coalescence between neighboring bubbles takes place and vapor escapes in the form of jet or column. This region (ca) is known as fully developed nucleate boiling regime. In this region, the liquid motion near the surface is caused due to the interference between densely populated bubbles. The highest heat transfer coefficients are observed in this regime at very small values of wall superheat. It is highly desirable to operate engineering systems in the nucleate boiling regime for maximum efficiency, safety and energy savings. Due to its numerous practical applications, many studies have been conducted to enhance nucleate boiling heat transfer.

Transition boiling

In the transition boiling regime ($\Delta T_a \leq \Delta T \leq \Delta T_b$) the bubble formation is so rapid that it leads to the formation of vapor film or blanket on the boiling surface. The heat flux value and wall superheat (ΔT_{sat}) continue to increase upto the limit when the agitating bubbles overcome the effects of the film. However, when the insulating effect of film dominates the bubble motion, the heat flux value tends to decrease with ΔT_{sat} (ab). Here, the condition may oscillate between film and nucleate boiling at any point on the surface. The formation, collapse and reformation of the film take place in this region. As the thermal conductivity of the vapor is much less than the liquid the heat transfer coefficient value tends to decrease with an increase in wall superheat.

Film boiling

The maximum achievable heat flux in the boiling curve is known as critical heat flux (CHF) and represented by point ‘a’ in the boiling curve (Fig. 1.3). If the heat flux is increased beyond CHF point the boiling mechanism changes from the nucleate boiling regime to the film boiling regime. The region 5 ($\Delta T \geq T_b$) in the boiling curve (Fig. 1.3) represents the film boiling region. Here, a stable vapor blanket is formed over the surface and it encapsulates the entire surface. The heat is transferred from the surface to pool liquid by conduction and radiation through vapor layer. The vapor film obstructs the contact of pool liquid with the boiling surface and results in very low value of heat transfer coefficient. With the decrease in the heat flux values, the stable vapor film cannot be sustained for a longer time and vapor film collapse takes place. The heat flux and temperature at this condition is termed as minimum heat flux (q_{min}) and minimum wall superheat (ΔT_{min}), respectively.

Critical heat flux (CHF)

The CHF condition is the upper limit for nucleate boiling process. For safe operation and maximum efficiency, the engineering systems are operated below the CHF limit. On reaching the CHF condition, an uncontrolled thermal condition is reached which leads to the sudden increase in the wall superheat values due to the decrease in heat transfer rates. This sudden increase in wall superheat value may result in burnout of surface or failure of the system. Therefore, in various practical applications such as boiling water reactors, steam generators and boilers, CHF condition must be avoided to prevent catastrophic failure.

1.3 Mechanism of pool boiling heat transfer

It is important to study and understand the key mechanism of bubble dynamics during pool boiling heat transfer. The heat transfer mechanisms during bubble growth on the heater surface are extensively studied by different researchers and are summarized by Kandlikar [2]. The mechanisms involved during pool boiling on flat heater surface can be classified in various categories such as microlayer evaporation, micro convection, transient conduction and contact line region. These are detailed below.

Microlayer evaporation: When a thin liquid film is entrapped beneath the growing bubble, the thin film interacts with the hot wall during initial superheat conditions, evaporates and heat transfer takes place to growing bubble. The evaporation of thin film may lead to an increase in the bubble growth rate. It is argued that a dry patch may be created depending on the complete evaporation of microlayer in the central region. The origin of the microlayer can be traced to the pioneering work by Moore and Mesler [3], Hendricks and Sharp [4], and Cooper and Lloyd [5].

Evaporation of this thin film leads to a substantial increase in the bubble growth rate [2]. The total energy from the microlayer can be estimated by analyzing (i) the heat transfer from the wall during the microlayer event, and (ii) the initial sensible energy of the microlayer [6]. The thickness of microlayer is considered to be in microscale and variation of temperature is assumed to be linear. The heat transferred during microlayer evaporation can be estimated as:

$$Q_{ME} = \frac{\rho_l v_{do} h_{lv}}{t} \tag{1.2}$$

where, Q_{ME}, ρ_l, v_{do}, h_{lv} and t denote the heat transferred from the microlayer, density of a liquid, volume of microlayer, latent heat and time, respectively.

Microconvection: The receding and advancing bubble interface on the heater surface during bubble growth and departure develops convective currents in the liquid near bubble base, disturbs the thermal boundary layer leading to enhancement in heat transfer. This is termed as microconvection. It was reported that the region of influence for microconvection is approximately two times of the bubble departure diameter [7]. For a higher value of heat flux, the interface motion increases and the contribution of microconvection increases. The heat flux values at the vicinity of the bubble, because of microconvection are estimated by using the following expression [9].

$$\frac{C_l(\Delta T)}{h_{lv}} = C_{sf}\left(\frac{q"}{\mu_l h_{lv}}\sqrt{\frac{\sigma}{g(\rho_l-\rho_v)}}\right)^{0.33} {P_{rl}}^{1.7} \tag{1.3}$$

where, C_l, h_{lv}, μ_l, ρ_l, ρ_g, C_{sf}, σ and q'' denote the specific heat, latent heat of vaporization, dynamic viscosity, liquid density, vapor density, surface-fluid factor, surface tension and microconvective heat flux, respectively.

Transient conduction: The bubble departure leads to the replenishment and removal of the liquid layer from the heater surface. The heat conduction in the liquid during this phase is termed as transient conduction. The velocity of contact line during advancement of liquid affects the transient heat conduction mechanism. The mechanism of transient heat conduction is reported by various researchers [7-10] and surface heat flux can be estimated by employing the following expression.

$$\dot{Q}_{TC} = \int_0^x \frac{k\,\Delta T}{\sqrt{\pi\,\alpha_l\,x}}\,dx \tag{1.4}$$

where, $\dot{Q}_{TC}$, k, α_l and x denote the heat transferred through transient conduction, thermal conductivity, thermal diffusivity and distance travelled by the contact line, respectively.

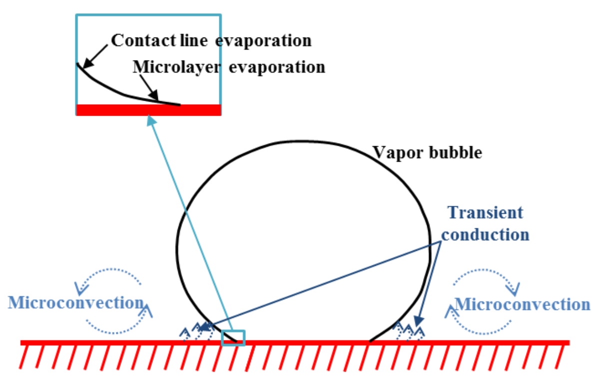

Figure 1.5: Mechanism of bubble dynamics during pool boiling heat transfer

Contact line region: This region exists at the boundary of the microlayer and liquid layer that undergoes the transient heat conduction (Fig. 1.5).

During the bubble growth period, this interface moves into liquid and the liquid layer experiencing the transient conduction is lifted around the bubble interface. Additionally, the high curvature of interface near the heater surface promotes higher evaporation and rapid cooling of liquid in this region leading to increase in local increase in the heat transfer coefficient. In contact line region heat transfer occurs is mainly due to relaxation of liquid superheat at the liquid–vapor interface. Hence, the contact line region represents the dynamic transition region from the microlayer to the bubble interface in the bulk meniscus region.

Heat transfer mechanism on porous and microchannel surfaces

Various authors have developed porous structures and studied the heat transfer mechanism during pool boiling. Neil et al. [11] suggested that vapor is generated in the porous network and is forced out of the pores. In such a case, the vapor tends to escape from the pores and fresh liquid is supplied through other pores. Bergles and Chyu [12] observed vapor formation, escape of vapor and supply of liquid through porous matrix. Wang et al. [13] proposed that numerous cavities developed in the porous network act as active nucleation sites. The fresh liquid fills in the nucleation sites every time when a bubble departs from it and the cycle continues. The nucleation frequency is found to be directly proportional to heat dissipation. The rapid growth and departure of bubble develop turbulent convective flows involving vapor columns resulting in the enhancement in heat transfer performance. The porous structure is found to promote the upward squirt effect. The representation of the boiling mechanism is shown in Fig. 1.6 (a). The liquid phase convection process that takes place in capillaries involving liquid is found to significantly affect the heat transfer performance of porous surface [14]. Cooke and Kandlikar [15] developed open microchannel geometry on the copper surface and conducted pool boiling experiments at atmospheric pressure. The authors reported that the nucleation occurs at comparatively low heat flux values and the nucleation occurs on the top of the microchannel. In such a case, the flooding of channels takes place with water and this acts as a pathway for water to the active nucleation sites. Fig. 1.6 (b) shows a schematic representation of bubble growth and departure on the microchannel surface as observed by the authors [15].

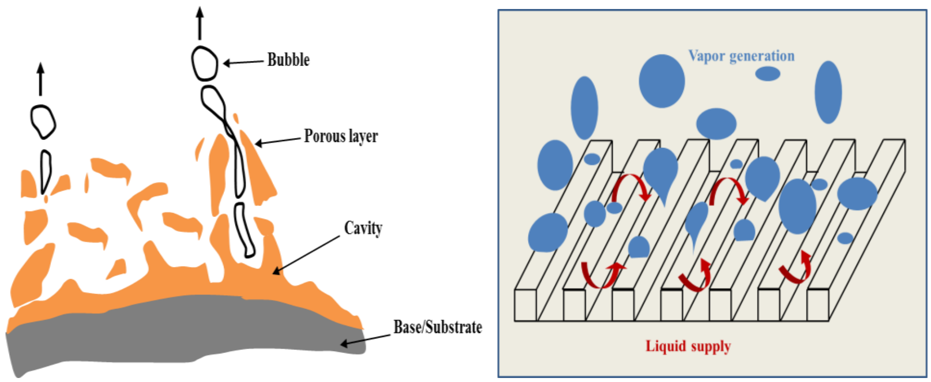

(a) (b)

Figure 1.6: Boiling mechanism (a) on a porous surface proposed by Wang et al. [13] (b) on open micro channeled surface proposed by Cooke and Kandlikar [15]

1.4 Techniques for enhancement in boiling heat transfer

Recent advances in technology, higher processing speeds and compact sizes of electronic components, reliability and safety issues associated with the reactor core cooling and energy efficiency of various thermal devices have motivated the researchers to develop techniques that can achieve significant enhancement in boiling heat transfer. The enhancement in boiling heat transfer can have various advantages such as higher energy efficiency, significant miniaturization of components, higher reliability and safety features, reduced weight and cost.

Therefore, boiling enhancement technologies have gained importance in refrigeration and air-conditioning industries, oil, gas and chemical processing industries and the microelectronics cooling (immersion cooling) industries, waste recovery for power generation and several other industries. Bergles et al. [16] have described different heat transfer techniques. These techniques are mainly classified into two groups such as passive and active techniques. The passive techniques use special geometries or fluid additives for enhancement and do not require an external power source. Whereas in active techniques an external power source is required to create surface vibrations or acoustic fields. The passive technique usually uses the coated surface, rough surface, structured geometries and additives in the coolant for enhancement in thermal performance. These are elaborated below.

- Coated surfaces: This technique involves metallic or non-metallic coating on the surface to develop nucleation sites. These include porous and high thermal conductivity metal coating on the surface.
- Rough surfaces: Roughness is developed on the surface by means of machining or restructuring of the surface. The roughness on the surface develops artificial nucleation sites which provide enhanced heat transfer performance compared to a plain or smooth surface.
- Channeled or structured geometries: By employing machining techniques, various structured geometries including channels are developed on the surface. These structured surfaces increase the surface area, provide better liquid-vapor interaction and lead to enhancement in heat transfer coefficient.
- Additives for liquids: Various nanoparticles (Al_2O_3, CuO, CNT) are added to the bulk fluid to prepare nanofluid. These nanofluids enhance thermal performance because of higher value of thermal conductivity.

In addition to this, various active techniques such as mechanical aids, electrostatic fields and fluid vibrations are used to enhance the thermal performance. These are detailed below.

- Mechanical aids: It involves stirrer or rotating surface to develop fluid motion by mechanical means. It promotes fluid mixing and better liquid flow over heated surface.

- Electrostatic fields: To promote bulk mixing of fluid, electrostatic fields are developed by employing direct or alternating current (DC or AC).
- Fluid vibrations: Vibrations for a varied range of frequency are introduced in the fluid to promote mixing in the fluid.

It may be noted that passive surface modification technique is preferred because of various advantages such as no need of external power source, easy to implement in real-time conditions, beneficial in accidental conditions and simple in design.

1.5 Literature review

The pool boiling heat transfer can be enhanced by using active techniques such as electrostatic fields, ultrasonic vibrations or by using passive methods such as surface modification. The passive techniques are widely used because these techniques are easy to implement and do not need any external power source. In view of this, numerous studies have been carried out to enhance heat transfer performance by using various surface modification techniques. These include mechanical machining, chemical processing, coating and microelectromechanical systems (MEMS), nanoelectromechanical systems (NEMS) technique (Lithography, etching) to develop novel surfaces with unique surface characteristics. These surfaces were used to enhance nucleate pool boiling heat transfer performance for various operating conditions. The Present literature study, reports various passive techniques used by different researchers to develop novel surfaces and their heat transfer performance. These are elaborated below.

Roughened surfaces

Initially, attempts have been made to employ different surface modification techniques, such as sand blasting and machining to alter the surface roughness [17]. Kurihara and Mayers [18] conducted pool boiling experiments on a copper surface roughened by using emery papers with water and different organic fluids. They observed a substantial increase in the boiling heat transfer coefficient values and reported that the increase in the area density of active nucleation sites is mainly responsible for the enhancement in heat transfer coefficient. Benjamin and Balakrishnan [19] developed copper surfaces with varying surface roughness values by polishing them using different grades of polishing papers. They conducted pool boiling experiments by using different pool liquids namely water, acetone, hexane and CCl_4. Numerous active nucleation sites, developed on the surface due to roughening of surfaces with polishing paper, are found to be responsible for the enhancement in heat transfer performance of stainless steel and aluminum surfaces. Kang [20] used different grades of sandpapers to increase the surface roughness value of stainless steel surfaces and achieved surface roughness of 60.9 nm. The SEM images of test surfaces developed by the authors are shown in Fig. 1.7 (a,b). Subsequently, these surfaces are used in pool boiling tests. The enhancement in heat transfer coefficient was observed with the treated surfaces [20].

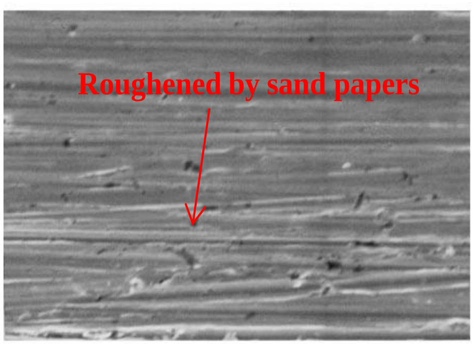

(a)

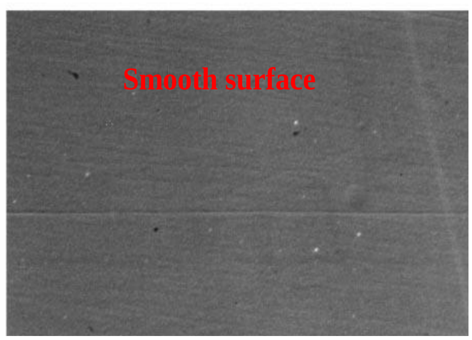

(b)

Figure 1.7: SEM images of test specimens developed by Kang et al. [20] with different surface roughness (a) Rough surface 60.9 nm (b) Smooth surface 15.1 nm

Jones et al. [21] employed a electro discharge method (EDM) machining technique to increase the surface roughness of the heater surface. Cavities are formed on the surface and the surface with 10 µm surface roughness value possesses higher cavity density. Cavities formed on the surface due to EDM machining, act as active nucleation sites and promote higher heat transfer rates. In addition to this, numerous studies [22-25] have been made that report enhancement in boiling heat transfer performance with roughed surface compared to plain surface.

Structured surfaces

Efforts have been made to develop various structured geometries such as channels/tunnels on the test surface by employing different machining techniques. Subsequently, these structured surfaces were used in pool boiling tests and their thermal performance was estimated. In general, micro fins are developed on the test surface and are found to promote heat transfer performance [26-39]. Siman-Tov [26] reported that extended surface enhances heat transfer performance and the fin spacing is found to play a crucial role in heat transfer enhancement. Klein and Westwater [27] conducted tests to study the effect of fin spacing on boiling heat transfer performance. The configuration with fin spacing of 1.57 mm is found to exhibit better thermal performance. The heat transfer performance of the finned structure reduces when the fins are brought very close to each other due to bubble interference. Bergles et al. [28] observed that the effectiveness of square shaped fins reduces with a decrease in the gap between two fins. Rainey and You [29] performed experiments on plain square pin finned surfaces and reported that pin fins create resistance to the departing vapor bubble and increase the flow resistance to liquid resulting in local dry out condition. These studies indicate that the dimension and shape of extended surface geometry significantly affect the heat transfer performance. Chen et al. [30] carried out pool boiling experiments on 3D printed helical fins (Fig. 1.8 a). It was argued that the helical fins exhibit superior heat transfer performance compared to plain surface. Various experimental studies are conducted on reentrant cavities by different authors [31-39]. Reentrant cavities are found to act as a vapor trap and support the nucleation process which enhances the heat transfer performance. In addition to this, efforts have been made to study the boiling heat transfer performance of interconnected reentrant tunnel geometries. Interconnected reentrant tunnels are found to enhance the heat transfer performance of surface compared to isolated reentrant cavities due to better vapor and liquid interaction inside tunnel geometries. A common example of such structure is tunnel pore geometry. Kim and Choi [39] used tubes with pore and connecting gaps to study pool boiling characteristics of tunnel pore structure. The schematic view of different geometries developed by the authors are shown in Fig. 1.8 (b-d). Initially, the authors studied the effect of pore sizes on heat transfer performance and the pore sizes that yield the higher heat transfer coefficient are used in the pool boiling experiment.

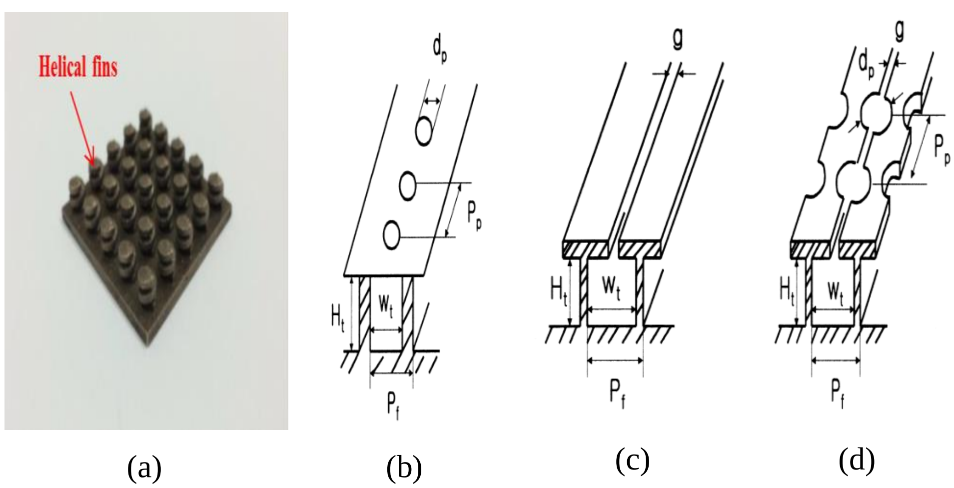

Figure 1.8: (a) Photographic view of helix fin used by Chen et al. [30] (b) Characteristic dimensions of structured enhanced tubes used by Kim and Choi [39] with pores (c) With gaps (d) Pores with connecting gaps

It was argued that the connecting gaps act as additional liquid supply path and delays dry out condition. Chien and Webb [40] carried out the visualization study on surfaces with tunnels and surface pores. Evaporation on the menisci in the corners is found to be the principal mechanism of heat transfer in these structures. Rajulu et al. [41] carried out tests to study boiling heat transfer performance of tubes with reentrant cavities for different mouth sizes by using different pool liquids such as acetone, isopropanol, ethanol and water. The heat transfer enhancement is found to depend on cavities on the surface. Pastuszko [42] studied boiling heat transfer over tunnel pore structure with fins of 5 mm height. They observed the highest heat transfer coefficient for water and ethanol with the pore of size 3 mm. Das et al. [43] developed different structures on a copper surface by employing the wire-EDM method (Fig. 1.9 a,b) and subsequently, these surfaces are used to estimate boiling heat transfer performance. Structured surfaces with bidirectional tunnel geometries exhibit the highest heat transfer coefficient values compared to unidirectional tunnel geometries. Cooke and Kandilkar [15] conducted pool boiling experiments over the microchannel surface. The heat transfer coefficient of surfaces involving microchannel is found to be 3.4 times higher compared to the plain surface. Based on the bubble dynamics study, it was argued that the channels improve liquid flow towards nucleation sites and provide better wetting. In addition to this, the authors studied the effects of different geometric parameters such as channel width, fin thickness and depth of channel geometry on pool boiling heat transfer [15]. Test geometries with wider and deep channels involving thin fins exhibit higher heat transfer performance. Tests have been conducted to study the effect of variation in dimensions of channeled geometries [15]. Guglielmini et al. [44] developed an extended surface geometry and carried out a pool boiling experiment with FC-72 as pool liquid for saturation pressure varying between 0.5 to 2 bar. It was argued that the extended surface geometries exhibit higher heat transfer performance compared to a plain surface. Xuenong et al. [45] studied the pool boiling heat transfer performance of machined porous tubes by using R134a and R142b as pool liquids. The enhancement in boiling heat transfer was found to vary within a ratio of 1.4 to 1.7 compared to the plain surface.

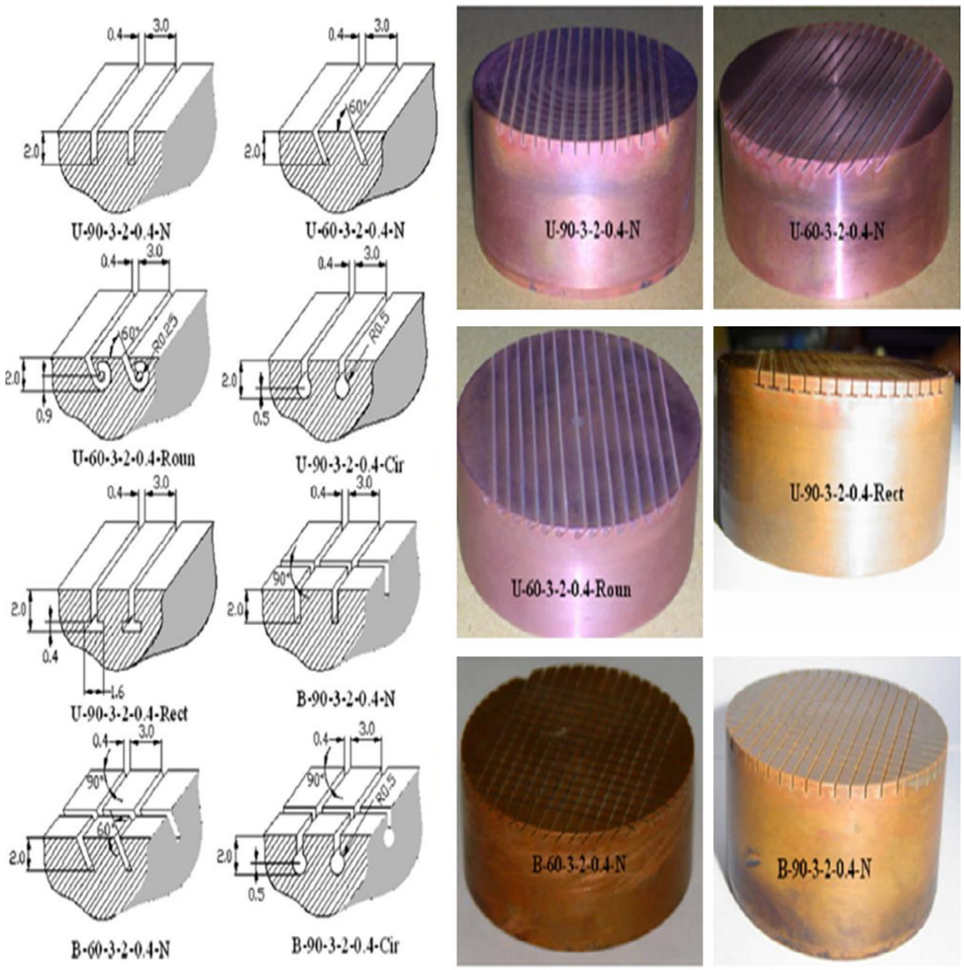

(a) (b)

Figure 1.9: Structured surfaces developed by Das et al. [43] (a) Schematic view of tunnel geometries (b) Pictorial view of test surfaces

Coated and micro/nanostructured surfaces:

A wide variety of studies have been made that employ advanced micro/nanostructure fabrication techniques such as coating methods, chemical processing and MEMS/NEMS fabrication techniques to develop novel surfaces. The surface coating methods consist of various fabrication techniques namely sputtering, vapor deposition, atomic layer deposition, spin coating, solution immersion and calcination to coat the material surface with numerous nanoparticles such as SiO_2, TiO_2, graphene oxide and carbon nanotubes (CNTs). In a recent study, Forrest et al. [46] coated silica nanoparticle on the stainless steel and nickel surface by employing layer by layer method. The SEM image of the test section fabricated by the authors is shown in Fig. 1.10 (a). In this method, the surfaces are repeatedly immersed in the solutions containing nanoparticles and subjected to the calcination process. The enhancement in heat transfer is found to be 100 % for nanoparticle coated surfaces.

Hsieh and Weng [47] employed plasma and flame spraying technique to coat molybdenum, aluminum and copper on the heater surface. The processed surfaces were found to exhibit 2.5 times higher heat transfer coefficient values compared to the smooth surface. Ahn et al. [48] used a chemical vapor deposition (CVD) method to coat vertically aligned multiwalled carbon nanotubes (MWCNT) on silicon wafers. Fig. 1.10 (b) depicts the SEM image of the test section developed by using CVD technique. Various factors are found to be responsible for the enhancement in heat transfer performance of coated surfaces. Li et al. [49] used a copper electron beam evaporator to deposit copper nanorods on copper substrate. The deposition of nanorods on surface develops nanostructures on a copper substrate and promote the enhancement of boiling heat transfer performance.

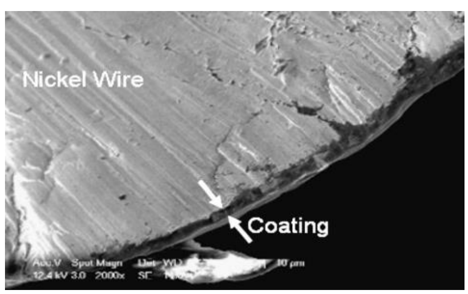

(a)

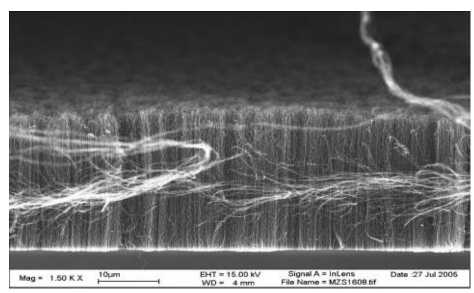

(b)

Figure 1.10: (a) SEM image showing the diametric view of 0.01" nickel wire with 40 bilayers PAH/SiO_2 Forrest et al. [46] (b) SEM image of type-B MWCNT synthesized on silicon substrate by using chemical vapor deposition (CVD) technique Ahn et al. [48]

Ramaswamy et al. [50] employed two microfabrication methods, namely, wet etching and wafer dicing to develop surfaces involving channels and pores (Fig. 1.11 a,b). The authors conducted pool boiling experiments by using FC-72 and reported the effect of pore size in the boiling heat transfer process. Chen et al. [51] studied the effect of Si and Cu nanowires developed on the surface by employing electroplating and electrochemical etching technique. The enhancement in heat transfer coefficient of these surfaces was found to be more than 100 % compared to plain surface. Apart from coating techniques, attempts have been made to develop nano and microstructures on the surface by using advanced semiconductor fabrication methods such as MEMS and NEMS.

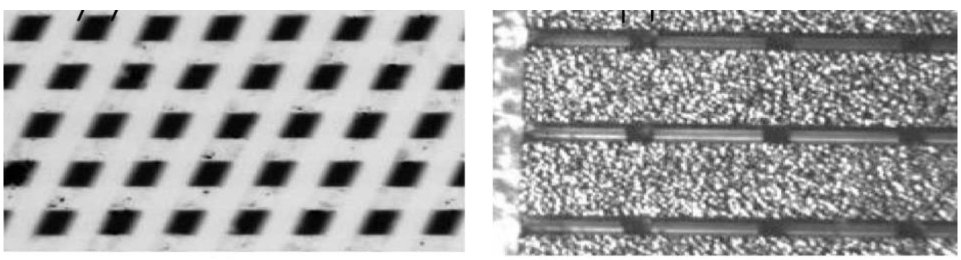

(a) (b)

Figure 1.11: Microfabricated enhanced structures fabricated by Ramaswamy et al. [50] by using (a) Wet-etched method (b) Wafer-dicing method

These fabrication techniques usually employ patterning and material deposition by etching and photolithography, respectively. A micro fin structure was developed on the surface using the dry etching technique by Honda et al. [52]. The authors developed a micro fin structure with a square cross section of 50 × 50 × 60 μm and conducted pool boiling experiments with FC-72 as pool liquid. Significant enhancement in heat transfer performance was observed compared to the smooth surface. Zhang and Lian [53] employed a LIGA (German acronym of **Li**thographie, **G**alvanoformung, **A**bformung) technique to develop microstructure on a silicon surface. In this technique, the microstructures are developed on a silicon surface using photolithography and wet etching. The development of microstructures on silicon surface was found to enhance the heat transfer performance. Later on, Coso et al. [54] used lithography and etching technique to prepare bi-porous media with micro fin arrayed structure on the silicon surface. It was argued that the overall heat transfer coefficient increases with the reduction in pore size that may be due to the increase in surface area. In addition to this, numerous pool boiling studies [55-67] have been made and these studies report significant enhancements in boiling heat transfer performance due to the addition of microstructures. These studies are summarized in Table 1.1.

Table 1.1: Different studies on microstructured surfaces

Author	**Surface type**	**Remarks**
Kubo et al. [55]	Reentrant cavities	The authors studied pool boiling with FC-72 as pool liquid on re-entrant cavities of 1.6 μm and 3.1 μm diameter with the pitch varying between 0.1 - 1 mm.
Kotthoff et al. [56]	Micro cavities	The authors reported that the change in behavior of bubble growth and departure is the reason behind boiling heat transfer enhancement.
Li et al.[57]	Horizontal highly conductive micro porous coated surfaces	The authors studied the effects of geometric parameters of the conductive microporous surface on pool boiling heat transfer and reported that various parameters such as the thickness of coating and porosity of coating strongly affects the boiling heat transfer performance.
Alam et al. [58]	Coated tube	Experiments were conducted on copper coated mild steel hot tubes with thicknesses

		varying between 19-60 μm. The authors reported that the value of heat transfer coefficient enhances up to certain thickness, beyond that a decrease in heat transfer is observed.
Wu et al. [59]	TiO_2 coated surface	The heat transfer coefficient and CHF of coated surface are found to increase by 91 % and 38 %, respectively compared to the smooth surface.
Sahu et al. [60]	Copper plated nanofiber	The nanofiber coated surface exhibits 33 % higher CHF than the smooth surface.
Hendricks et al. [61]	Nanostructured surfaces	The authors employed the microreactor-assisted nanomaterial deposition (MAND) technique to develop nanostructure on aluminum and copper surface. They used ZnO as the coating material. The average pore size and surface roughness were 50–100 nm and 80–6000 nm, respectively. Authors conducted pool boiling experiments with water to measure boiling heat transfer coefficients and CHF.
Launay et al. [62]	Microstructured surfaces	The authors employed various MEMS fabrication techniques, to develop seven types of microstructured surfaces on Si wafers. They conducted pool boiling test with water and PF5060.
Feng et al. [63]	Aluminum oxide-coated	Authors developed an aluminum oxide-coated platinum wire by employing the atomic layer deposition (ALD) technique. They measured the average roughnesses

		values of the Pt and Pt/Al_2O_3 surfaces and were 357 and 378 nm, respectively. They conducted pool boiling experiments by using water as pool liquid.
Yao et al. [64]	Nanostructured surfaces	The authors developed nanostructured surfaces by using electrochemical deposition method. They coated Cu nanowires on different substrates such as Ag–Si, Au–glass, and Cu. The pool boiling tests were conducted by using water as pool liquid.
Kim et al. [65]	Wet etching	Multiscale geometries were fabricated on Si wafer and the authors conducted pool boiling experiments with water.
Zou and Maroo [66]	Etching technique	The authors fabricated structures by employing Bosch etching technique following patterning by deep ultraviolet photolithography. Pool boiling tests were conducted on ridge structured surfaces on Si wafers using water pool liquid.
Dong et al. [67]	Dry and wet etched surface	The authors fabricated nanocavity-structured surfaces on Si wafers using dry etching and wet etching technique and conducted pool boiling tests with ethanol. The pool boiling heat transfer performance was found to be better when compared to the plain surface.

Miscellaneous pool boiling studies on enhanced surface developed using different methods

Lu et al. [68] developed a porous layer by using the sintering method. Introduction of the porous matrix on the heater is found to enhance the pool boiling heat transfer performance. In their study, Li et al.

[69] developed various modulated porous structures on the heater surface with different thickness values. The thickness of the porous structure was found to play an important role in the enhancement of heat transfer performance. Authors observed a relatively constant heat transfer coefficient on a thin uniform porous structure surface. Whereas the thick porous structure exhibits poor heat transfer performance but the CHF value observed on thick porous structure was found to be twice compared to the plain surface. Ali and El-Genk [70] developed copper microporous surfaces using an electrochemical process and studied the effect of inclination on pool boiling heat transfer performance. The porous surface possesses higher heat transfer coefficient values compared to plain surface. Also, the heat transfer coefficient decreases with the increase in the inclination angle.

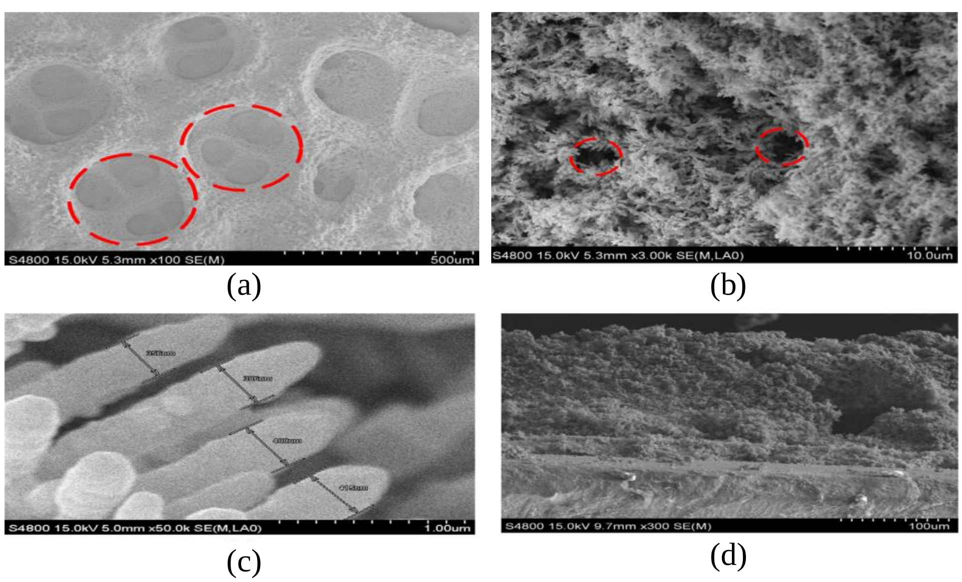

Figure 1.12: SEM micrographs of the composite porous surface developed by Xu et al. [72] (a) Macroporous (b) Microporous (c) Dendritic structure (d) Side view of the porous surface

Different structured porous surfaces were synthesized using acid etching and sintering process by Rioux et al. [71]. The enhancements in HTC and CHF were found to 200 % and 350 % for hierarchical multiscale modulated porous surface, respectively compared to plain surface. Xu et al. [72] developed a composite porous copper surface by employing electrochemical method (Fig. 1.12 a-d). Porous structures exhibit the enhancement in heat transfer coefficient values by 120 % compared to plain surface. Mori et al. [73] conducted pool boiling heat transfer experiments on commercially available honeycomb porous plate and nanoparticle deposited surface. These surfaces were found to enhance heat transfer performance. Yang and Takizawa [74] conducted pool boiling tests using Freon 113 as pool liquid on a commercial graphite fiber-reinforced copper (Gr–Cu) heater surface with graphite fiber diameter varying between 0.008–0.01 mm. It was argued that boiling heat transfer performance was enhanced due to the higher value of thermal conductivity of the graphite fibers. Vemuri and Kim [75] developed nano porous surface (Fig. 1.13 a) and their pool boiling heat transfer performance by using FC-72 dielectric fluid as pool liquid. The nano porous surface was found to reduce the incipient superheat by 30 %.

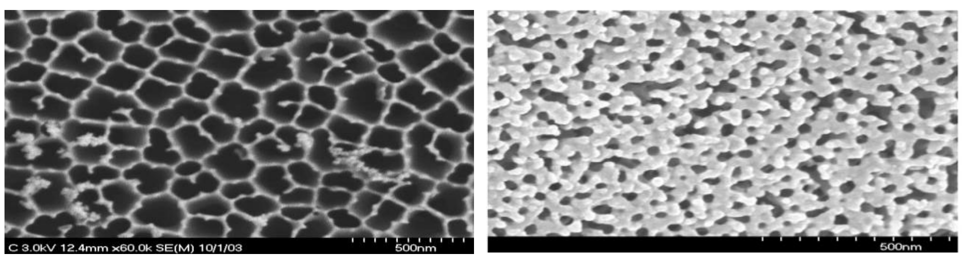

(a) (b)

Figure 1.13: (a) SEM photograph of nano-porous surface developed by Vemuri and Kim [75] (b) FESEM image of nano-porous surface developed by using the anodizing technique by Lee et al. [76]

The anodizing was employed by Lee et al. [76] to develop nano porous surface on an aluminum alloy (Fig. 1.13 b). The nano porous coated surface was found to exhibit better nucleate pool boiling heat transfer performance compared to non-coated plain surface. Lu et al. [77] employed a wafer-scale electroless etching method to coat the heater surface with silicon nanowires (Fig. 1.14 a-d). They reported that the silicon nanowires enhance the heat transfer performance of surface due to the improved liquid spreading on the coated surface compared to the plain surface. Apart from these, various authors [78-90] have conducted pool boiling experiments with nanofluids to study the boiling heat transfer performance of surface and the effect of nanoparticle deposition on surface during nanofluid boiling.

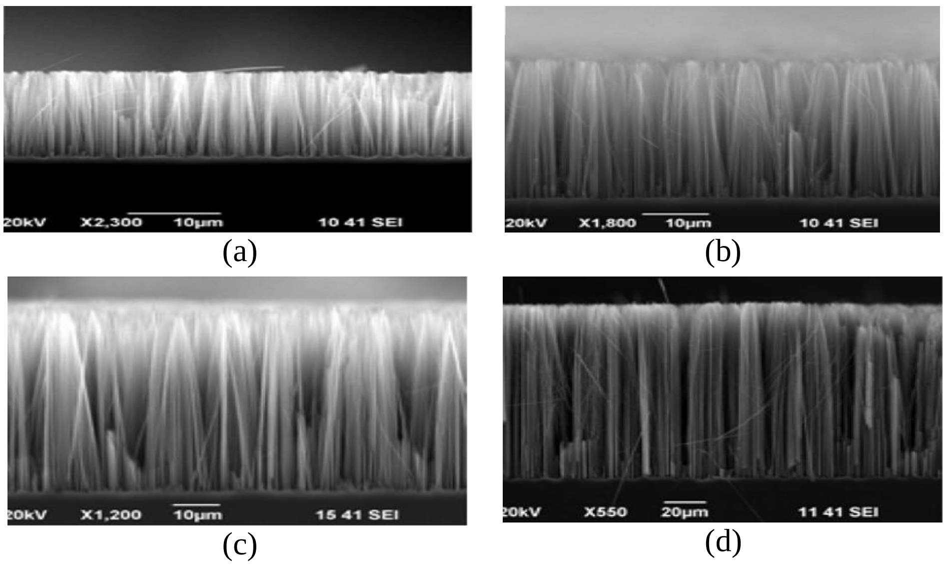

Figure 1.14: SEM images of SiNW array with different heights developed by Lu et al. [77] (a) 16 µm (b) 32 µm (c) 59 µm, (d) 122 µm

A number of studies have been made that employ numerous techniques such as machining, coating, MEMS and NEMS to develop novel surfaces. Subsequently, these processed surfaces were used to estimate the boiling heat transfer performance. However, surfaces developed by employing these techniques exhibit various drawbacks such as thermal stability, mechanical strength, difficulty in large scale fabrication, difficult fabrication method, expensive and bonding material limitations. Recent studies [91-97] report the development of organized microstructure on the material surface because of direct exposure of the material surface to laser irradiation. Also, the microstructure developed using laser processing does not possess limitations as reported by other methods.

Recently, laser processing techniques have been used to develop novel microstructures on the surface by various researchers [98-100]. Subsequently, the authors analyzed the pool boiling heat transfer performance of these surfaces. The pool boiling performance was found to be superior compared to plain surface.

1.6 Scope and objective of the present investigation

The present literature review reports various experimental studies associated with the enhancement of boiling heat transfer performance of surface using various surface modification techniques such as sandblasting, polishing, milling, wire-electro discharge machining (wire-EDM), microelectromechanical systems (MEMS). These processed surfaces are found to exhibit higher pool boiling performance compared to the plain surface. Limited studies are reported that analyze the pool boiling performance of laser processed surfaces. Nevertheless, various issues pertaining to laser processing parameters, physical characteristics of laser test surfaces, pool boiling heat transfer performance need further investigation. These are detailed below:

- Development of various tunnel geometries with varying width and depth by employing wire-electro discharge machining (wire-EDM) process and study the pool boiling performance for a varied range of input heat fluxes.
- The influence of various parameters such as width and depth of structured surfaces developed by wire-EDM on pool boiling performance, for different pool liquids such as water and isopropyl alcohol need to be studied.
- Efforts should be made to develop multiscale functionalized copper surfaces by employing pulsed and continuous wave laser surface processing techniques and study the pool boiling heat transfer performance of processed surfaces for a varied range of input heat fluxes.

- The influence of numerous parameters, namely, laser type, laser power, laser wavelength on pool boiling heat transfer performance must be studied.
- The physical characteristics of laser processed surfaces need to be studied by utilizing photographic view, stereo microscopic images, scanning electron microscope images, the 3D roughness profile of the test section.
- The pool boiling performance of laser processed surface for a varying range of input heat flux values with different pool liquids such as water and acetone must be studied.
- The physical characteristics and pool boiling performance of test surfaces developed by employing pulse laser and continuous wave laser processing technique are to be compared.

The objective of the present study is to obviate some of the issues highlighted above. The aim of the present thesis is to study the pool boiling performance of test surfaces developed by using wire-EDM, nanosecond pulsed laser, continuous wave laser techniques. The effects of variation of laser type, laser power and laser wavelength on physical characteristics of test surface are studied in this thesis. Also, the effects of a varied range of input heat fluxes, different pool liquid on the pool boiling performance are studied.

The organization of the present thesis is as follow:

Chapter 1: This chapter introduces the phenomenon of pool boiling and various boiling regimes during pool boiling. The heat transfer enhancement techniques and their fabrication processes are discussed. A brief review of the literature is reported. Finally, the scope of the present investigation is highlighted.

Chapter 2: This chapter reports the design, development and fabrication of the experimental test facility for studying nucleate boiling heat transfer performance. The heat transfer performances of the structured geometries fabricated by using wire-EDM machining method are discussed.

Chapter 3: This chapter provides information about the fabrication of novel surfaces by using a nanosecond pulsed laser system. The effects of variation of various laser processing parameters such as laser power and laser wavelength on the microstructure formation are discussed in this chapter.

Chapter 4: This chapter discusses the fabrication of test surface by using continuous wave laser system. The microstructure formation using two different laser systems such as continuous wave laser system and nanosecond pulsed laser system is discussed in this chapter. Pool boiling heat transfer performance of surfaces developed by employing both nanosecond laser system and the continuous wave laser is provided in this chapter.

Chapter 5: Conclusions obtained from the present experimental investigations are presented in this chapter. In addition, the scope for further investigations is discussed.

Chapter 2

Enhancement of nucleate pool boiling performance by using structured surfaces

2.1 General Background

Over the last few decades, researchers have employed numerous active and passive techniques to augment heat transfer performance. Passive techniques are preferred because they do not need external power for the augmentation of heat transfer performance. Various passive techniques such as surface modification techniques, involving mechanical machining, chemical processing, coating and microelectromechanical systems (MEMS) are widely used to develop novel surfaces for heat transfer augmentation. Mechanical machining techniques include various techniques such as milling, polishing, electro discharge machining (EDM) and wire-EDM. Efforts have been made to develop various structured geometries such as channels/tunnels on the test surface by employing different machining techniques. Subsequently, these structured surfaces were used in pool boiling tests and their thermal performance was estimated. In general, micro fins are developed on the test surface and are found to promote heat transfer performance [26-39]. It is argued that fin spacing plays a crucial role in heat transfer enhancement. The heat transfer performance of the finned structure reduces when the fins are brought very close to each other due to bubble interference [26-28]. Chen et al. [30] reported that the helical fins exhibit superior heat transfer performance compared to plain surface. These studies indicate that the dimension and shape of extended surface geometry significantly affect the heat transfer performance. Various studies [31-39] on re-entrant cavities report that the re-entrant cavities act as a vapor trap and support the nucleation process which enhances the heat transfer performance. Interconnected reentrant tunnels are found to enhance the heat transfer performance of surface compared to isolated reentrant cavities due to better vapor and liquid interaction inside tunnel geometries. Rajulu et al. [41] studied boiling heat transfer performance of tubes with reentrant cavities for different mouth sizes by using different pool liquids such as acetone, isopropanol, ethanol and water. They reported that the heat transfer enhancement depends on cavities on the surface. Das et al. [43] developed different structures on a copper surface by employing the wire-EDM method and subsequently, these surfaces are used to estimate boiling heat transfer performance. They reported that the structured surfaces with bidirectional tunnel geometries exhibit the highest heat transfer coefficient values compared to unidirectional tunnel geometries. Compared to various machining techniques, wire-EDM has been considered for fabrication due to its inherent precise machining capability. Although the structured geometries manufactured by wire-EDM process exhibit better heat transfer performance, limited studies are reported in the literature. Compared to other configurations, the bidirectional tunnel structured geometry, developed by employing wire-EDM exhibit better heat transfer performance [43]. In addition to this, limited studies are available with structured geometries with isopropyl alcohol as pool liquid. Here, efforts have been made to develop structured surfaces on the copper test section. The pool boiling characteristics of the structured surfaces are estimated through experimental investigation.

In the present study, an experimental investigation has been carried out to investigate the nucleate boiling heat transfer performance of various orthogonally intersecting structured surfaces. Tests were carried at atmospheric pressure and saturated pool boiling conditions by using water and isopropyl alcohol as pool liquid. The orthogonally intersecting tunnel structured geometries with varying tunnel depth of 0.5 mm, 1 mm and width of 0.61 mm, 0.725 mm were developed on copper test sections by using wire-EDM process. Tests were carried by varying input heat flux in the range of 0-300 kW/m^2 for water and 0-250 kW/m^2 for isopropyl alcohol. The effects of geometrical parameters of structured surfaces on the heat transfer performance are studied. Also, the mechanism of heat transfer on the structured surfaces is highlighted.

2.2 Fabrication of experimental test facility and test surface

2.2.1 Experimental test facility

The schematic of the experimental test facility for the present pool boiling experiments on horizontal, smooth and various structured surfaces at atmospheric pressure condition is shown in Fig. 2.1 (a). The experimental test facility includes a cylindrical boiling container (1), a heater assembly (2), a condensing coil (3), power supply (8), measuring instrumentation (4). A cylindrical borosilicate glass container, with 130 mm diameter, 5 mm thickness and 300 mm in length was used as a boiling container which stores the pool liquid. The ends of the container were closed with the 12 mm thick metal flanges and the bottom flange was covered with 5 mm thick silicon insulation to reduce heat loss. The bottom plates also hold the test section, emerging in the liquid pool from a circular opening resting on the copper block. A press fitted Teflon bushing was provided between bottom plate opening and copper block. This also ensured the leak proof joint and prevented pool liquid from leaking in heater assembly (2). A 40 mm diameter copper disc is used as the test section and fitted on the copper block heater protruding in boiling container from the bottom plate using nut and bolt arrangement. The copper block of 40 mm diameter and 87 mm length is the part of the heater assembly. Two high density cartridge heaters with 500 watt capacity each were fitted in the copper block. The copper block in heater assembly was heavily insulated from sides and bottom to ensure a unidirectional heat transfer in upward direction. A ceramic fiber blanket was used to cover the copper block in multiple layers forming a 50 mm thick insulation around the copper block. The bottom face of copper block is resting on ten ceramic plates (each 6 mm thick) joined together forming

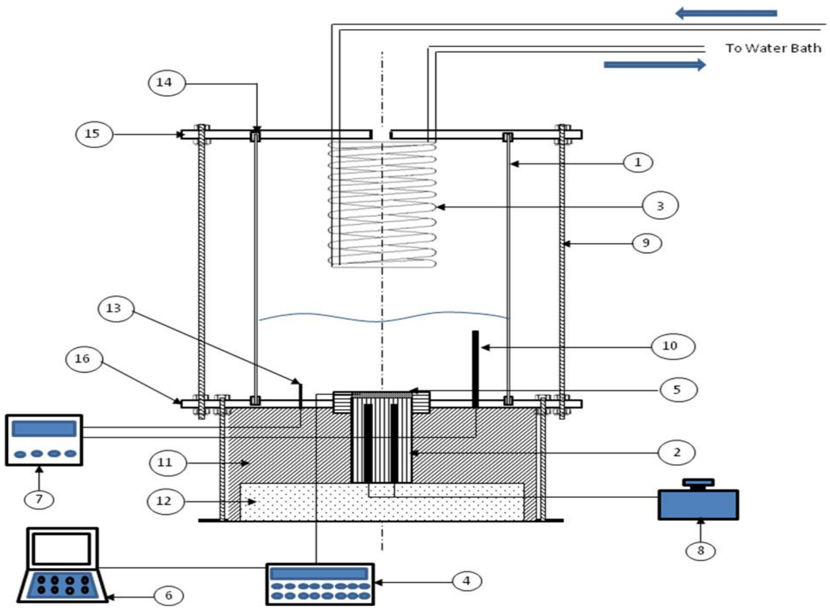

1	Boiling container	2	Heater assembly
3	Condensing coil	4	DAS
5	Test section	6	Computer
7	PID Controller	8	Dimmerstat
9	Studd	10	Pool heater
11	Ceramic blanket insulation	12	Bottom ceramic insulation
13	Pool thermocouple	14	Rubber gasket
15	Top flange	16	Bottom flange

(a)

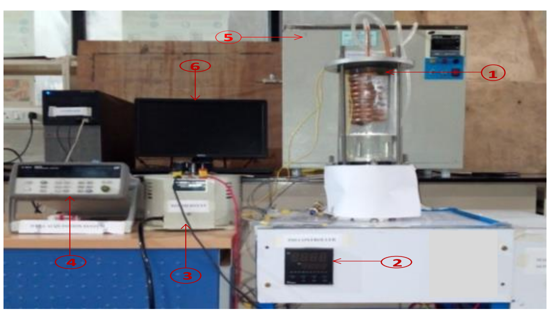

1	Boiling container	2	PID Controller
3	Dimmerstat	4	DAS
5	Water bath	6	Computer

(b)

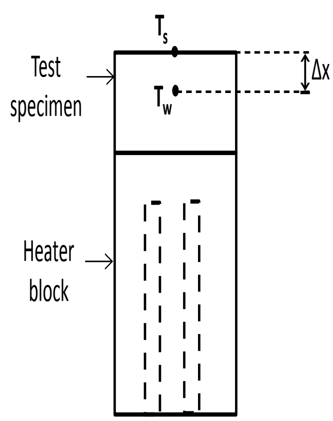

(c)

Figure 2.1: (a) Schematic diagram of the experimental setup (b) Photographic view of the experimental set up (c) Location of thermocouple in test specimen to measure temperature

60 mm thick insulation covered by a ceramic blanket on the bottom side of the copper block. This insulation arrangement reduced heat loss from heater assembly. The heat loss to surrounding was calculated by using data from the thermocouples, which are fixed in the insulation layers. Heat loss estimate shows that heat loss to surrounding from heater assembly outer surface is within 2 % peak heat load. The test section is firmly held in a Teflon cap to minimize heat losses and fixed on top of the heater block. All the joints were filled with high temperature silicon based sealants to curb the leakage of pool liquid. Liquid evaporated from the liquid pool was condensed by a condensing coil (3), suspended in the boiling container from the top plate. The condensate falls in the liquid pool maintaining pool liquid level in the boiling container. This also avoids any pressure build up inside the boiling container due to continuous liquid evaporation. A cryostat water bath (Biotechnics BTI-35) was used to cool the water, which was circulated from the condensing coil in the boiling container. Three 8 mm diameter and 60 mm long cartridge heaters with a power capacity of 300 watt were fixed inside the boiling container on bottom plate acting as auxiliary heaters to heat the pool liquid to saturation temperature and to maintain the temperature through the experimentation. The power supply to auxiliary heaters was controlled by PID controller (UDIAN Make AI 509 Model) and arrangements were made to cut off the power supply of individual heater when required. The liquid pool temperature data was provided to the PID controller by using thermocouple located in the boiling container just above the test surface. A photographic view of test facility is show in Fig. 2.1 (b). The temperature of the test section was measured by using a K-type calibrated thermocouple embedded just 1.5 mm (Fig. 2.1 c) below the test surface. The voltage signals from this thermocouple were examined by using a data acquisition system (Agilent 34970A) and stored in a desktop. The heat flux supplied was calculated by recording voltage and current inputs of heater recorded by using a digital multimeter (Meco). A leakproof joint

between a glass container and metal flanges was achieved by using circular rubber gaskets on the glass ends resting in the circular grooves provided on the flanges. This arrangement avoids any possible leakage of pool liquid as well as liquid vapor from the boiling container. The smooth surface was polished progressively using fine grades of polishing paper on polishing machine in order to reduce surface structure effect on nucleate boiling of the reference smooth test surface.

2.2.2 Fabrication of the test surfaces

While selecting the fabrication process for the development of augmented surfaces, one needs to consider the following points:

- A simple fabrication process.
- It is desirable that the fabrication process should be capable of producing the same structure precisely with similar surface characteristics. This ensures similar heat transfer performance for all the developed surfaces.
- It is desirable to develop a compact and robust surface structure, which needs to perform well in different working conditions.

Various machining techniques have been employed in the past to fabricate enhanced surfaces with different surface characteristics. A Wire-EDM machining technique satisfies above requirements and can develop different surface structures. In the present work, wire-EDM machining process has been used as a single machining process to develop precise tunnel structure on test sections. In this machining process, the material is removed from the workpiece by controlled erosion via successive electrical discharges or sparks in between two electrodes separated by dielectric fluid. The heat of each electrical spark erodes away a tiny bit of material that is vaporized and melted from the workpiece. These particles are flushed away from the cut with a stream of de-ionized water through the top and bottom flushing nozzles. The water also prevents heat build-up in the workpiece.

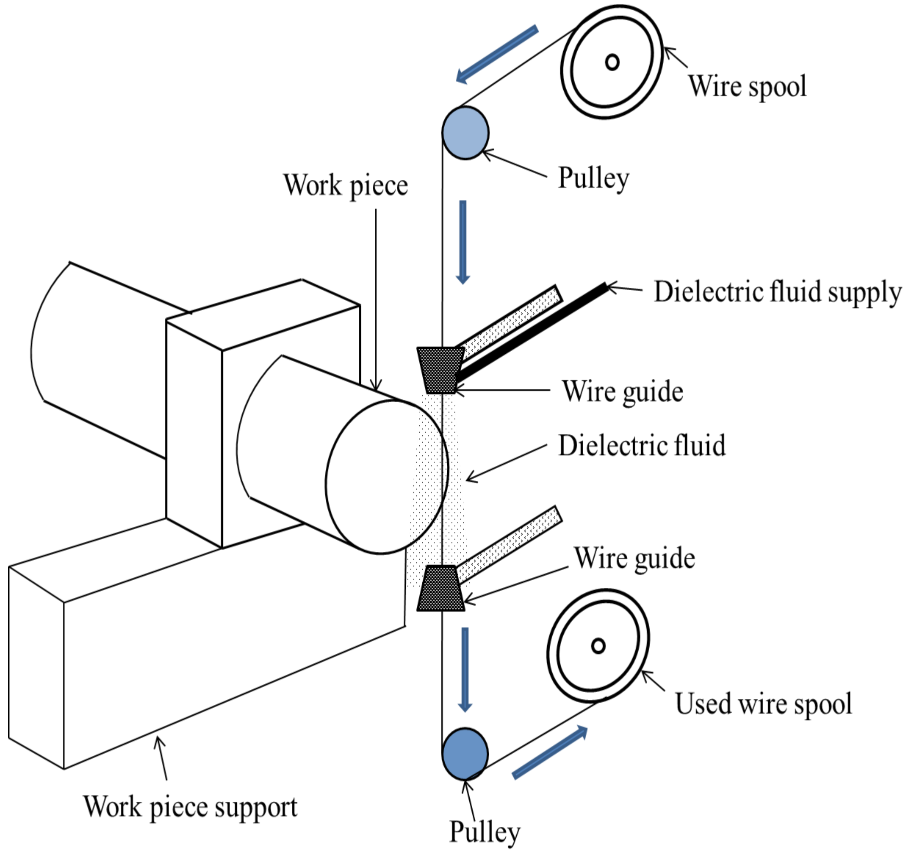

Figure 2.2: Schematic diagram of wire-EDM process

Fig. 2.2 depicts the schematic view of the wire-EDM process. A brass wire (Nickunj, Delhi) with 0.25 mm diameter from wire spool is fed through the workpiece. Machining pass was conducted using a low sparking energy by applying 20 volt and a maximum current of 1 amp with 1.0 μs ON and OFF time pulse durations. The contact in brass wire and workpiece leads to continuous electric sparks between the brass wire and a test surface. These sparks generate heat and remove tiny material from the surface. This machining process maintains a uniform and good surface finish during material removal. This helps to maintain identical surface characteristics over all augmented surfaces, reducing possibilities of variation in boiling heat transfer performance of surfaces due to varied surface characteristics and helps to study the boiling heat transfer performance of surface with varied tunnel geometry dimensions. Following Das et al. [43] here the developed geometries are named as tunnel geometries (these geometries are also known as micro fin geometries).

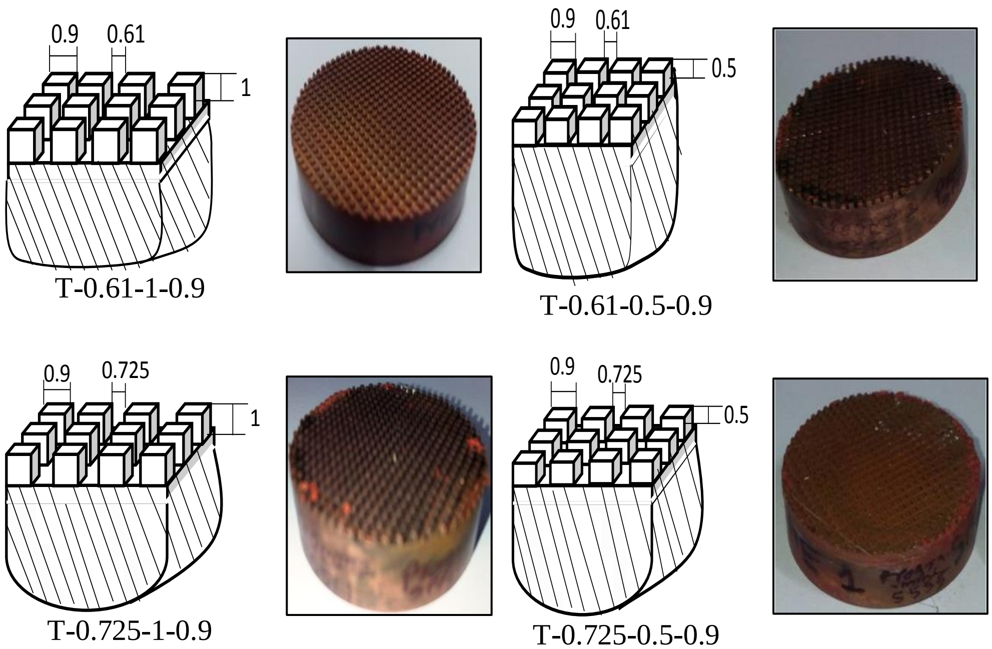

Figure 2.3: Schematic and photographic view of test surfaces

Table 2.1: Summary of surfaces used in the present investigation

Surface	Specification	Width (mm)	Depth (mm)	Pitch (mm)	Area enhancement factor
Smooth Surface	Smooth	NA	NA	NA	1.0
Structured 1	T-0.725-0.5-0.9	0.725	0.5	0.9	1.63
Structured 2	T-0.725-1-0.9	0.725	1	0.9	2.27
Structured 3	T-0.61-0.5-0.9	0.61	0.5	0.9	1.72
Structured 4	T-0.61-1-0.9	0.61	1	0.9	2.44

Tunnel geometries having a constant pitch with varying width and depth from the top of the surface have been prepared. The tunnel surface geometries were designated using a four character symbolic representation in which the first letter ‘T’ used to represent test surface, followed by numbers representing the width of the tunnel, depth of tunnel and pitch. The details of the surfaces with dimension in mm are given in Table 2.1 and schematically shown in Fig. 2.3 with their pictorial view.

2.2.3 Experimental procedure

Initially, few trial tests were conducted to ensure the experimental test setup is leak proof and to verify that all components of the test facility are working in a satisfactory manner under various operating conditions. After ensuring the satisfactory performance of the experimental test facility the experimentation was started with the smooth surface. The polished and cleaned smooth surface was embedded in Teflon cap mounted on the copper heater block inside the thoroughly cleaned boiling container. Here, thermal conductive paste (Cooler Master, RG-ICV1-TW20-R1 with thermal conductivity of 1.85 W/m-K) was used in between the test section and copper block contact to reduce contact resistance. Subsequently, the boiling container was filled with distilled water and degassed by vigorous boiling using the auxiliary heaters in pool liquid. After degassing the top flange was fixed and the cooling water circulation pump was switched on to circulate water in the condensing coil to condense the vapor inside the boiling container. The PID controller was set to saturation temperature to maintain the liquid pool to saturation temperature. Simultaneously the main heaters fixed in the copper block were switched ON and power to this heater was regulated using a dimmerstat (8). The temperature of pool liquid, test surface and the supply voltage, current were recorded and monitored throughout the experimentation. The supply voltage varied in the steps and for each varied supply voltage setting, sufficient time was given to achieve a steady state temperature. The readings were noted when the test surface temperature reading was found within ± 0.5 °C.

2.2.4 Data reduction

The input heat flux supplied to the test section is calculated by using voltage and current readings across the heater terminal using Eq. (2.1) and is expressed below [43]:

$$q'' = \frac{V \times I}{\frac{\pi}{4} \times d_{cyl}^2} \tag{2.1}$$

where, V is voltage measured across heater terminals in volts, I is the current measured across heater terminals in amps and d_{cyl} is the diameter of copper heater block in meter.

The direct measuring of the temperature at the heated surface is difficult as it can affect the bubble growth and departure process due to the alteration of the test surface geometry. Initially, three thermocouples are inserted in the test section at different locations to measure the temperature. But the variation in the temperature of these thermocouples is very small, only a thermocouple is inserted in the test section at a distance Δx from the top surface of the test section (Fig. 2.1 c) to measure the test section temperature (Tw). Therefore, the surface temperature (T_s) was calculated using the temperature of the test section (T_w) (Fig. 2.1 c). The surface temperature (T_s) was calculated by using a one-dimensional heat conduction equation as expressed below [101].

$$T_s = T_w - \frac{q'' \times \Delta T}{k} \tag{2.2}$$

where, T_s, q'', Δx and k denotes surface temperature, supplied heat flux, the distance of thermocouple located in test surface from the top and thermal conductivity of the material, respectively.

The heat transfer coefficient (HTC) was calculated from measured heat flux and wall superheat [101] expressed as in Eq. 2.3.

$$h = \frac{q''}{\Delta T} \tag{2.3}$$

where, h, q'' and ΔT denotes the heat transfer coefficient, supplied heat flux and wall superheat, respectively.

The wall superheat can be obtained as the difference of surface temperature and saturation temperature of pool liquid: $\Delta T = T_s - T_{sat}$

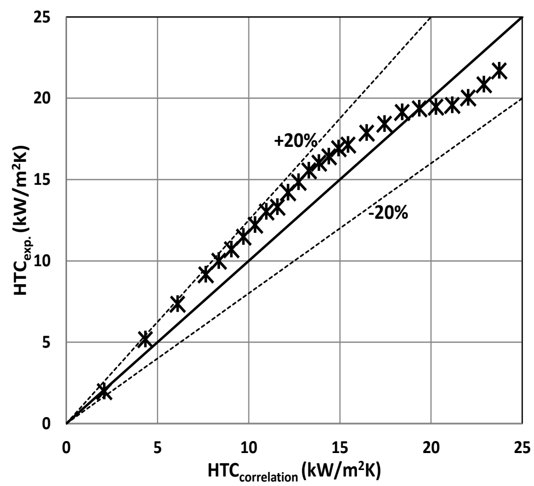

(a)

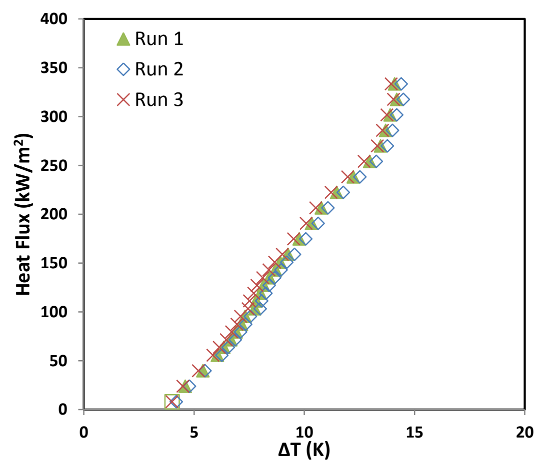

(b)

Figure 2.4: (a) Comparison of experimental heat transfer coefficient with correlation (b) Test Run on smooth surface

Initially, the reference smooth polished surface was fixed inside the boiling chamber and its pool boiling heat transfer performance was studied. Heat transfer coefficient values of the smooth surface were calculated by using the test data at different input heat flux values. The heat transfer coefficient values of smooth surface calculated experimentally are compared with the heat transfer coefficient calculated by using Rohsenow correlation [102] (Eq. 2.4) and is shown in Fig. 2.4 (a).

$$\frac{C_{pl} \times \Delta T}{h_{lg}} = C_{sf} \left\{ \frac{q"}{h_{lg}\ \mu_l} \left[\frac{\sigma}{g(\rho_l - \rho_g)} \right]^{0.5} \right\}^m \left[\frac{C_{pl}\ \mu_l}{k_l} \right]^n \tag{2.4}$$

where, c_{pl}, h_{lg}, μ_l, k_l, σ, and ρ_l denotes the specific heat, latent heat of vaporization, dynamic viscosity, thermal conductivity, surface tension and density of pool liquid, respectively. While, $q"$, ΔT, g and C_{sf} represent the supplied heat flux, wall superheat, acceleration due to gravity, the density of vapor, and surface liquid parameter used in Eq. (2.4), respectively. The Fig. 2.4 (b) depicts test runs conducted on the smooth surface.

2.3 Results and discussion

Here, four different orthogonally intersecting tunnel geometries with two different tunnel depths (0.5 mm and 1 mm) and width (0.61 mm and 0.725 mm) are developed on copper test section by wire-EDM process. Tests are conducted at atmospheric pressure and saturated pool boiling condition. Two different fluids such as water and isopropyl alcohol are used as pool liquid. Efforts have been made to investigate the effect of tunnel width and depth on heat transfer performance of the augmented surface with different liquids. The present experimental investigation involves the measurement of various physical quantities such as the temperature of the test section, a diameter of the test section, supply voltage and current. Here, a voltmeter and ammeter is used to measure voltage and current supplied to the heaters, respectively. A Vernier caliper is used to measure dimensions of the test section and K-type thermocouples are used to measure the temperature of the test section. The individual uncertainties involved in various measuring parameters such as V, I, d, Δx and T are found to be 1V, 0.01 A, 0.02mm, 0.02 mm and ±0.2 ˚C, respectively. Utilizing, Eqs. (2.1-2.3), the individual uncertainties in each parameter, the error analysis are made to estimate the errors associated in various parameters following the procedure suggested by Cole-man and Steele [103]. The details of calculation procedure for the smooth surface is elaborated in Appendix I. For, the wire-EDM processed surfaces, the maximum uncertainty was found for T-0.725-1-0.9. The uncertainty in the estimated results for various parameters such as heat flux (q″) and heat transfer coefficient (h) was found to be 1.85 % and 28.06%, respectively. The details of the result are elaborated below.

The visual observation showed that, with the gradual increase in heat flux, active nucleation sites on the surface increases. Initially, at lower heat flux input, very few distinct nucleation sites were observed on the test surface, from which growth of small diameter bubbles was observed. While, at higher heat flux input setting, with higher wall superheat values, a number of nucleating sites were observed with the growth of larger diameter bubble. On further increase in wall superheat with heat flux, bubble merger was observed.

2.3.1 Effect of surface structure on heat transfer performance

The detailed dimension of the tunnel structures is summarized in Table 2.1. Initially, efforts have been made to test structured surface (T-0.725-0.5-0.9) for boiling heat transfer performance. The heat flux input given to this enhanced surface is maintained following the same procedure as provided to the smooth surface. Fig. 2.5 (a) shows the boiling curve for the structured surface (T-0.725-0.5-0.9). Here, the boiling curve shifts significantly towards the left side for the structured surface. This signifies the reduction in wall superheat for the structured surface compared to the smooth surface. The comparison of the heat transfer coefficient for the structured surface (T-0.725-0.5-0.9) and smooth surface are shown in Fig. 2.5 (b). The increment in the heat transfer coefficient for the augmented surface is significantly higher compared to the smooth surface. These results indicate that the tunnel structure developed on the surface is found to significantly enhance the heat transfer performance of the test section. The experimental investigation carried by Das et al. [43] on similar type bidirectional tunnel geometry showed 260 % enhancement in the heat transfer performance of the structured surface.

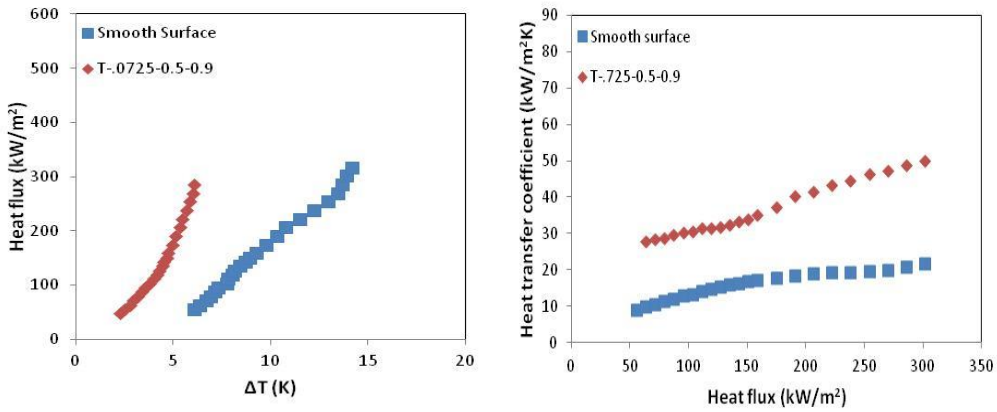

(a) (b)

Figure 2.5: (a) Comparison boiling curve for a smooth surface and T-0.725-0.5-0.9 (b) Comparison heat transfer coefficient for a smooth surface and T-0.725-0.5-0.9

The comparison of pool boiling curve for smooth and four orthogonally cut tunnel structured surfaces are shown in Fig. 2.6 (a). A considerable decrease in incipient superheat values was observed for all the structured surfaces. The reduction in the incipient wall superheat values indicates the presence of a large number of active nucleation sites promoting the generation of vapor bubbles and enhancing heat transfer performance. Many studies on pool boiling involving various roughened surfaces [18-25], surface structures [26-39], porous coated surfaces [68-73] suggested that the altered surface characteristics developed a large number of cavities on the test surface.

These cavities act as active vapor traps and promote rapid growth of the bubble. The existence of a large number of such active vapor traps on the surface helps in better nucleation and enhances the liquid-vapor movement on the surface enhancing heat transfer performance of the test surface. The complex two phase hydrodynamics is involved in such geometries; separate pathways are developed in these geometries for liquid and vapor transport. Liquid enters at random locations and vapor in bubble form ejects from different locations. This process develops strong convection on the boiling surface and enhances the heat transfer performance.

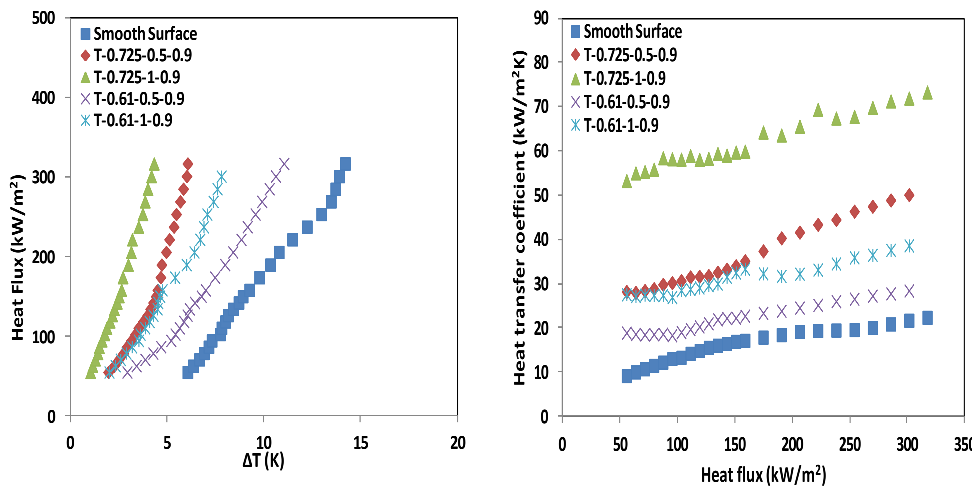

(a) (b)

Figure 2.6: (a) Comparison of heat flux versus wall superheat with water as pool liquid (b) Comparison of heat transfer coefficient versus heat flux with water as pool liquid

The comparison of boiling curve for surface T-0.725-0.5-0.9 and T-0.61-0.5-0.9 indicates that the surface with smaller tunnel width possesses higher wall superheat values compared to the surface with a larger tunnel width. This indicates that the reduction in the tunnel width adversely affects the heat transfer performance of the structured surface. The comparisons of structured surface T-0.725-0.5-0.9 with T-0.725-1-0.9 and T-0.61-0.5-0.9 with T-0.61-1-0.9 exhibits better heat transfer performance with the increase in the tunnel depth. A leftward shift in a boiling curve is observed for surfaces with the increase in tunnel depth for various tunnel width.

The comparison of heat transfer coefficients for various structured surfaces is shown in Fig. 2.6 (b). It is observed that the surface (T-0.725-1-0.9) with higher tunnel depth and higher tunnel width exhibits better heat transfer performance compared to other surfaces. The heat transfer coefficient for T-0.725-1-0.9 is found to be 250 % higher compared to the smooth surface. While the heat transfer coefficient for the surface T-0.725-1-0.9 is found to be 40 % higher compared to the surface T-0.725-0.5-0.9. Also, the heat transfer coefficient for the surface T-0.61-1-0.9 is found to be 35 % higher compared to the surface T-0.61-0.5-0.9. It may be noted that the heat transfer performance decreases because of the decrease in tunnel width. All structured surfaces exhibit better heat transfer performance compared to the polished smooth surface. These results indicate that the proposed orthogonally intersecting tunnel structure not only increases the surface area with numerous active nucleation sites but also develops a better liquid-vapor transport over the test surface resulting in a multifold increase in the heat transfer coefficient values. Here, the efforts have also been made to study the heat transfer performance of these intersecting structures by using isopropyl alcohol as pool liquid. The test results have shown a considerable decrease in the wall superheat, indicating that the tunnel structure provided better heat transfer performance with different pool liquid as well (Fig. 2.7 a).

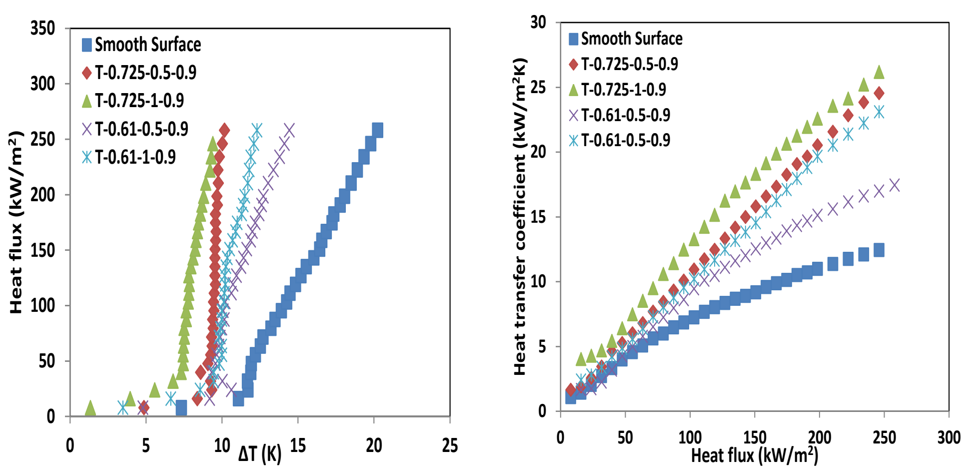

(a) (b)

Figure 2.7: (a) Comparison of heat flux versus wall superheat with isopropyl alcohol as pool liquid (b) Comparison of heat transfer coefficient versus heat flux with isopropyl alcohol as pool liquid

A similar shift in pool boiling curve for isopropyl alcohol is observed as was observed in the case of water. The comparison of the boiling curve for surface T-0.725-0.5-0.9 and T-0.61-0.5-0.9 is shown in Fig. 2.7 (a). A higher wall superheat values are obtained for the surfaces with smaller tunnel width. This indicates that reduction in tunnel width affects the heat transfer performance for the case of isopropyl alcohol as well. However, the variation in the depth of the structured surface has little influence on the pool boiling curve in case of isopropyl alcohol as a pool liquid (Fig. 2.7 a). The comparison of the heat transfer coefficient with supplied heat flux for various structured surfaces with isopropyl alcohol as pool liquid is shown in Fig. 2.7 (b). The results indicate significant enhancement in heat transfer coefficient of the structured surface compared to a smooth surface for different pool liquid as well. It is observed that the surface (T-0.725-0.5-0.9) with higher tunnel depth and higher tunnel width exhibits better heat transfer performance compared to other surfaces. The heat transfer coefficient for the surface T-0.725-1-0.9 is found to be 100 % higher compared to the smooth surface, whereas a marginal increase in heat transfer coefficient is observed when compared to T-0.725-0.5-0.9 surface with lower tunnel depth. It may be noted that the decrease in heat transfer coefficient values is also observed in the case of isopropyl alcohol, with the decrease in the tunnel width.

The performance of various structured surfaces with two different pool liquids such as water and isopropyl alcohol for different heat inputs are shown in Fig. 2.8 (a) and Fig. 2.8 (b), respectively. It may be noted that for different heat fluxes, the variation in the depth of the structured surface exhibits significant improvement in heat transfer performance with water compared to isopropyl alcohol. The enhancement in heat transfer coefficient for the structure (T-0.725-1-0.9) compared to the structure (T-0.725-0.5-0.9) is found to be 85 %, 75 %, and 60 % for various input heat fluxes of 103 kW/m^2, 150 kW/m^2 and 222 kW/m^2, respectively. While, in case of isopropyl alcohol as the pool liquid, the heat transfer enhancement of structure (T-0.725-1-0.9) compared to the structure (T-0.725-0.5-0.9) is found to be 21 %, 15 %, and 6 % for several supplied heat flux values of 103 kW/m^2, 150 kW/m^2 and 222 kW/m^2, respectively. This indicates that the enhancement in heat transfer coefficient because of change in depth exhibits better thermal performance with water compared to isopropyl alcohol as pool liquid. This trend is observed for other structures as well and shown in Fig. 2.8 (a,b).

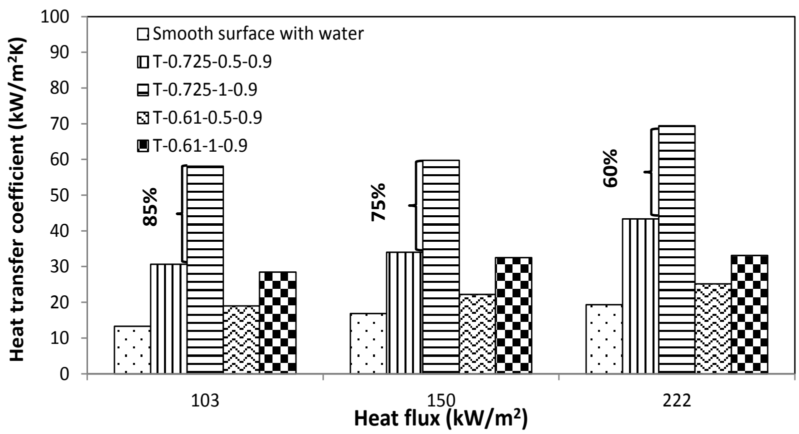

(a)

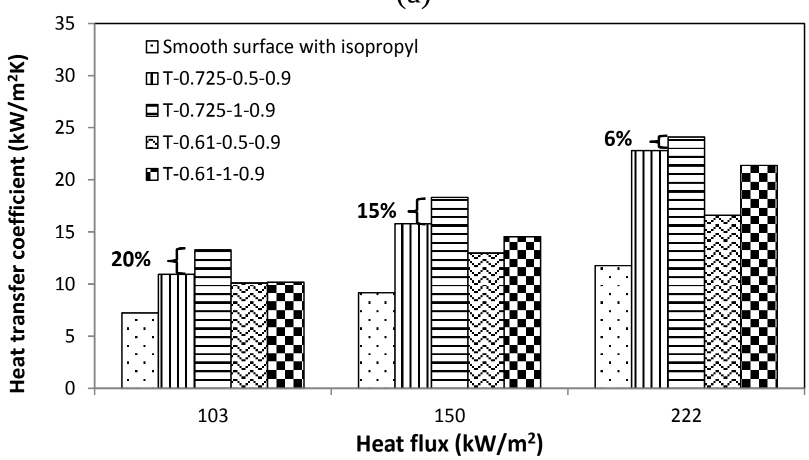

(b)

Figure 2.8: Comparisons of heat transfer coefficient over the structured surface with (a) Water (b) Isopropyl alcohol

2.3.2 Boiling mechanisms

Here, an effort has been made to propose the boiling mechanism in the structured surfaces. The liquid is found to enter the intersecting tunnel geometry at random locations and vapor in the form of bubbles ejects from

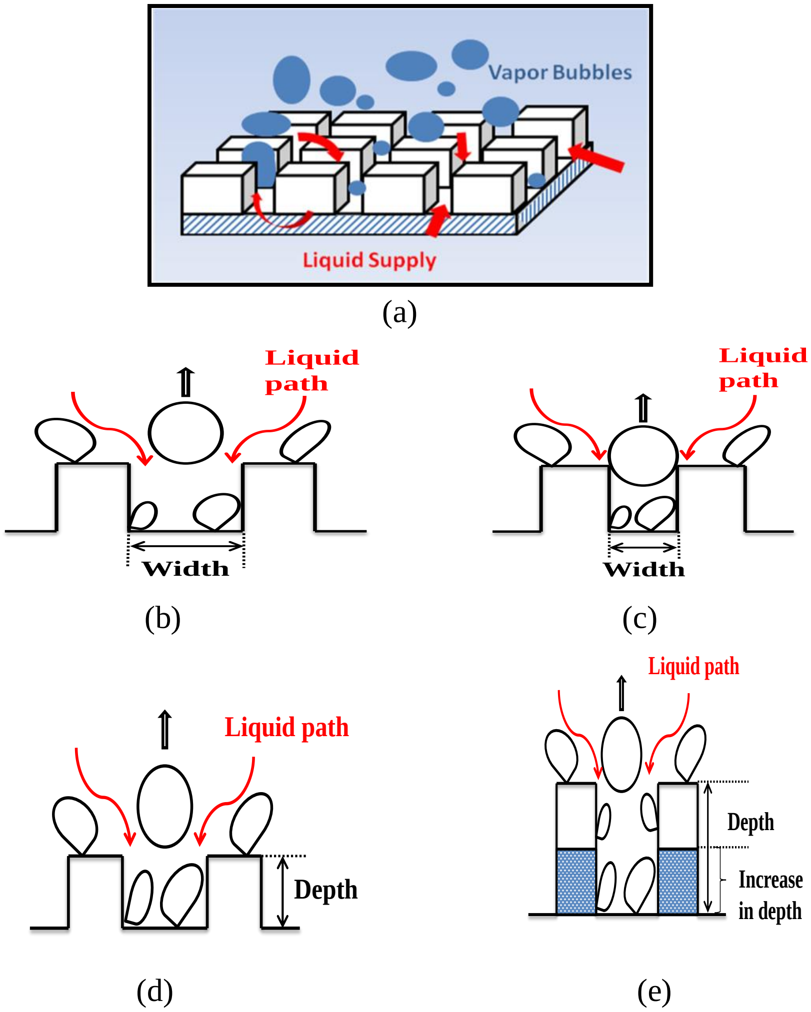

Figure 2.9: (a) Boiling mechanism over structured surface (b) Representation of Bubble growth on the surface with 0.725 mm width (c) Representation of Bubble growth on the surface with 0.61 mm width (d, e) Representation of Bubble growth on the surface with 0.5 mm and 1 mm depth

different locations on the tunnel surface as depicted in Fig. 2.9 (a). This bubble and liquid movement over the exposed surface develops strong free convection resulting in the increases in the heat transfer performance of the surface. Also, the intersecting tunnel geometry develops a square network for transportation of liquid. This provides a constant liquid supply to active nucleation sites on the surface and delays the dry out condition for the nucleation sites, leading to enhancement in the heat transfer performance. It was observed that the width of the tunnel plays an important role in heat transfer performance. The deterioration in heat transfer performance was observed with a reduction in the width of surface for both the fluids such as water and isopropyl alcohol. The reduction in heat transfer performance with width as observed in Fig. 2.8 (a,b), may be due to various reasons.

First, the bubble growth is obstructed because of less width of the tunnel. Also, with the progress of time, as more bubbles are formed, they do not find sufficient space to escape from the tunnel. In addition to this, the liquid supply is obstructed because of the counter flow of liquid and vapors bubble in the narrow channel of the structure and is shown in Fig. 2.9 (b). Also, in the case of reduced tunnel width, the liquid flow suffers resistance because of the merging of bubbles and the growth of larger vapor bubbles. While, in case of the structure with a larger width, the resistance between the inward liquid flow and upward moving vapor bubbles is less resulting in enhanced convection and better heat transfer performance and is shown in Fig. 2.9 (c). It may be noted that the structure with larger depth provides better heat transfer performance. This may be due to the fact that, with the increase in depth, the heat transfer area increases (Fig. 2.9 d-e) and result in the increase in active nucleation sites, leading to an increase in heat transfer performance.

The test results indicate that the structured surfaces developed by using wire-EDM machining process exhibit enhanced heat transfer performance compared to the smooth surface. It may be noted that nano sized porous coating on the surface exhibits significant heat transfer enhancement [68-73]. However, limited studies are available that report the combination of structured geometry developed by wire-EDM with nano sized porous coating on the surface. In case of such geometries, the structured surface developed by a wire-EDM process can provide higher surface area, better liquid transport network. While the nano-coating on the structured surface can provide numerous nucleation sites, which may result in better heat transfer. Such combined geometries can be used in future for boiling heat transfer enhancement.

2.4 Concluding remarks

Here, an experimental investigation has been carried out to investigate the nucleate boiling heat transfer performance of various structured surfaces developed by using wire-EDM machining method. The heat transfer performance of four different structured geometries with two different pool liquids such as water and isopropyl alcohol are studied in this investigation. Tests are carried for varying heat flux input in the range of 0-300 kW/m^2 and 0-250 kW/m^2 for water and isopropyl alcohol, respectively. The enhancement in heat transfer because of change in depth/width was found to be significant for water as pool liquid. While no significant enhancement in heat transfer due to change in width/depth is noticed for isopropyl alcohol. A multifold enhancement in heat transfer coefficient values ranging up to 250 % was observed on the structured surfaces compared to the smooth surface, indicating that the introduction of such structured geometries helps in the enhancement of heat transfer performance. The enhancement was observed in both pool liquids, though the percentage enhancement in case of isopropyl alcohol is less compared to the water. Efforts have been made to highlight the heat transfer mechanism of structured surfaces. Introduction of such structure geometries on the surface provides additional pathways for liquid vapor interaction and delays the dry out of nucleation sites. This may be one of the reasons for enhancement in heat transfer.

Chapter 3

Enhancement of nucleate pool boiling heat transfer performance by using a novel nanosecond laser processing fabrication method

3.1 General background

The multiscale functionalized surfaces, developed by using micro/nano technology, can promote superior heat transfer performance because of the higher rate of energy conversion between the wall and adjacent liquid. Various advanced fabrication techniques have been employed to develop micro and nanostructured surfaces to enhance pool boiling heat transfer. These include various coating techniques like vapor deposition, sputtering, atomic layer deposition (ALD), pulsed laser deposition (PLD), spin coating, painting, chemical processing and MEMS/NEMS techniques [46-67]. These techniques have enabled researchers to fabricate compact and complex surface structures. These methods are either expensive or find difficulty for a larger surface area. Some of these methods involve bonding between two different materials which may fail in the case of different heat loading conditions. Therefore, efforts have been made to use the laser ablation process to develop surfaces with several multiscale features. This technique enables the formation of self-organized micro/nanostructures on the surface and promotes heat transfer performance. This is a one step process and capable of processing any size of area with precision. However, limited studies are available that report the effect of various laser type and laser power on the physical characteristics of the test surface and their boiling heat transfer performance. The objective of the present study is to investigate the heat transfer performance of copper multiscale functionalized surfaces fabricated by employing the nanosecond laser surface process (NLSP). This technique utilizes an ultra-fast laser to ablate the copper surface.

Present chapter reports the experimental investigation of pool boiling heat transfer on multiscale functionalized copper surfaces. Multiscale functionalized surfaces are fabricated by employing the nanosecond laser surface processing (NLSP) technique. The laser (Nd:YAG) used in this study to fabricate different multiscale functionalized surfaces produces laser light with wavelengths of 1064 nm, 355 nm and 532 nm with varying laser powers. Two different fluids such as water and acetone are used to estimate the boiling heat transfer performance. Tests are performed at atmospheric pressure and saturated pool boiling condition with heat flux varying between 0-330 kW/m^2. The enhancement in heat transfer coefficient of laser processed surfaces is compared with reference smooth surface. Also, efforts have been made to study the physical characteristics of the test sections.

3.2 Fabrication of experimental test facility and test sections

A test facility has been developed to study the pool boiling heat transfer performance of laser processed surfaces. The details of the test facility, test procedure and data reduction are elaborated in the previous chapter (Section 2.2.1, Ch. 2) and therefore not reported here. The different multiscale functionalized surfaces are fabricated by employing the nanosecond laser surface processing technique. The details of this technique are elaborated below.

3.2.1 Test surface fabrication by laser processing

Different types of pulsed laser are available based on pulse duration such as nanosecond, femtosecond, picosecond lasers. The effect of multiscale surface structure, fabricated by using nanosecond laser on the heat transfer performance of the copper test section is investigated in this study. Various physical surface characteristics such as surface roughness and surface microstructure are found to depend on laser power and incident laser pulses. Fig. 3.1 (a) represents the schematic of the nanosecond laser surface processing setup used to develop microstructure on copper test sections. Here, a Neodymium-Doped Yttrium Aluminum Garnet (Nd:YAG) laser (Quanta-Ray ND, Spectra Physics) capable of producing 5-8 nanosecond pulses with wavelengths of 1064 nm, 532 nm and 355 nm at a repetition rate of 10 Hz was used develop microstructure on copper test surfaces. The Nd:YAG laser power was controlled by using a Q-switch which consists of a pockels cell, polarizer, and a quarter wave-plate. The copper test sections were mounted on a 3D translation stage which is controlled by a computer program. A combination of prism and lens was used to focus the laser beam on the copper test section. An area larger than the spot size of the laser beam was processed by moving the copper test section through the laser beam path. Identical translation speed of the 3D stage was maintained for all the test sections in order to ensure that the incident pulses are same for all the test sections during laser processing.

3.2.2 Laser ablation

Efforts have been made by various authors to study the mechanism of microstructure formation on the metallic surface due to direct laser ablation [91-97]. In this process, the laser beam produced by a laser is focused on the metallic surface using a lens. A laser beam is a narrow, intense beam of light produced by a laser. The laser beam consists of photons. It is argued when the laser beam strikes a metal surface, a high amount of heat is generated as a result of photon electron interaction and it develops a temperature field in the test specimen. Depending upon the temperature achieved, the melting of material takes place. Subsequently, it either evaporates or transfers to a plasma state. The 3D stage is moved continuously during the laser ablation process, which shifts the laser processing zone to the next point (Fig. 3.1b). The shifting of laser processing zone exposes the melt pool developed at the previous point to surrounding cooler temperature. The large temperature difference between the melt pool and surrounding leads to rapid cooling of molten metal on

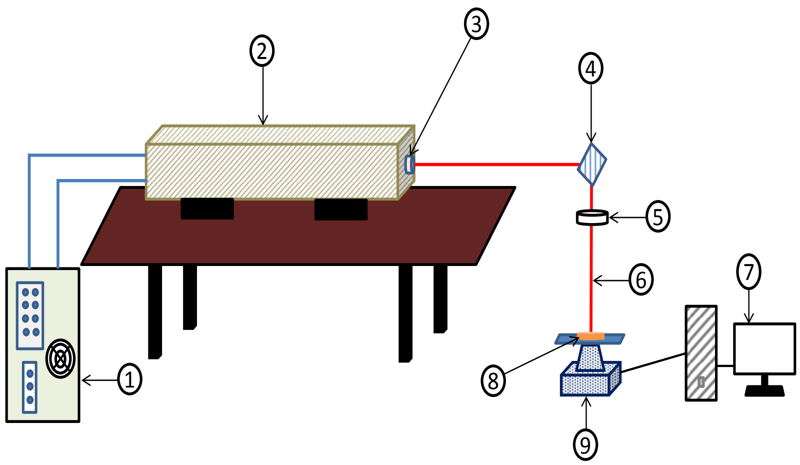

1	Laser power supply and control	2	Laser enclosure
3	Laser head	4	Prism
5	Lense	6	Laser beam
7	Computer	8	Test section
9	Translation stage		

(a)

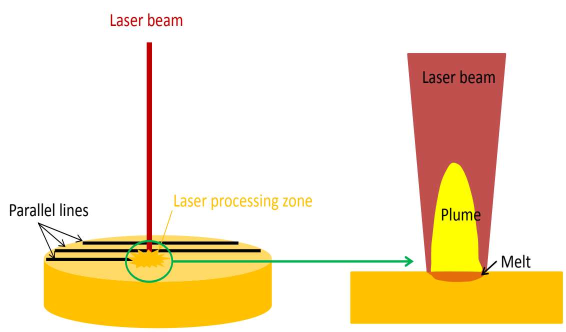

(b)

Figure 3.1: (a) Schematic diagram of nanosecond laser surface processing (NLSP) setup used in the present investigation (b) Schematic of the laser ablation process

the substrate. This process is very fast and the temperature difference between the molten metal with the surrounding is very high resulting in rapid solidification of molten material. This melting, plasma formation and solidification process develop microstructure on the surface. These microstructures consist of peaks, micropores and micro fins. In the present investigation, a parallel line laser scanning pattern was selected for laser processing of the copper test sections. This is done to ensure that the nucleation sites developed in microstructure act independently. Earlier studies report that the presence of such surface structures helps in the formation of a large number of nucleation sites resulting in the enhancement of boiling heat transfer performance of the surface [46-67].

3.2.3 Characterization of laser processed surface

Initially, microstructure on three copper test sections was developed using 1064 nm laser wavelength by varying laser power from 4 to 4.6 W and the heat transfer performance of this surfaces were studied using water and acetone as pool liquid. Four more test surfaces were developed by using two different laser wavelengths (532 nm and 355 nm) with two different laser powers in each wavelength to study the effect of microstructures developed using different laser wavelengths on boiling heat transfer performance.

Table 3.1 summarizes various physical characteristics of the laser processed copper test sections used in the current experimental investigation with the different laser parameters. It is evident from the literature [98-99] that different laser processing parameters (laser power and laser wavelength) affect the microstructure development process on the surface. We have a Neodymium-Doped Yttrium Aluminum Garnet (Nd:YAG) laser (Quanta-Ray, Spectra Physics) system at IIT Indore. The laser system is capable of producing 5-8 nanosecond pulses with wavelengths of 1064 nm, 532 nm and 355 nm at a repetition rate of 10 Hz. The Nd:YAG laser power was controlled by using a Q-switch which consists of a pockels cell, polarizer, and a quarter wave-plate. Based on configuration of laser system available at IIT Indore and taking a cue from other studies, various parameters are selected in the present investigation. Fig. 3.2 (a) depicts the photographic view, stereo microscopic images (EZ4HD, Leica), scanning electron microscope (SEM) (Supra55, Zeiss) images. The SEM images in Fig. 3.2 (a) depict the presence of microstructure and pores on the test section surface. The microstructure developed on the surface is found to be dependent on different laser para-

Test section	Photographic view	Microscope images	SEM images
FS1	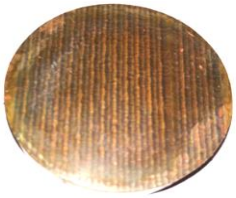	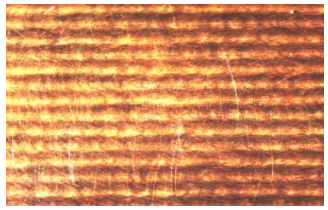	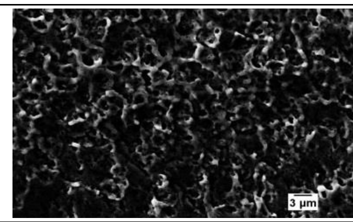
FS2	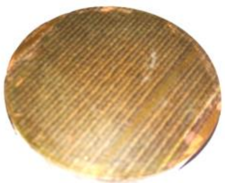	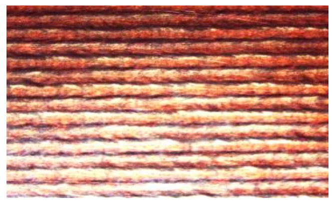	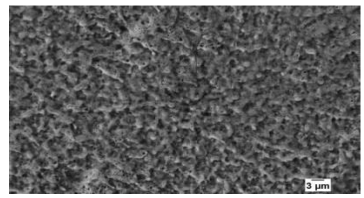
FS3	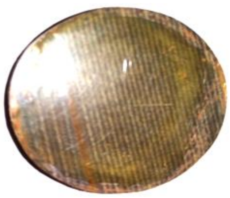	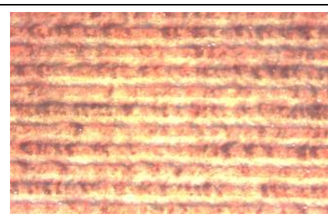	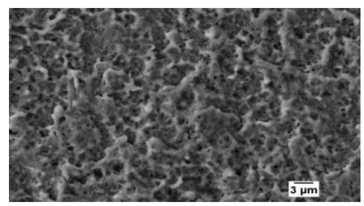
FS4	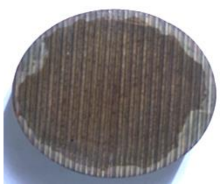	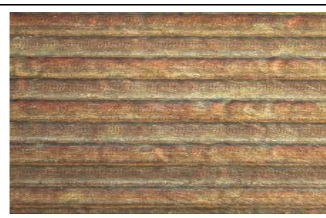	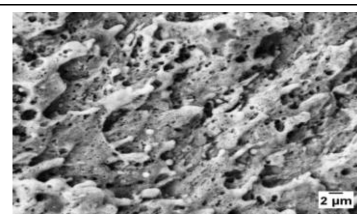
FS5	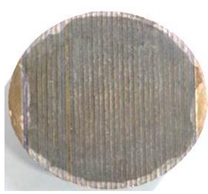	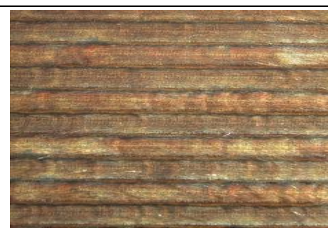	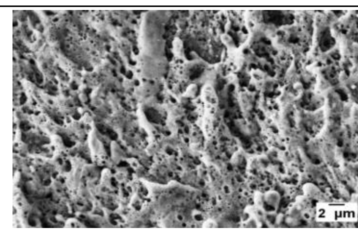
FS6		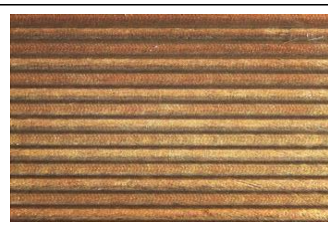	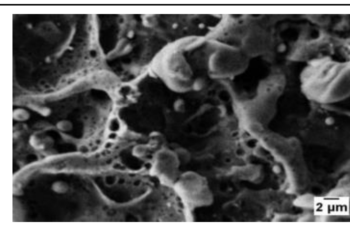
FS7	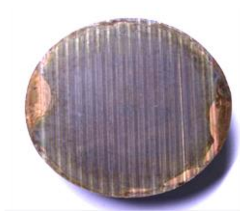	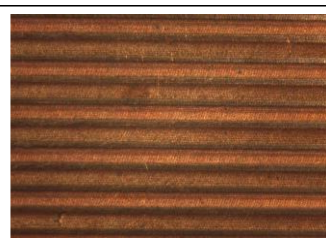	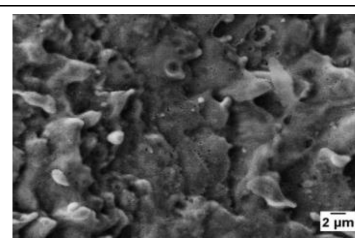

(a)

Test section	3D topography images	Test section	3D topography images
FS1	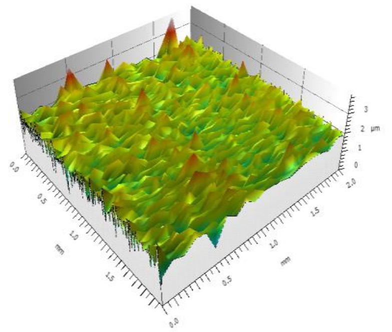	FS4	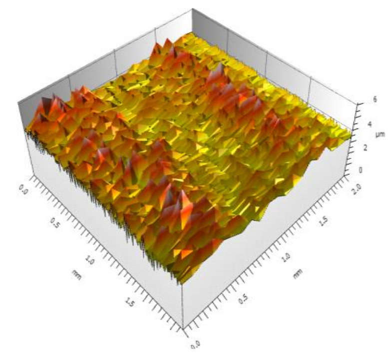
FS2	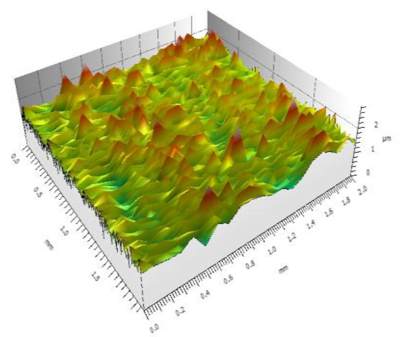	FS5	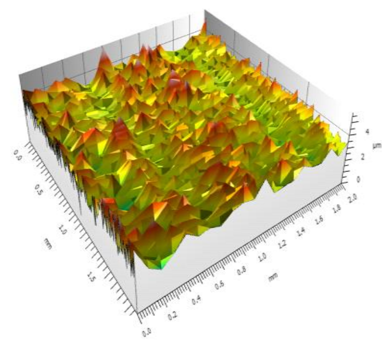
FS3	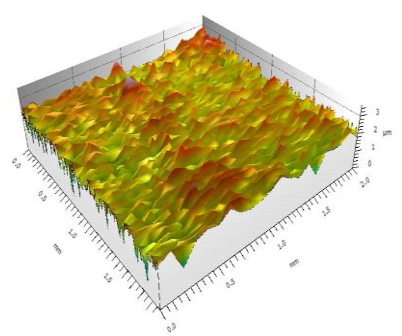	FS6	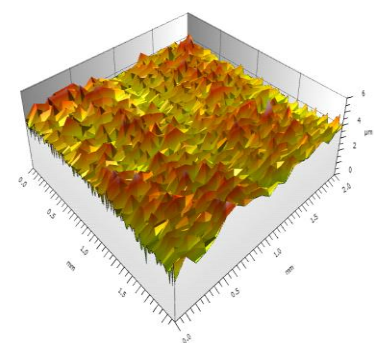
FS7	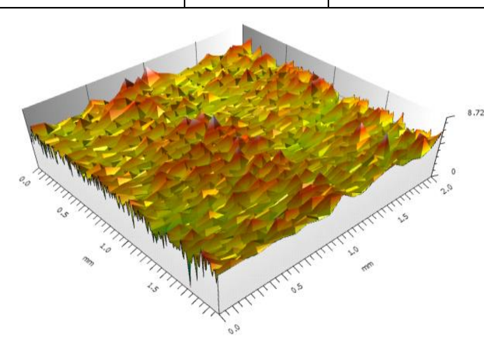		

(b)

Figure 3.2: (a) Microscopic and SEM images of laser processed test sections (b) Topography images (3D) of laser processed test sections

-meters. A variation in microstructure involving a number of pores and micro fin structure was observed in SEM images of test surfaces that are processed at different laser power and laser wavelengths. Fig. 3.2 (b) depicts the 3D topography images (MarSurf LD 130) showing microroughness profile of the functionalized test sections. The 3D profile of the microstructure is obtained by moving probe of the profilometer on the laser processed region of test sections. The movement of the probe is recorded by software (MarSurf) which generates a 3D profile based on probe movement. The presence of a large number of irregular peak and valleys can be observed in these 3D plots. All of the laser processed test sections possess roughness values in the micron scale. The surface roughness values of test sections for different laser power and wavelength are shown in Table 3.1.

Table 3.1: Surface characteristics of test sections

Surface	**Specification**	**Laser Power (W)**	**Laser Wavelength (nm)**	**Surface Roughness (µm)**	**HTC (kW/m^2) at q″=253 W/m^{2}K**	**% Increase in HTC compared to smooth surface per watt of corresponding laser power**
Test Section 1	FS1	4.6	1064	0.271	37698	20 %
Test Section 2	FS2	4.2	1064	0.237	27157	9 %
Test Section 3	FS3	4.0	1064	0.290	22624	3.8 %
Test Section 4	FS4	1.8	532	0.496	29888	28 %
Test Section 5	FS5	1.6	532	0.427	27683	25 %
Test Section 6	FS6	1.0	355	0.445	31813	62 %
Test Section 7	FS7	0.8	355	0.411	26925	46 %
Test Section 8	Smooth surface	--	--	0.07	19574	--

3.3 Results and Discussion

Initially, pool boiling heat transfer performance of three nanosecond laser processed micro structured copper surfaces namely, FS1, FS2 and FS3 are studied. These test surfaces are processed at different laser power with 1064 nm wavelength. Experiments were conducted on these test sections at saturated pool boiling condition and atmospheric pressure. Two different pool liquids such as water and acetone are used in experiments. Attempts have been made to assess the effect of laser power on the heat transfer performance of the laser processed copper surface with water and acetone. Following the procedure as discussed in the previous section and Appendix I, the uncertainty for nanosecond pulsed laser processed surfaces were evaluated in this chapter. The maximum uncertainty was found on surface FS4. The maimum uncertainty in the estimated results for heat flux (q'') and heat transfer coefficient (h) was found to be 1.85 % and 8.4%, respectively. The microstructured surfaces are useful in the miniaturized high heat flux cooling systems to enhance heat transfer performance. Many times, it is difficult to use larger size heat sinks during cooling of miniaturized electronic devices. That restricts the use of conventional enhanced macroscale surface structures. The details of the experimental test results are elaborated below.

3.3.1 Effect of laser power with 1064 nm wavelength on heat transfer performance

Variation of heat flux with wall superheat for both laser processed and polished copper surface with water as pool liquid is shown in Fig. 3.3 (a). The reduction in local maximum wall superheat corresponding to the input heat flux values vary among various laser processed surface. For the wall heat flux value of 285 kW/m^2, the maximum reduction in wall superheat of various test sections FS1, FS2 and FS3 was found to be 48 %, 26 % and 10 % respectively, compared to the smooth surface. This indicates that the processed surface exhibit better heat transfer performance compared to the smooth polished surface. This may be due to the increase in the number of active nucleation sites which are developed on the laser processed surface as a result of microstructure formation compared to the smooth polished surface. These surfaces have numerous active nucleation sites that are being activated with increasing input heat flux and promotes nucleate boiling, resulting in a reduction in local wall superheat values. A leftward shift in the boiling curve was observed for all the laser processed test surfaces. This indicates an enhancement in heat transfer coefficient which allows a large amount of heat transfer at relatively lower surface temperature.

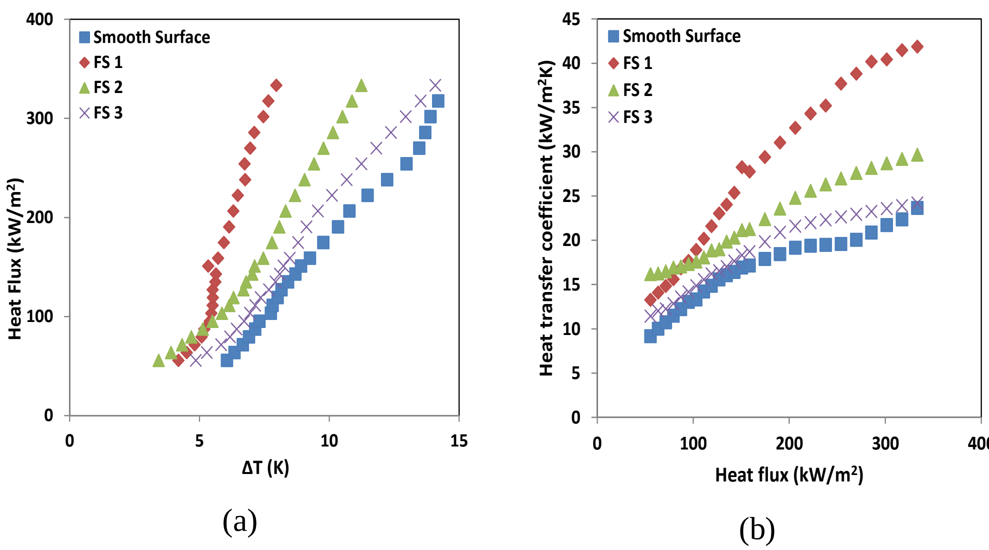

Figure 3.3: (a) Variation of heat flux with wall superheat for laser processed and smooth surface with water as pool liquid (b) Variation of heat transfer coefficient with heat flux for laser processed and smooth surface with water as pool liquid

The variation of heat transfer coefficient with heat flux values for both laser processed and the smooth polished surface has been shown in Fig. 3.3 (b). It is observed that the heat transfer coefficient values are higher for all the laser processed surfaces compared to smooth polished surfaces. For a given input heat flux value of 285 kW/m^2 the increases in heat transfer coefficient were found to be 92 %, 37 % and 11 % for FS1, FS2 and FS3, respectively compared to the smooth surface. It may be noted that higher laser power is used to prepare FS1 compared to FS2 and FS3. The heat transfer performance of the laser processed surface with higher laser power exhibits better heat transfer performance. At higher laser power, melting of more material takes place and after solidification dense mound structures are formed on the surface. The SEM image of FS1 (Fig. 3.2 a) shows the mound structures are densely packed and narrow channels/cracks are formed between microstructures. Apart from the generation of active nucleation sites, these microstructures allow capillary wicking effects and help to replenish the heater surface with cold fluid after the local evaporation takes place. It is noticed from the SEM images that the pore size of the microstructures reduces from FS1 to FS3. This may be due to the reduction in laser power, used during fabrication of test surfaces.

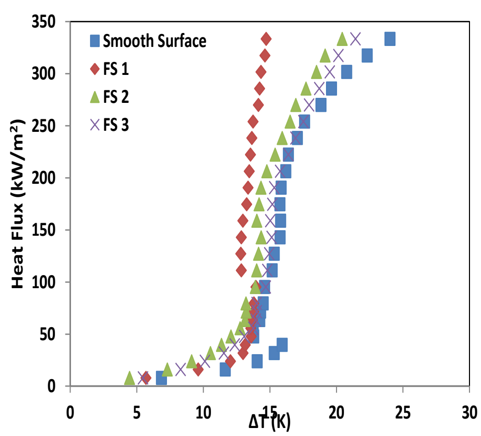

(a)

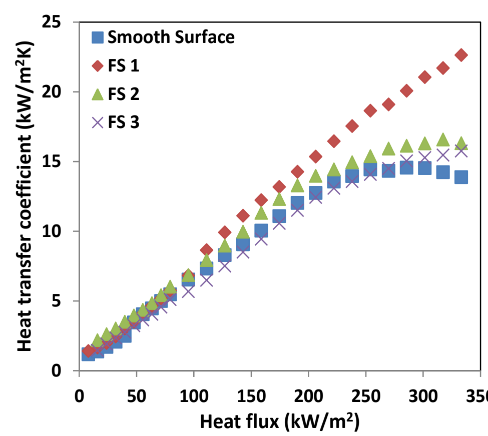

(b)

Figure 3.4: (a) Variation of heat flux with wall superheat for laser processed and smooth surface with acetone as pool liquid (b) Variation of heat transfer coefficient with heat flux for laser processed and smooth surface with acetone as pool liquid

In the present investigation, an attempt has been made to study the heat transfer performance of laser ablated test section with acetone as pool liquid. The test results with acetone as the pool liquid exhibit a marginal increase in the heat transfer performance of the laser processed test surface over a smooth polished test surface. Variation of input heat flux with wall superheat for both laser processed and smooth polished copper surface with acetone is shown in Fig. 3.4 (a). The local maximum reduction in wall superheat values corresponding to the input heat flux is found to vary among various laser processed surface.

The reduction in wall superheat of various test sections FS1, FS2, FS3 was found to be 27 %, 9 % and 4 %, respectively, compared to the smooth surface. This indicates the laser processed surface exhibits better heat transfer performance compared to the smooth polished surface. This may be due to the numerous nucleation sites developed on the laser processed test surface. The variation of heat transfer coefficient with heat flux values for both laser processed and the smooth polished surface has been shown in Fig. 3.4 (b). It is observed that the heat transfer coefficient values are higher for all the laser processed surfaces compared to smooth polished surface. For a given input heat flux value of 285 kW/m^2, the increase in heat transfer coefficient was found to be 37%, 10 % and 4 % for FS1, FS2 and FS3, respectively compared to the smooth surface. In both the pool liquids, FS1 exhibits best heat transfer performance compared to the smooth, FS2 and FS3 test surfaces. The heat transfer performance of the laser processed surface is found to be better compared to the smooth surface for different pool liquids and various heat flux values. This may be due to the fact that the microstructures developed on the test surface during laser processing have developed more active nucleation sites. Also, the variation of nanosecond pulsed laser power affects the restructuring of the metallic top layer.

3.3.2 Effect of laser wavelength on heat transfer performance

Here, efforts have been made to study the effect of laser wavelength on microstructure formation and on the boiling heat transfer performance. Materials have different laser light absorptivity in different laser wavelengths and the heat generated during laser processing is dependent on laser light absorption. Here, four different test sections (FS4, FS5, FS6, FS7) are developed with different laser wavelength and laser power (Table 3.1). Tests are conducted at saturation temperature and atmospheric pressure condition by using water as pool liquid.

The pool boiling curve for six nanosecond laser surface processed surfaces and smooth surface are shown in Fig. 3.5 (a). A substantial leftward shift was observed in the boiling curve for nanosecond laser processed surfaces compared to the smooth surface. This leftward shift in pool boiling curve for nanosecond laser processed surface indicates the reduction in the wall superheat values for laser processed test surface. The reduction in wall superheat temperature values was observed on all of the nanosecond laser processed surfaces compared to smooth surfaces.

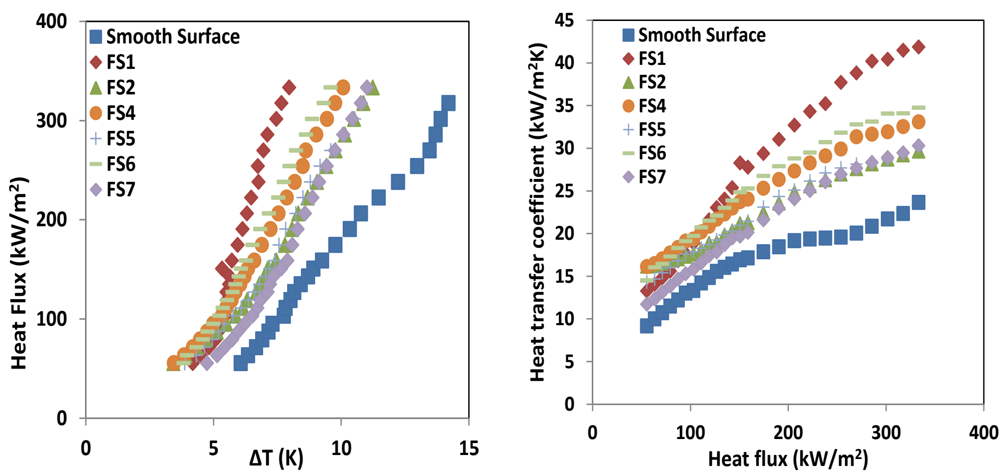

(a) (b)

Figure 3.5: (a) Comparison of heat flux versus wall superheat with water as pool liquid (b) Comparison of heat transfer coefficient versus heat flux with water as pool liquid

Fig. 3.5 (b) depicts the variation in heat transfer coefficients with supplied heat flux values for a smooth surface and nanosecond laser processed surfaces. The laser processed test surface FS1 exhibits better heat transfer performance compared to other laser processed test surfaces

(FS2, FS3, FS4, FS5, and FS6). The enhancement in heat transfer coefficient value for FS1 was found to vary within 41 % to 93 % higher compared to the smooth surface. The test surface (FS1) has been developed with 4.6 W laser power and 1064 nm wavelength. It is argued that higher laser power develops a high temperature on the test surface. This results in the development of a larger melt pool and microstructure in a large volume of material. While the test surface (FS2) developed with 4.2 W laser power and 1064 nm wavelength exhibits reduced heat transfer coefficient values compared to test surface FS1. All the nanosecond laser processed surfaces demonstrate better heat transfer performance compared to the reference smooth surface.

The enhancement in heat transfer performance of nanosecond laser processed surfaces is attributed to the formation of microstructure in the form of pores and micro fins during the laser ablation process. This is due to rapid melting and fast cooling of surface material in the top surface layer. The formation of pores and micro fins structure on these surfaces may act as active nucleation sites resulting in the enhancement in heat transfer coefficient values compared to the smooth surface.

3.3.3 Effect of variation in laser wavelength and laser power

Here, an effort has been made to study the effect of microstructure developed using different laser wavelength and laser power on heat transfer performance of copper test sections. It is important to note that the laser ablation process depends on the amount of laser light absorption. It can be observed from SEM images in Fig. 3.2 (a) that different microstructure was developed on copper test sections with different wavelengths. A comparison of heat transfer coefficient for different nanosecond laser processed test surfaces developed by varying laser wavelength and laser power for different input heat flux values is presented in Fig. 3.6. The heat transfer performances of laser processed test surfaces are compared with the smooth surface. For each laser wavelength, the test surfaces developed by using higher laser power yields better heat transfer performance. This may be due to the fact that at higher laser power, a large amount of heat is generated owning to higher laser pulse energy. This results in rapid melting and fast cooling of surface material developing microstructure with more nucleation sites in the form of pores. This can be observed in SEM images in Fig. 3.2 (a). Also, it was observed that, even the microstructure developed with lower laser power of 1 W and 1.8 W in 355 nm and 532 nm laser wavelength yield enhancement in heat transfer coefficient values ranging up to 60 %. This may be attributed to the higher optical absorption of laser light on the copper surface at these wavelengths. The percentage increase in HTC of test surfaces for per watt of laser power is shown in Table 1. It may be noted that the test surfaces developed at 355 and 532 nm wavelengths exhibit better enhancement for per watt of laser power.

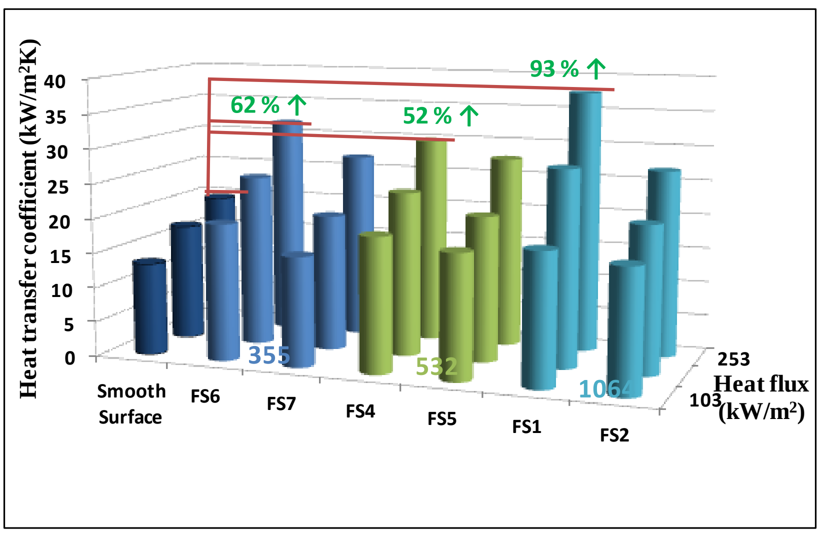

Figure 3.6: Comparison of heat transfer coefficient with different laser wavelength and laser power

3.3.4 Comparison of present test data with the results of other laser microstructured surfaces

The comparisons of present experimental results with the experimental results of Kruse et al. [98], Zupancic et al. [99], Kim et al. [103] and Jones et al. [21] is shown in Fig. 3.7. Zupancic et al. [99] used a nanosecond laser with a laser wavelength of 1064 nm to develop microstructure on the test surface.

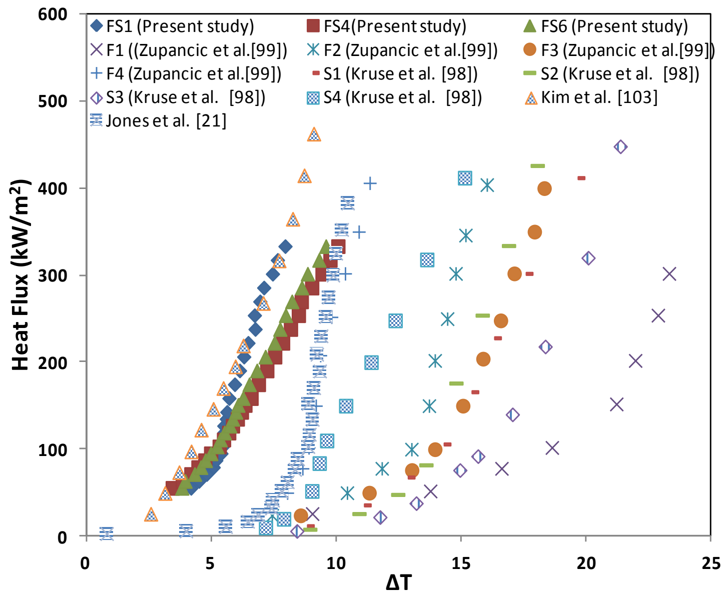

Fig. 3.7: Comparison of present test data with other test results [21, 98-99, 104]

Four different microstructured surfaces were developed using a thin stainless steel foil by varying scan line separation. They reported that laser micro structuring promotes the formation of numerous active nucleation sites. The enhancement in heat transfer coefficient of laser processed surfaces was found to be 100 % compared to the smooth surface. Kruse et al. [98] used a femtosecond laser to develop microstructure on the stainless steel surface. They developed four microstructured surfaces by varying laser fluence. It is argued that the microstructures enhance heat transfer coefficient values compared to the smooth surface. Kim et al. [104] developed microporous structures by employing the coating technique proposed by You and O'Connor [105-106] and termed as ABM coating following its various contents such as aluminum particles, brushable ceramic epoxy, and methyl ethyl ketone. The ABM coatings with the largest particle size of 17-30 μm reduce the wall superheat value by 5℃ and exhibit enhancement in heat transfer coefficient by 47 %

compared to plain surface. It is argued that the use of such coatings result in an increase in microcavities that act as active nucleation site. Jones et al. (2009) reported that the test surface developed by using EDM with 10 µm surface roughness possess more and larger cavities. The cavities were found to promote enhancement in heat transfer coefficient values. The enhancement in heat transfer coefficient is found to be 100 % compared to the smooth surface.

The present study uses Nd:YAG laser to develop various test surfaces. Present test results exhibit maximum enhancement in heat transfer coefficients values by 90 to 93 % on FS1 surface compared to the reference smooth surface. This comparison indicates that the laser processing technique is useful in developing enhanced surfaces. The microstructure developed using laser processing method helps to enhance the heat transfer coefficient values on the test surface made of different materials.

3.3.5 Proposed boiling mechanism for augmentation in heat transfer performance

Here, an attempt was made to propose the boiling mechanism responsible for the enhancement in heat transfer performance of laser processed surfaces. Based on the SEM images (Fig. 3.2 a), an attempt has been made to show the graphical representation of multiscale functionalized surfaces in Fig. 3.8 (a). The heat generated due to incident laser pulses results in the melting of the top metal surface layer. Subsequently, the rapid cooling of melt formed due to incident laser pulse leads in the formation of micro fins, pores and craters on the metal surface. Fig. 3.8 (b) represents the liquid vapor interaction on the laser processed surface. The formation of micro fins increases the available surface area. Also, the surface craters and pores spread over laser processed area act as active nucleation sites resulting in the enhancement of heat transfer performance. Also, the presence of micro fins with pores provides additional liquid pathways to nucleation sites and enhances liquid vapor interaction over the surface. This leads to a steady liquid supply to active nucleation sites and enhanced heat transfer performance.

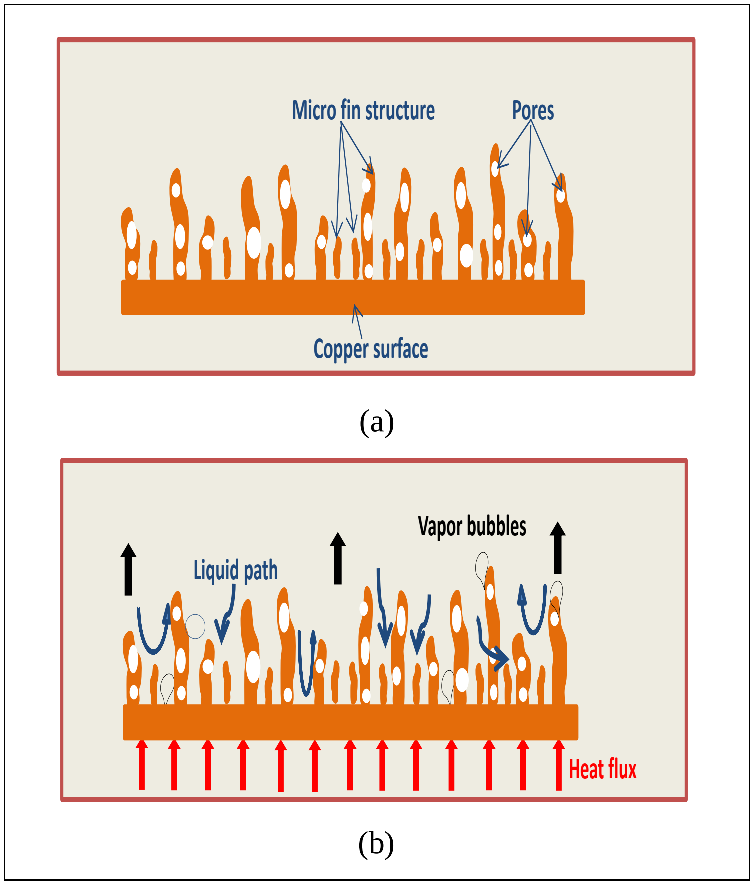

Figure 3.8: (a) Graphical representation of multiscale functionalized surfaces (b) Proposed boiling mechanism

3.4 Concluding remarks

In this chapter, experiments are performed to study the nucleate pool boiling heat transfer performance of microstructured surfaces developed by using nanosecond laser processing technique. The laser is Nd:YAG (Quanta-Ray ND, Spectra Physics) that produces 5-8 nanosecond pulses with a wavelength of 1064 nm at a repetition rate of 10 Hz.

Initially, three test surfaces are developed by using different laser powers varying within 4 W – 4.6 W for a wavelength of 1064 nm. The physical characteristics of processed surfaces are studied by using stereo microscopic images (EZ4HD, Leica), scanning electron microscope

(SEM) (Supra 55, Zeiss) images and 3D (Mahr Surf 130D) profile of the test section. Tests are conducted at atmospheric pressure and structured pool boiling condition with input heat flux varying between 0-330 kW/m^2 by using two different pool liquids (water and acetone). For both the pool liquids, the test surfaces developed at the highest laser power exhibits the highest value of heat transfer enhancement compared to the other surfaces. Also, efforts have been made to propose the boiling mechanism responsible for the enhancement in heat transfer performance of laser-processed surfaces.

Next, efforts have been made to develop laser processed surfaces for a varied range of laser wavelength (355 nm – 1064 nm) and varied laser powers. The physical characteristics of laser ablated surfaces are studied. It was observed that the variation in laser light absorptivity in different laser wavelengths affects the microstructure development on surface and their boiling heat transfer performance. The heat transfer performance of present microstructured surfaces developed by laser ablation techniques is compared with the experimental results of various microstructured surfaces used by other researchers.

Chapter 4

Nucleate boiling performance of continuous wave laser processed surfaces

4.1 General background

Over the years, numerous novel surfaces are developed by employing various fabrication techniques such as machining, polishing, coating, MEMS/NEMS. These novel surfaces were found to exhibit better heat transfer performance compared to the plain surface. However, these techniques have several limitations such as involves difficult manufacturing processes, expensive, difficult to scale up for system components, mechanical and thermal instabilities and not applicable to all materials. Efforts have been made to employ alternative techniques to develop novel surfaces. Recently, laser processing technique has been employed to develop micro/nano structure on the test surface. Laser processing technique possesses various advantages such as reproducibility, precision and less surface contamination. Laser processed surfaces were found to exhibit better heat transfer performance compared to plain surfaces. It is argued that type of laser, laser wavelength and laser fluence affect the laser ablation process and type of microstructure development on the surface. The laser processing technique is a simple one step fabrication process which can be easily employed on curved and larger surface areas. It was observed that the laser processing develops micro cavities inside the grooves that act as active nucleation sites and promotes heat transfer. However, limited studies have been made that employ laser processing technique to develop novel surface by employing different lasers, various laser power and laser wavelength to investigate the effect of micro structured surfaces on pool boiling performance.

The objective of the present study is to investigate the augmentation of boiling heat transfer of different laser processed test surfaces. Present chapter reports the nucleate pool boiling characteristics of micro structured copper surface developed by utilizing continuous wave laser. Tests were conducted at atmospheric pressure and saturated pool boiling condition by using water as pool liquid with varying heat flux values. Six different test sections are developed by varying laser power between 40-50 Watt. The heat transfer performance of surfaces developed by continuous wave laser and pulsed laser are compared in this investigation. The characterization of test surfaces is reported and present results are compared with the test results obtained by previous researchers.

4.2 Development of test facility and fabrication of test surface

A test facility has been developed to study the pool boiling heat transfer performance of laser processed surfaces. The details of the test facility, test procedure and data reduction are elaborated in the previous chapter (Section 2.2.1, Ch. 2) and therefore not reported here. The different multiscale functionalized surfaces are fabricated by employing the nanosecond laser surface processing technique. The details of this technique are elaborated below.

In this study, various channeled/grooved surfaces are developed by using laser marking machine (SCANTECH, India). Fig. 4.1 (a) depicts the schematic diagram of laser marking machine. This consists of various modules such as laser source, scan head and a computer system. Here, Ytterbium (Yb) doped continuous wave fiber laser (IPG Photonics) is used as laser source. In case of fiber laser, an optical fiber doped with the rare earth element is used as an active medium. In such a case, light is already coupled into flexible fiber and it has high optical quality with compact size. Here, a scan head (basiCube 10, Scanlab, Germany) is used to deflect laser beam in working plane. A scan head consists of a galvanometer based scanning motor with optical mirrors mounted on the shaft. It has a detector that provides a positional feedback to control board. The laser beam enters through the input scan head aperture centrally and exit from output scan head lens following two mirrors. Two mirrors in the scan head are used to deflect laser beam in both X and Y directions as per the requirement. The scan head is provided with a linear power supply of 15 volts and 3 amps. This has a focal length of 160 mm and can scan area with 100 mm in length and 100 mm in width.

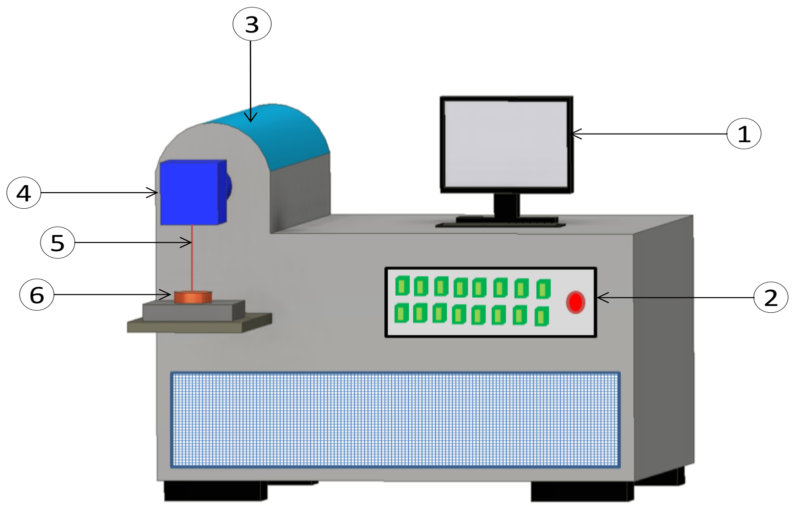

1	Desktop	2	Laser and Galvo controls
3	Laser enclosure	4	Scan head
5	Laser Beam	6	Test section

(a)

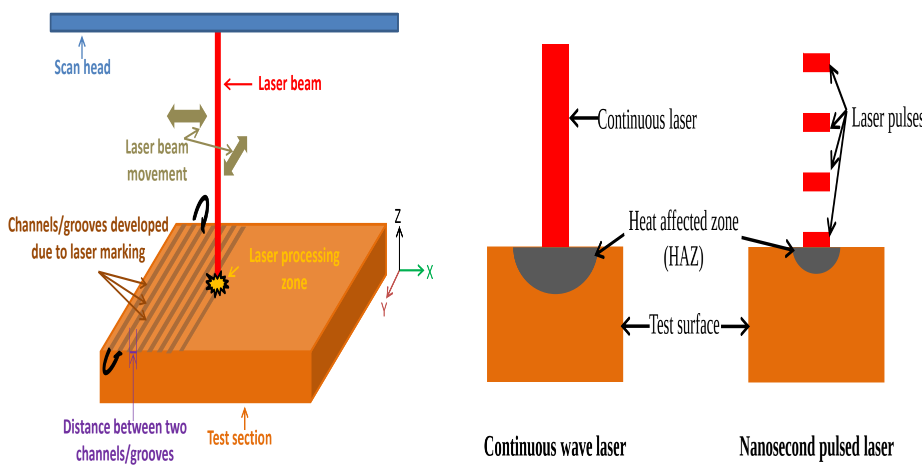

(b) (C)

Figure 4.1: (a) Schematic diagram of laser marking machine (b) Schematic representation of laser processing (c) Representation of nanosecond and continuous laser wave

The laser marking process is controlled by HPGL Scanlab software. By using this software, the user can select or draw customized geometries, with desired dimensions as per the requirement. It also allows the user to select different laser parameters as per the need. Based on the user inputs the software controls the scan head and laser to

Test section	Photo graphic view	Test section	Photo graphic view
LM-1-50-1064		LM-0.5-50-1064	
LM-1-45-1064	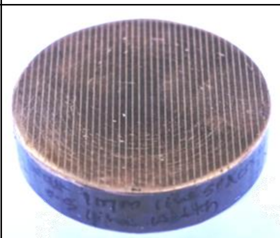	LM-0.5-45-1064	
LM-1-40-1064		LM-0.5-40-1064	

Figure 4.2: Photographic view of test surfaces

develop required geometry on the surface. Fig. 4.1 (b) depicts the laser marking process. The laser beam is precisely focused and moved on the test surface from scan head. The laser produces a laser beam that includes photons and it develops high amount of heat at the incident point due to photon electron interaction. This heat melts and evaporates metal present at incident point. Here, the laser beam is moved continuously to create parallel channels/grooves on the surface. The laser system can be classified as continuous wave and pulsed laser system. As shown in Fig.

4.1 (c) continuous electromagnetic wave is emitted in case of CW laser, whereas pulsed laser emits an electromagnetic wave consisting of a pulse train in nano, pico or femto second time interval.

Test section	SEM images	Microscope images
LM-1-50-1064	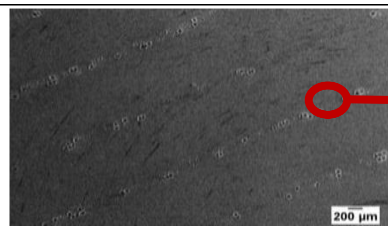	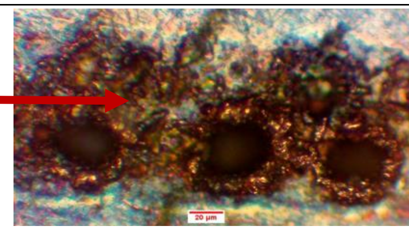
LM-1-45-1064	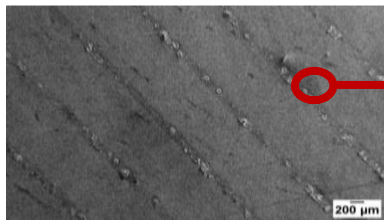	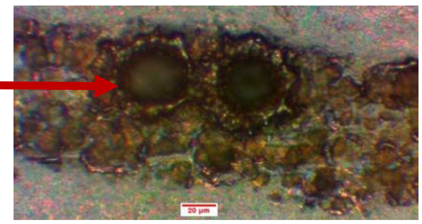
LM-1-40-1064	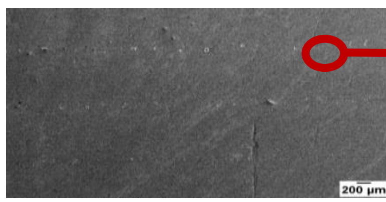	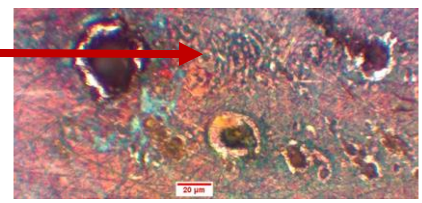
LM-0.5-50-1064		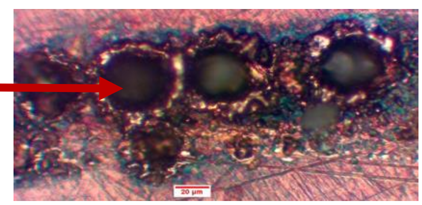
LM-0.5-45-1064		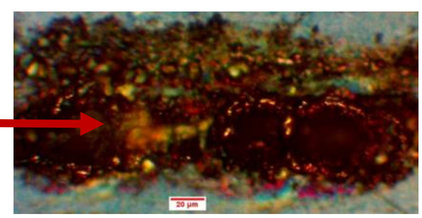
LM-0.5-40-1064	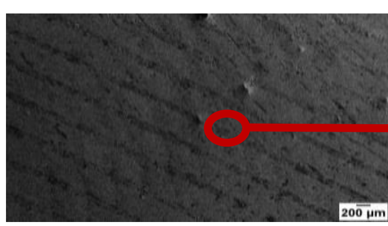	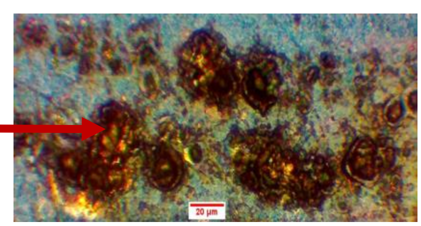

Figure 4.3: SEM and Microscopic images of test sections

Test section	**SEM images of microcavities**	
LM-1-50-1064	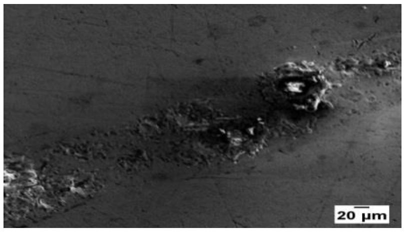	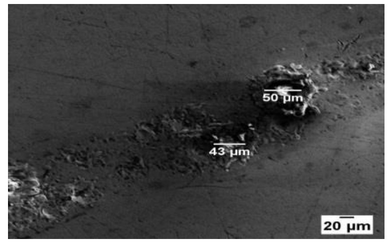
LM-1-45-1064	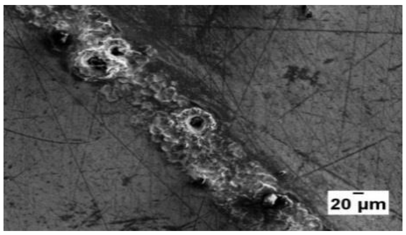	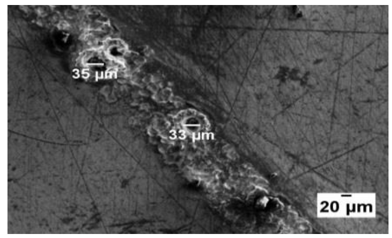
LM-1-40-1064	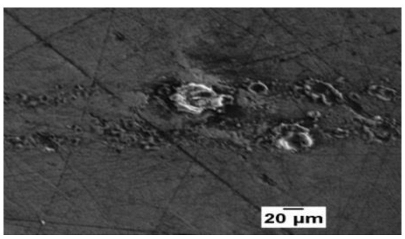	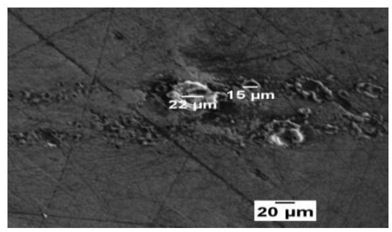
LM-0.5-50-1064	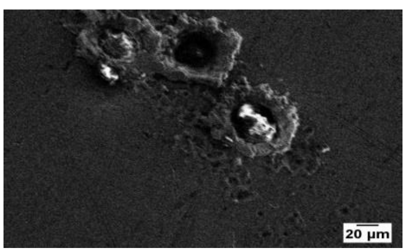	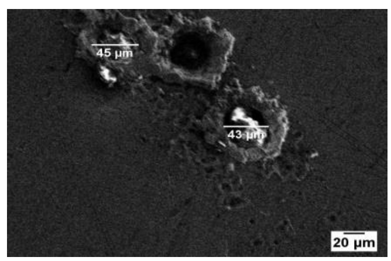
LM-0.5-45-1064	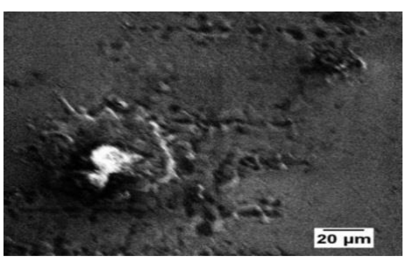	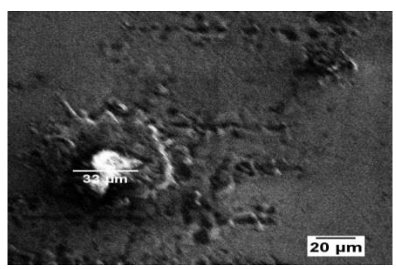
LM-0.5-40-1064	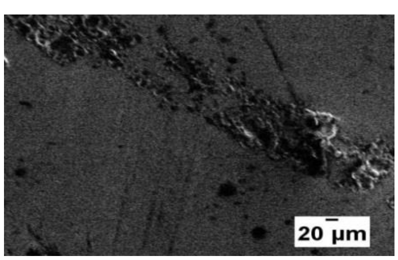	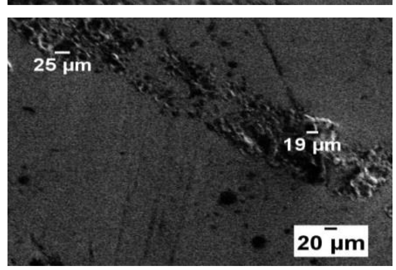

Figure 4.4: SEM images of microcavities

Six different test surfaces (LM-1-50-1064, LM-1-45-1064, LM-1-40-1064, LM-0.5-50-1064, LM-0.5-45-1064, LM-0.5-40-1064) are produced by varying the laser power and spacing between the channels/grooves on the copper surface. Here, the surfaces are prepared with a single pass of laser beam to create a channel/groove on surface. The laser movement is controlled using computer program. Three different laser powers (40 W, 45 W, 50W) and two different marking distances (1 mm and 0.5 mm) have been used to develop the test surfaces. The different laser parameters and physical dimensions used for fabrication of test sections are enlisted in Table 4.1. The photographic view (Fig. 4.2), SEM (Supra 55) images (Fig. 4.3) and microscopic (Dewinter) images (Fig. 4.3) of laser processed test sections are studied to observe surface morphology of the processed surfaces. The SEM images depict the presence of large number of micro pits in the channels/grooves on the test surfaces. The number of micro cavities developed in channels/grooves is increased with the increase in laser power. The micro cavities can be studied through microscopic and SEM images.

Table 4.1: Surface characteristics of test sections

Surface	Specification	Distance between makings (mm)	Laser Power (W)	Wavelength (nm)
Test Section 1	LM-1-50-1064	1	50	1064
Test Section 2	LM-1-45-1064	1	45	1064
Test Section 3	LM-1-40-1064	1	40	1064
Test Section 4	LM-0.5-50-1064	0.5	50	1064
Test Section 5	LM-0.5-45-1064	0.5	45	1064
Test Section 6	LM-0.5-40-1064	0.5	40	1064

Also, variation in number of micro cavities with laser power is observed in these images similar to SEM images (Fig. 4.3). The size of the micro pits was found to vary with reducing laser power. Here, an attempt has been made to measure the approximate size of micro cavities developed inside channels/grooves using higher magnification SEM images. The approximate size of micro cavities was found to decrease with the decrease in laser power (Fig. 4.4). The size of micro cavities was found to vary between 40-50 µm, 30-35 µm and 15-25 µm for laser processed surfaces developed with 50 W, 45 W and 40 W laser power, respectively.

4.3 Results and Discussion

In the present investigation, tests were conducted to study the nucleate pool boiling heat transfer performance of six laser processed copper test sections (Table 4.1). Tests are conducted at atmospheric pressure and saturated pool boiling condition by using water as pool liquid. Attempt has been made to study the effect of variation of laser power and distance between channels/grooves on the processed surface on heat transfer performance. Following the procedure as discussed in the previous section and Appendix I, the uncertainty for continuous wave laser processed surfaces were evaluated in this chapter. The maximum uncertainty was found on surface LM-0.5-50-1064. The maximum uncertainty in the estimated results for heat flux (q'') and heat transfer coefficient (h) was found to be 1.85 % and 13.4%, respectively.

4.3.1 Effect of laser markings on heat transfer performance

The details of laser processed surfaces are summarized in Table 1. Here, three different laser power such as 40 W, 45 W and 50 W with two marking distance (1 mm, 0.5 mm) for each laser power is considered to fabricate the test surfaces. Fig. 4.5 (a) depicts the variation of heat flux with wall superheat for six different laser processed surfaces and smooth surface. A significant leftward shift in boiling curve was observed for laser processed surfaces compared to smooth surface. The leftward shift in boiling curve is an indication of reduction in the wall superheat for laser processed test surface. The reduction in wall superheat is found to vary between 60-68 % and 25-35 % for LM-0.5-50-1064 and LM-1-40-1064, respectively. It is observed that all of the laser processed surfaces exhibits reduction in wall superheat values compared to the smooth surfaces.

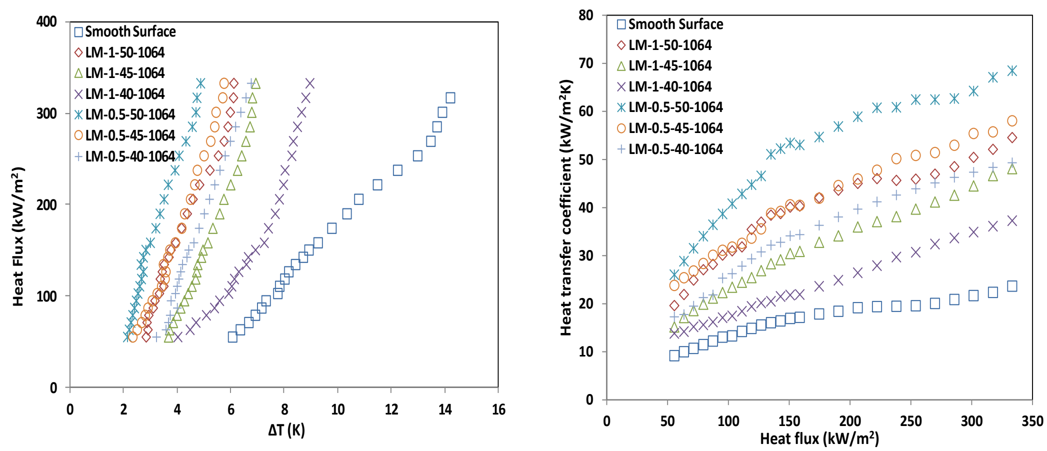

(a) (b)

Figure 4.5: (a) Comparison of heat flux versus wall superheat with water as pool liquid (b) Comparison of heat transfer coefficient versus heat flux with water as pool liquid

Fig. 4.5 (b) shows the variation of heat transfer coefficients with the supplied heat flux values for laser processed surfaces and smooth surface. The test surface LM-0.5-50-1064 exhibits better heat transfer performance compared to other test surfaces (LM-0.5-45-1064, LM-1-50-1064, LM-0.5-40-1064, LM-1-45-1064 and LM-1-40-1064). The enhancement in heat transfer coefficients values for LM-0.5-50-1064 was found to vary from 180 to 219 % compared to the smooth surface. It may be noted that we have maintained a reduced marking distance (0.5 mm) and higher laser power (50 W) for preparing the test surface LM-0.5-50-1064. This increases the number of channels and the material removal is higher because of higher laser power. The test surface LM-1-40-1064 fabricated with larger laser marking distance (1 mm) and lowest laser power (40 W) exhibits lowest enhancement in heat transfer coefficient. The enhancement in heat transfer coefficient for LM-1-40-1064 was found to be 50-53 % higher compared to the smooth surface. All the laser processed surfaces exhibit better heat transfer performance compared to smooth surface. They have shown significant enhancements in heat transfer coefficient values compared to the smooth surface.

The enhancement in heat transfer performance of laser marked surfaces is attributed to the formation of channel/grooved structure and formation of numerous nucleation sites during laser processing due to melting of top surface layer. The formation of channeled/grooved structure on surface enhances the liquid supply to active nucleation sites by providing additional liquid flow path ways and delays the possible occurrence of dry out at the test surface.

4.3.2 Effect of variation in laser power and distance between channels/grooves

Fig. 4.6 depicts the comparison of heat transfer coefficient for various laser processed surfaces produced by varying laser power and marking distance for different input heat flux values. The performances of laser processed surfaces are compared with the smooth surface. It is observed that all the test surfaces exhibit higher value of heat transfer coefficient with the increase in the input heat flux values. The laser processed surfaces produced by using higher laser power yield better heat transfer performance for all the input heat flux values. This may be due to fact that at higher laser power the rapid melting and fast cooling promotes development of more nucleation sites. The number of micro cavities increases with the increase in the laser power (Fig. 4.4). In addition to this, the distance between channels/grooves plays a significant role in creating the surface structure. With the reduced distance between consecutive channels/grooves, the number of channels/grooves increases on the surface. This increment provides more number of liquid pathways and allows continuous liquid flow to active nucleation sites delaying the dry out condition. In addition to this, more number of nucleation sites are developed on the boiling surface as larger surface area is exposed to the laser process. This combination of enhanced liquid supply network and increased nucleation site density on test surface with 0.5 mm laser marking distance promotes the enhancement of nucleate boiling heat transfer performance. At q″=95 kW/m^2, the enhancement in heat transfer coefficient of LM-0.5-45-1064 and LM-1-50-1064 compared to smooth surface is found to be 131 % and 196 %, respectively (Fig. 4.6). While, at q″=142 kW/m^2, the enhancement in heat transfer coefficient of LM-0.5-45-1064 and LM-1-50-1064 compared to smooth surface is found to be 218 % and 136 %, respectively. In addition to this, the enhancement in heat transfer coefficient of LM-0.5-45-1064 and LM-1-50-1064 compared to smooth surface is found to be 219 % and 135 %, respectively, for q″=253 kW/m^2.

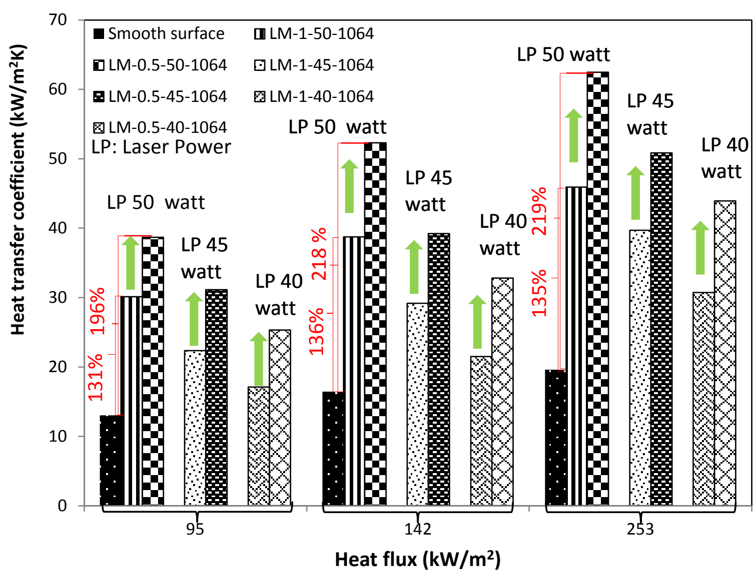

Figure 4.6: Comparison of heat transfer coefficient with laser power and 1 mm and 0.5 mm laser channel/groove distance

4.3.3 Liquid vapor interaction on test surface

The SEM images depict the presence of large number of micro cavities in the channels/grooves on the test surfaces developed by laser marking machine (Fig. 4.4). The microscopic (Fig. 4.3) and SEM images (Fig. 4.4) depict the closer look of these micro cavities. Fig. 4.7 (a-c) represents the graphical representation of test surface, the possible liquid vapor interaction and actual photographic view of bubble generation on laser processed test surface, respectively. In past, researchers have reported that the presence of channels/grooves on the surface helps in the enhancement of liquid vapor interaction on the test surface. Bubble growth was observed (Fig. 4.7 c) at numerous locations on the laser processed surface. This indicates the presence of active nucleation sites in channles/grooves. Here, micro cavities are acting as nucleation sites and the channels/grooves formed on the surface provides additional liquid pathways. In the present investigation the presence of micro pits and channels/grooves on the test surface is seen as the main reason behind heat transfer enhancement.

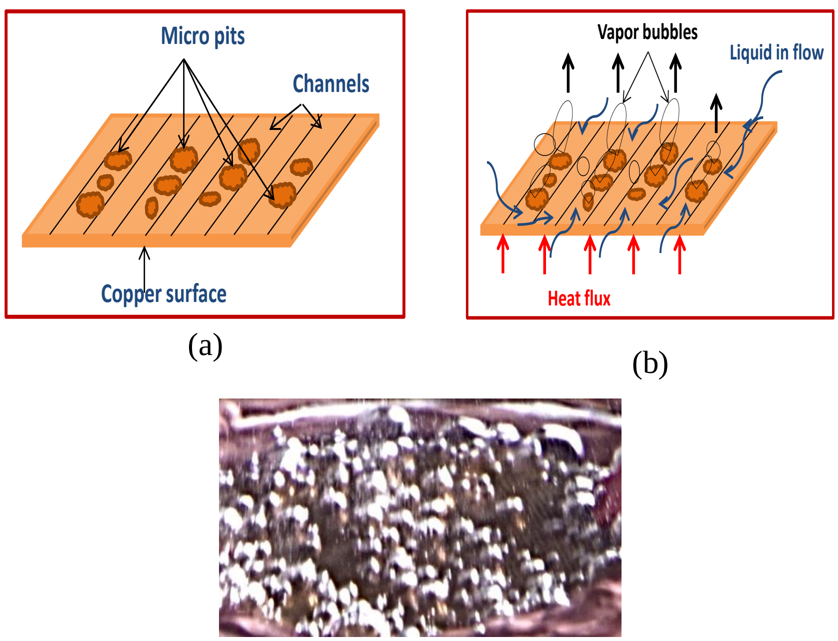

LM-0.5-50-1064 test surface at 31kW/m^2

(c)

Figure 4.7: (a) Graphical representation of microscope images (b) Graphical representation of liquid vapor interaction on the test surface (c) Photographic view of bubble generation

4.3.4 Comparison of present study with other test data

Here, an effort has been made to compare present test data with the experimental results of Dehghani-Ashkezari and Salimpour [107] for triangular grooved copper surfaces prepared by wire-cut machining, Jones et al. [21] for surfaces produced by electric discharge machining (EDM), Kathiravan et al. [108] for stainless steel surfaces with silver nanofluids with surfactant and Kim et al. [104] for ABM coated surface and is shown in Fig. 4.8.

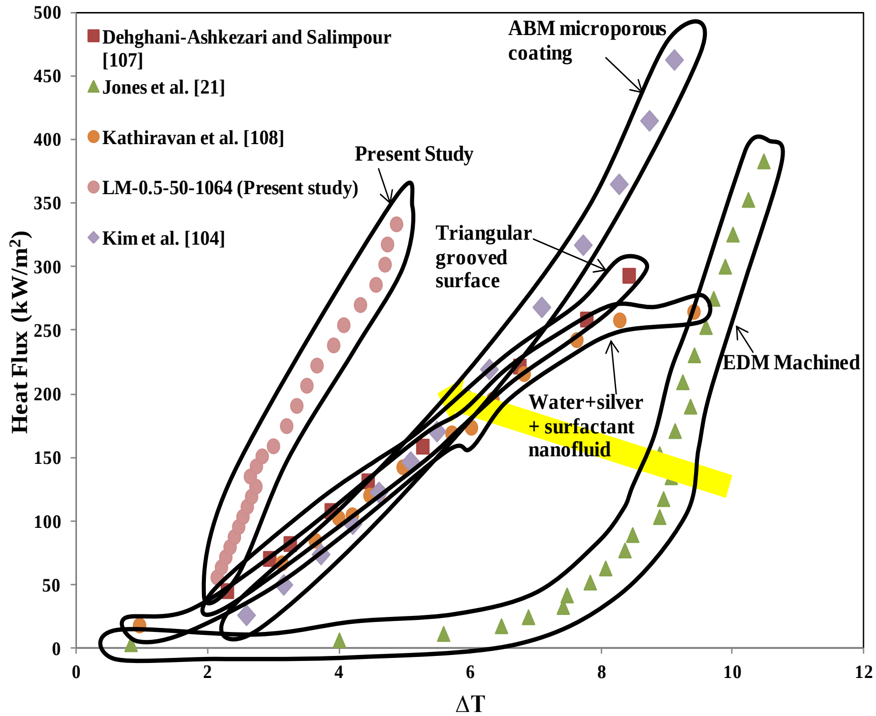

Fig. 4.8: Comparison of present result with test data of Dehghani-Ashkezari and Salimpour [107] Jones et al. [21] Kathiravan et al. [108] and Kim et al. [104]

Dehghani-Ashkezari and Salimpour [106] reported that the triangular geometry possesses the highest surface area, which helps in the enhancement of heat transfer coefficients compared to other grooved geometries. Jones et al. [21] in their experimental investigation reported that the EDM process develops cavities on surface and the test surface developed by using EDM with 10 μm surface roughness possess higher cavity density. They attributed the enhancement of heat transfer coefficient to the presence of these cavities. They reported an approximate 100 % enhancement in heat transfer coefficient values on this surface.

While, Kathiravan et al. [108] reported that the use of silver nanoparticles enhances the heat transfer performance. The authors observed that the aqueous surfactant solution with silver nanoparticle concentration of 0.75 % exhibits the highest enhancement in heat transfer compared to pure water. Kim et al. [104] developed microporous structures by employing the coating technique proposed by You and O'connor [105-106]. This technique is termed as ABM coating following its various contents such as aluminum particles, brushable ceramic epoxy, and methyl ethyl ketone (You and O'connor [105-106]). The surfaces prepared by ABM coatings with largest particle size of 17-30 μm exhibit reduction in wall superheat by 5 °C and enhancement in heat transfer coefficient by 47 % compared to plain surface. It is argued that the use of such coatings result an increase in micro cavities that act as active nucleation site.

Results obtained by present experimental investigation with LM-0.5-50-1064 exhibit better heat transfer performance than the test data of Dehghani-Ashkezari and Salimpour [107], Jones et al. [21], Kathiravan et al. [108], Kim et al. [104]. This indicates that the use of channeled/grooved surface developed using laser marking machine has better heat transfer performance characteristics compared to other techniques.

4.4 Effect of pulsed and continuous wave laser processing on heat transfer performance

Fig. 4.9 (a) depicts the variation of heat flux with wall superheat for smooth and all laser processed test sections with water as pool liquid. The maximum wall superheat values were found to vary among various laser processed test surfaces. A leftward shift in boiling curve of all laser processed test sections was observed, suggesting reduction in wall superheat values compared to smooth surface test section. The continuous wave laser processed test sections LM-1-50-1064, LM-1-45-1064, LM-1-40-1064 have shown overall 20 % to 57 % reduction in wall superheat values compared to the smooth test section. Whereas the pulsed laser processed test sections FS1, FS2, FS3 have shown overall 5 % to 48 % reduction in wall superheat values compared to the smooth test section. The reduction in wall superheat values is attributed to the increased nucleation site density on laser processed test sections compared to smooth surface test sections. The leftward shift in boiling curve also indicates the enhancement in heat transfer coefficient at relatively lower surface temperatures.

Fig 4.9 (b) depicts the variation in heat transfer coefficient values with heat flux for laser processed and smooth surface. Enhancement in heat transfer coefficient values was observed for all laser processed surfaces compared to smooth surface. In case of continuous laser processed test surfaces, an enhancement in heat transfer coefficient values ranging up to 136 % was observed for test surface LM-1-50-1064 compared to smooth surface, which is highest among (LM-1-45-1064 and LM-1-40-1064) test surfaces developed using continuous laser. Whereas, an enhancement ranging up to 93 % in heat transfer coefficient values was observed over test surface FS1 compared to smooth surface and is highest among (FS2 and FS3) test surfaces developed using nanosecond pulsed laser. It has been observed that the test surfaces developed using peak laser power has best heat transfer performance and the heat transfer performance of test surfaces decreases with decreasing laser power used during laser processing. This trend of heat transfer performance was observed in case of both of the laser systems used here. This trend suggest that laser power used during laser processing affects the microstructure development on surface and is important parameter in developing augmented surfaces using laser processing technique. One of the main reasons behind this is, at higher laser power the amount of heat generated is higher, which causes more topographical chances on surface layer developing conditions favorable for heat transfer enhancement by increasing number of active nucleation sites.

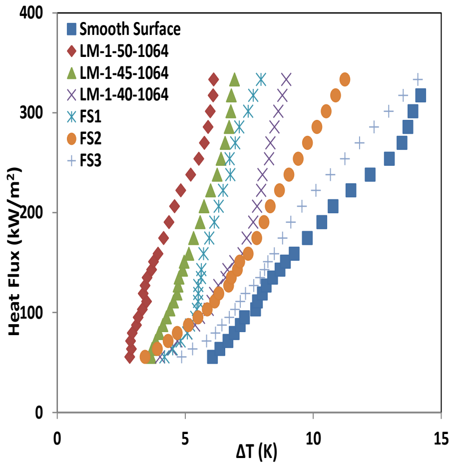

(a)

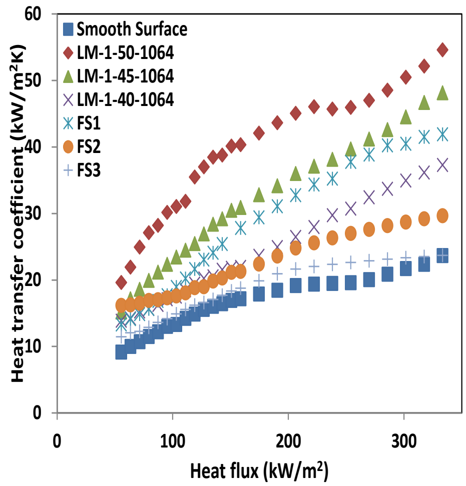

(b)

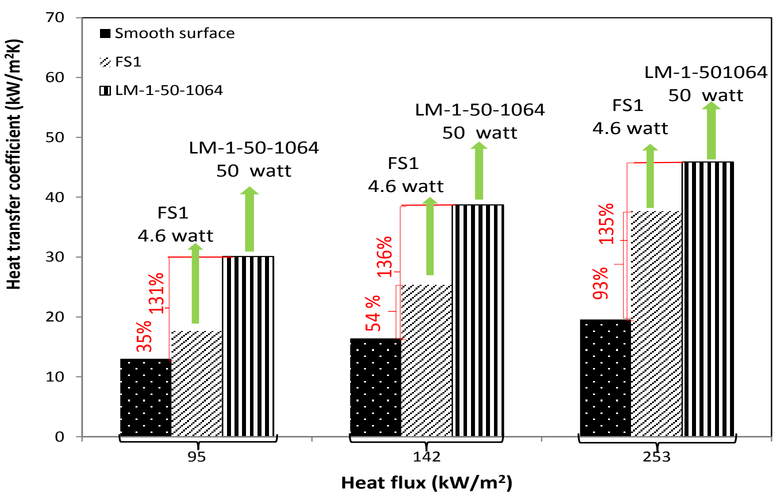

(c)

Figure 4.9: (a) Variation of heat flux with wall superheat (b) Variation of heat transfer coefficient with heat flux for both laser processed and smooth copper surface with water as pool liquid (c) Comparison of percentage enhancement in HTC at various heat flux input compared to smooth surface for FS1 and LM-1-50-1064

The topographical changes in microstructures can be observed in SEM images for test sections developed using continuous wave (Fig. 4.3) and pulsed laser (Fig. 3.2 a, Ch. 3). In case of test sections LM-1-50-1064, LM-1-45-1064 and LM-1-40-1064 developed using continuous wave laser, the number of cavities developed inside the channels/grooves decreases from LM-1-50-1064 to LM-1-40-1064, which were developed with decreasing laser processing power. These cavities are expected to be acting as nucleation sites and their decreasing number results in decreasing heat transfer performance from LM-1-50-1064 to LM-1-40-1064 (Fig. 4.9 b). Whereas, from the SEM images (Fig. 3.2 a, Ch. 3) of test sections FS1, FS2 and FS3, it can be observed that the decrease in laser processing power results in development of microstructure with less number of pores and micro fins which are helping in the enhancement of heat transfer performance. The reduced number of micro fins and pores lead to the decoration in heat transfer performance from FS1 to FS3 (Fig. 4.9 b).

The comparison of increment in heat transfer coefficient values with respect to smooth surface reveal that the test surfaces developed using continuous wave laser has higher heat transfer coefficient value than the test surfaces developed using nanosecond pulsed laser. However, the laser power used in case of continuous wave laser is much higher compared to the nanosecond pulsed laser (Fig. 4.9 c). This suggests that the development of microstructure using pulsed laser system can be more beneficial. At heat flux input of 95 kW/m^2, 142 kW/m^2 and 253 kW/m^2 the continuous wave laser processed test section LM-1-50-1064 shown enhancement in heat transfer coefficient by 131 %, 136 % and 135 %, respectively, whereas, pulsed laser processed surface FS1 shown enhancement in heat transfer coefficients by 35 %, 54 % and 93 %, respectively.

4.5 Comparison of heat transfer performance different structured surfaces

The variation of q'' vs ΔT and h vs q'' for different surfaces developed by using various surface modification techniques considering same liquid is shown in Figs. 4.10 (a-b), respectively. These include the surfaces developed by wire-EDM method, continuous wave laser ablation technique and nanosecond pulsed laser ablation technique. The structured surface T-0.725-1-0.9 developed with wire-EDM method exhibits the lowest wall superheat values (Fig. 4.10 a) and highest values of heat transfer coefficient (Fig. 4.10 b). The structured surface T-0.725-1-0.9, developed using wire-EDM machining exhibits highest enhancement in heat transfer performance among all test surfaces. This is followed by the test surfaces developed by continuous wave laser processed surfaces LM-0.5-50-1064, LM-0.5-45-1064, which exhbits the second and third best heat transfer performance. This may be due to the increased surface area with enhanced liquid vapour interaction compared to microstructured surfaces developed by continuous wave and nanosecond pulsed laser processing techniques. The combination of number of micro cavities acting as nucleation sites with micro grooves is found to be the main reason in the enhancement of heat transfer coefficient values on surfaces processed by continuous wave laser. While, the formation of microstructure with micro fin and pore is the prime reason of heat transfer enhancement on nanosecond pulsed laser processed surface.

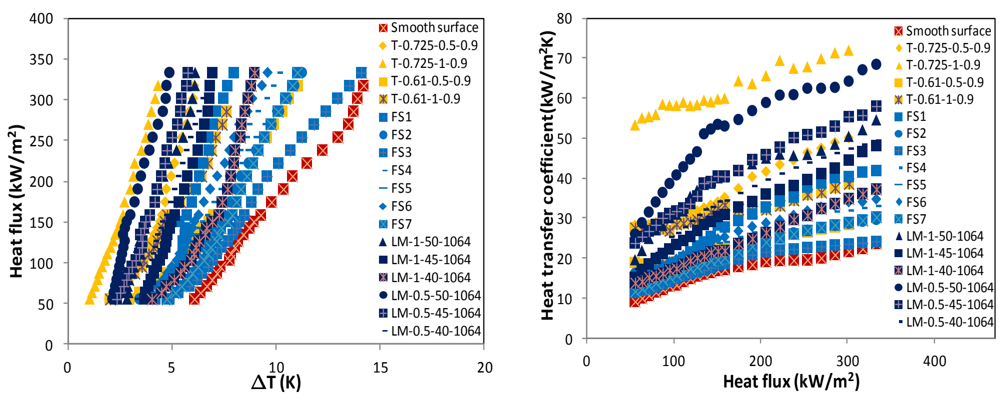

(a) **(b)**

Figure 4.10: (a) Comparison of heat flux versus wall superheat with water as pool liquid, (b) Comparison of heat transfer coefficient versus heat flux with water as pool liquid

In case of the test surfaces (T-0.725-1-0.9, T-0.725-0.5-0.9, T-0.61-1-0.9, T-0.61-0.5-0.9) developed using wire-EDM machining the method, the tunnel structure developed on the surface provides separate vapor and liquid pathways enhancing vapour-liquid interaction on the surface and delays the possible dry out situation at active nucleation sites. Also, the dimension of structure is found to play an important role in enhancement. The bubble growth is obstructed because of reduced width of the tunnel and with the progress of time, as more bubbles are formed, they do not find sufficient space to escape from the tunnel. In addition to this, counter flow of liquid and vapour bubble obstructs liquid flow. While, in case of the structured surface with a larger width, the resistance between the inward liquid flow and upward moving vapor bubbles is less resulting in enhanced convection and better heat transfer performance. It can be observed from the (Figs. 4.10 a-b) that the test surfaces (T-0.725-1-0.9 and T-0.725-0.5-0.9) with larger width exhibit lower wall superheat values and higher heat transfer coefficient values compared to the test surfaces (T-0.61-1-0.9 and T-0.61-0.5-0.9) involving lower width. Also, the structure with larger depth (T-0.725-1-0.9 and T-0.61-1-0.9) provides better heat transfer performance. This may be due to the fact that with the increase in depth, the heat transfer area increases and result in the increase in active nucleation sites, leading to an increase in heat transfer performance. It was observed from Figs. 4.10 (a-b) that the structured surface (T-0.725-1-0.9) with higher width and depth is found to exhibit the highest enhancement values ranging up to 250% compared to the smooth surface (Fig. 4.10 b). In case of continuous wave laser processed surfaces (LM-1-50-1064, LM-1-45-1064, LM-1-40-1064, LM-0.5-50-1064, LM-0.5-45-1064, LM-0.5-40-1064) the grooved structure with microcavities help in the enhancement of heat transfer coefficient. Here, micro cavities act as nucleation site and the channels/grooves formed on the surface provides additional liquid pathways. The SEM images of continuous wave laser processed surfaces show that the size and number of microcavities in grooves reduces with reduction in the laser power. The size of micro cavities was found to vary between 40-50 μm, 30-35 μm and 15-25 μm for 50 W, 45 W and 40 W laser power, respectively. The surface processed with highest laser power and reduced groove spacing (LM-0.5-50-1064) is found to exhibit the highest enhancement (up to 219%) in heat transfer coefficient (Fig. 4.10 a). In case of nanosecond pulsed laser processed test sections (FS1, FS2, FS3, FS4, FS5, FS6, FS7) the formation of pore and fin microstructure is seem to be the main reason of enhancement in heat transfer coefficient values. The microstructure developed on the surface is found to be dependent on different laser parameters. A variation in microstructure involving a number of pores and micro fin structure was observed in SEM images of test surfaces that are processed at different laser power and laser wavelengths. The heat transfer performance of the laser processed surface with higher laser power exhibits better heat transfer performance. At higher laser power, melting of more material takes place and after solidification dense mound structures are formed on the surface. The SEM image of the surface processed with higher laser power (FS1, FS4 and FS6) shows densely packed mound structures and narrow channels/cracks between microstructures. It is noticed from the SEM images that the pore size of the microstructures reduces with reduction in laser power in case of all laser wavelengths. The test surface developed with highest laser power (FS1) for all laser wavelengths exhibits the highest enhancement in heat transfer coefficient values (up to 93%) among all processed surfaces (Fig. 4.10 b).

4.6 Concluding remarks

This chapter reports the investigation of the nucleate pool boiling performance of laser processed surfaces developed by continuous wave laser processing technique. Here, ytterbium (Yb) doped fiber laser (IPG Photonics) is used as the laser source. Six different test surfaces are developed by varying laser power (40-50 W) and spacing between the channels/grooves (1 mm and 0.5 mm) on the copper surface. Tests are conducted with water at atmospheric pressure condition and saturated pool boiling condition. The surface morphology of the processed surface is studied by using SEM images. The maximum enhancement in heat transfer coefficient of laser processed surface was found to 219 % higher compared to smooth surface. Present test results are compared with the experimental results of the other researchers. Also, the mechanism of heat transfer on laser processed surface was discussed.

Next an attempt has been made to investigate the nucleate pool boiling heat transfer performance of micro structured copper surfaces developed by using two different laser systems, namely, pulsed Nd:YAG laser and continuous wave laser. Laser processed surfaces, developed by employing different laser systems, were found to exhibit superior heat transfer performance compared to smooth surface. The test surfaces developed by employing continuous wave laser processing technique exhibit channeled/grooved structure with micro cavities or micro holes. While, the microstructure involving micro pores and micro fins are observed on the test section developed by using nano second pulsed laser. Different microstructures are developed on the surface by employing pulsed Nd:YAG laser and continuous wave laser. These microstructures were found to affect the heat transfer performance. The heat transfer performance is found to increase with the increase in laser power. The reduction in wall superheat values for continuous wave laser processed surface is found to be higher compared to the pulse laser processed surfaces.

Chapter 5

Summary and Conclusions

The present dissertation reports experimental investigations pertaining to the pool boiling heat transfer performance of test surfaces developed by using wire-EDM, nanosecond pulsed laser and continuous wave laser with different pool liquids such as water, isopropyl alcohol and acetone. The objective of the present work is to develop different test surfaces and to analyze the effects of variation of laser type, power and wavelength on physical characteristics and pool boiling heat transfer performance of the test surface.

Design and development of a test facility involving various modules such as cylindrical boiling container, heater assembly, condensing coil, power supply system and temperature measurement scheme have been made to study the pool boiling heat transfer characteristics of smooth and different structured surfaces. Initial tests are conducted at atmospheric pressure at the saturated condition for a smooth copper test surface. The input heat supplied to the test section is calculated by measuring the voltage and current values across the heater terminals. The surface temperature of the boiling surface is calculated by using the measured temperature data of the test section and input heat flux. Subsequently, the heat transfer coefficient is evaluated by using the input heat flux and wall superheat values. Later on, structured surfaces are prepared by using wire-EDM, nanosecond pulsed laser and continuous wave laser. Tests are conducted with different pool liquids such as water, isopropyl alcohol and acetone. The conclusions obtained from the present dissertation are summarized below.

5.1 Conclusions from the present work

Pool boiling heat transfer performance of structured surfaces developed by the wire-EDM method

Here, an effort has been made to develop different structured geometry on the copper surface by using a non-conventional wire-EDM machining technique. Tests are conducted at atmospheric pressure and saturation condition by using water and isopropyl alcohol as pool liquids. The significant outcomes of the experimental investigation are discussed below.

- The structured surfaces are found to exhibit better heat transfer performance compared to the smooth surface with water and isopropyl alcohol.
- For the structured surface, the boiling curve is found to shift towards a leftward direction. The reduction in incipient boiling superheat occurs in the structured surface compared to a smooth surface for given heat flux value.
- The maximum decrease in the wall superheat in case of the structured surface was found to be 70 % and 55 % in case of water and isopropyl alcohol, respectively.
- The maximum heat transfer enhancement of the structured surface compared to the smooth surface was found to be 250 % and 100 % for water and isopropyl alcohol, respectively.
- The heat transfer enhancement because of the change in depth/width was found to be significant in the case of water. While no significant enhancement in heat transfer because of change in width/depth is noticed for isopropyl alcohol.

Pool boiling heat transfer performance of nanosecond pulsed laser processed surface

In the present experimental investigation, an attempt has been made to use a novel surface modification method “laser processing”. In this chapter, experiments are performed to study the nucleate pool boiling heat transfer performance of microstructured surfaces developed by using nanosecond laser processing technique. The laser used here is Nd:YAG

(Quanta-Ray ND, Spectra Physics) that produces 5-8 nanosecond pulses with a wavelength of 1064 nm, 532 nm, 355 nm at a repetition rate of 10 Hz.

Initially, three test surfaces are developed by using different laser powers varying within 4 W to 4.6 W for a wavelength of 1064 nm. Tests are conducted to study the pool boiling heat transfer performance of microstructured surfaces by using two different pool liquids such as water and acetone. Next, four test surfaces were fabricated using 532 nm and 355 nm wavelength at peak laser power, two surfaces in each wavelength. The pool boiling heat transfer performance of laser processed surfaces was tested using water as pool liquid at saturation temperature. Significant findings obtained from the experimental investigations are summarized below:

- Experimental findings indicate that the microstructure developed on nanosecond laser processed test surfaces help in the enhancement of heat transfer performance compared to the smooth surface.
- A substantial leftward shift was observed in pool boiling curve for all laser processed microstructured surfaces, indicating a reduction in wall superheat at given input heat flux value.
- The maximum decrease in the wall superheat on microstructured test surface was found to be 40 % to 43 % compared to the smooth surface.
- The maximum enhancement in heat transfer coefficient for FS1 was found to be 93 % with water and 30 % with acetone compared to plain surface.
- The laser processing wavelength plays an important role in the enhancement of the heat transfer coefficient. The test surface FS6 and FS4 developed using laser wavelength of 355 and 532 nm have shown around 60 % and 50 % enhancement in heat transfer

coefficient values, respectively at considerably low laser power compared to FS1.

- It is observed that the heat transfer performance of laser processed surfaces increases with an increase in laser fluence.
- The heat transfer enhancement is found to dependent on laser fabrication parameters such as laser wavelength, the processed surface area and laser power.

Pool boiling heat transfer performance of continuous wave laser processed surfaces

Here, an effort has been made to develop copper test surfaces using a continuous wave laser and study their pool boiling heat transfer performance. The test surfaces were processed at different laser powers and with different scanning line separation distances with a laser wavelength of 1064 nm. The laser processing is found to develop grooved/ channeled structures on the surface with microcavities inside these channels. The pool boiling experiments were carried by using water as pool liquid at saturation temperature. In addition to this, the heat transfer performance of test surfaces developed by using two different laser systems, namely, pulsed and continuous wave laser system has been studied. The significant findings of the present investigation are summarized below.

- Experimental results indicate that test surfaces with channels/grooves developed using laser marking machine, exhibits enhanced heat transfer performance compared to the smooth surface.
- A significant leftward shift in the pool boiling curve was observed on channeled/grooved surfaces, which indicates the reduction in incipient boiling superheat for given heat flux values.
- The maximum decrease in the wall superheat on laser channels/grooves surface was found to be 60 % to 68 %.

- At q''=253 kW/m^2, LM-0.5-50-1064 exhibits maximum heat transfer coefficient value compared to other processed surfaces. The enhancement in heat transfer coefficient of LM-0.5-50-1064 is found to be 219 % higher compared to the smooth surface at q''=253 kW/m^2.
- The heat transfer enhancement is found to depend on the laser fabrication parameter such as laser power. The higher laser power, generates more heat, melting a large amount of surface material developing deeper grooves on the surface with more microcavities.
- The type of laser used in laser processing plays an important role in the development of microstructure on the test surface. Subsequently, the microstructure is found to affect the pool boiling performance.

5.2 Contributions from the present work

Following contributions are made from the present work.

- Present work adds significant experimental test data on pool boiling heat transfer.
- A novel laser processing technique has been developed to develop novel test surfaces.
- The effect of nanosecond pulsed laser for varied range of laser power and laser wavelength on microstructure development was studied.
- The effect of continuous wave laser for varied range of laser power on microstructure development was studied.
- The nucleate pool boiling heat transfer performance different laser processed surfaces (nanosecond pulsed laser, continuous wave laser) was obtained using different pool liquids (water, isopropyl alcohol).
- Nucleate pool boiling heat transfer performance of structured surfaces developed with wire-EDM machining method was obtained by using different pool liquid (water, isopropyl alcohol).
- Heat transfer enhancement mechanisms were proposed using graphical representation.

- The microstructure developed on laser processed surfaces was studied using SEM and microscopic imaging.
- Pool boiling curves for various structured surfaces with different pool liquid were obtained.

5.3 Limitations of the present work

Unfortunately, we could not report test data for CHF. This would be a important information to the existing pool boiling data. Also, different laser techniques involving range of laser power, laser frequency could be made because of certain constrain. Also, more surface characterization method need to made to explore the dependence of various parameters on performance. Apart from this sub cooling experimental tests, effect of inclination, gravity and different saturation pressure are not reported in the present study.

5.4 Scope for future work

The enhancement in pool boiling performance of structured surface is useful for various industrial applications such as boilers, nuclear reactors, chemical processing, refrigeration industry and microelectronics cooling systems (immersion cooling). Various surface modifications have been achieved by using different fabrication techniques. Although, numerous techniques have been employed to develop structured surfaces, they possess several limitations. The research work carried out in the present dissertation introduces novel techniques to develop modified surfaces. These include the use of wire-EDM and laser ablation techniques. Subsequently, these processed surfaces are tested to estimate the boiling performance. The test results may provide useful information for further research in this area. In view of these certain directions for future investigation are elaborated below.

- Efforts should be made to use different advanced laser systems for surface modification. Subsequently, the processed surfaces need to be tested to estimate the boiling heat transfer performance.

- Efforts should be made to develop different patterned surfaces with varied range of laser parameters including laser power and laser wavelengths.
- The optimal laser parameters for surface modification need to be studied.
- The heat transfer performance of surfaces developed by using combination of various surface modification techniques such as wire-EDM and laser ablation should be studied.
- Heat transfer performance of laser processed surfaces under various operating conditions such as varied range of pressure and different subcooling need to be studied.
- Effect of different pool liquids on the pool boiling heat transfer performance of modified surfaces needs to be studied.

References

[1] Nukiyama, S. (1934), Maximum and minimum values of heat transmitted from metal to boiling water under atmospheric pressure, Soc. Mech. Eng. Jpn. J., 37(206), 367–374.

[2] Kandlikar S.G. (2017), Enhanced macroconvection mechanism with separate liquid–vapor pathways to improve pool boiling performance, J. Heat Transfer, 139, 051501-1.

[3] Moore F.D., Mesler R.B. (1961), The measurement of rapid surface temperature fluctuations during nucleate boiling of water, AIChE Journal, 7(4), 620-624.

[4] Hendricks R.C., Sharp, R. R. (1964), Initiation of cooling due to bubble growth on a heating surface. Natl. Aeronaut. Space Adm., Tech. Note, Washington, [D.C.], D-2290.

[5] Cooper M.G., Lloyd A.J.P. (1969), The Microlayer in Nucleate Pool Boiling, Int. J. Heat Mass Transf., 12(8), 895–913.

[6] Moghaddam S., Kiger K. (2009), Physical mechanisms of heat transfer during single bubble nucleate boiling of FC-72 under saturation conditions-I: theoretical analysis, Int. J. Heat Mass Transf., 52(5–6), 1284–1294.

[7] Han C.Y., Griffith P. (1962), The mechanism of heat transfer in nucleate pool boiling, Technical report - heat transfer laboratory, Massachusetts Institute of Technology, no. 19.

[8] Mikic, B.B., Rohsenow W.M. (1969), A New Correlation of Pool-Boiling Data Including the Effect of Heating Surface Characteristics, J. Heat Transf., 91(2), 245–250.

[9] Mikic B.B., Rohsenow W.M., Griffith P. (1970), On Bubble Growth Rates, Int. J. Heat Mass Transf., 13(4), 657–666.

[10] Haider S.I., Webb R.L. (1997), A transient micro-convection model of nucleate pool boiling, Int. J. Heat Mass Transf., 40(15), 3675-3688.

[11] O'Neill P.S., Gottzmann C.F., Terbot J.W. (1972), Novel heat exchanger increases cascade cycle efficiency for natural gas liquefaction, Advances in Cryogenic Engineering, Springer, Boston, MA, 420-437.

[12] Bergles A.E. Chyu M.C. (1982), Characteristics of nucleate pool boiling from porous metallic coatings, J. Heat Transf., 104, 279–285.

[13] Wang X.S., Wang Z.B., Chen Q.Z. (2010), Research on manufacturing technology and heat transfer characteristics of sintered porous surface tubes, Adv. Mater. Res., 97-101, 1161–1165.

[14] Mankovskij O.N., Ioffe O.B., Fibgant L.G., Tolczinskij A.R. (1976), About boiling mechanism on flooded surface with capillary-porous coating, Ing Fiz J, 30(2), 975–782.

[15] Cooke, D., Kandlikar S.G. (2011), Pool boiling heat transfer and bubble dynamics over plain and enhanced microchannels, ASME. J. Heat Transfer, 133(5), 052902.

[16] Bergles A.E., Heat transfer enhancement—the encouragement and accommodation of high heat fluxes, J. Heat Transfer., 119(1), 8-19.

[17] Webb R.L. (2004), Odyssey of the enhanced boiling surface, J. Heat Transfer vol. 126 1051–1059.

[18] Kurihari H.M., Myers J.E. (1960), Effects of superheat and roughness on the boiling coefficients, AIChE J., 6, 83–91.

[19] Benjamin R.J., Balakrishnan A.R. (1997), Nucleation site density in pool boiling of saturated pure liquids: effect of surface micro-roughness and surface and liquid physical properties, Exp. Therm. Fluid Sci., 15, 32–42.

[20] Kang M.G. (2000), Effect of surface roughness on pool boiling heat transfer, Int. J. of Heat and Mass Transfer, 43, 4073-4085.

[21] Jones B.J., McHale J.P., Garimella S.V. (2009), The influence of surface roughness on nucleate pool boiling heat transfer, J. Heat

Transfer, 131, 121009.

[22] Jabardo J.M.S., Ribatski G., Stelute E. (2009), Roughness and surface material effects on nucleate boiling heat transfer from cylindrical surfaces to refrigerants R-134a and R-123, Exp. Therm Fluid Sci., 33, 579–590.

[23] Nishikawa K., Fujita Y. (1982), Effect of the surface roughness on the nucleate boiling heat transfer over the wide range of pressure, Proceedings of the Seventh International Heat Transfer Conference, Munchen, Germany, 61-66.

[24] Marto P.J., Moulson J.A., Maynard M.D. (1968), Nucleate pool boiling of nitrogen with different surface conditions, ASME J. Heat Transfer, 90, 437-444.

[25] Berenson P.J., (1965) Experiments on pool-boiling heat transfer, Int. J. Heat Mass Transfer, 5, 985-999.

[26] Siman-Tov M. (1970), Analysis and design of extended surfaces in boiling liquids, Chem. Engrg. Progr. Symp. Ser., 66, 174–184.

[27] Klein G.J., Westwater J.W. (1971), Heat transfer from multiple spines to boiling liquids, AIChE J., 17, 1050–1056.

[28] Bergles A.E., Guglielmini G., Misale M., Schenone C. (1995), Pool boiling from multiple square shaped spines in highly-wetting fluid, Proceedings of Pool Boiling 2: Eurotherm Seminar No. 48, Paderborn, Germany, 149–155.

[29] Rainey K.N., You S.M. (2000), Pool boiling heat transfer from plain and microporous, square pin-finned surfaces in saturated FC-72, ASME J. Heat Transfer, 122, 509–516.

[30] Chen K., Yan C., Kurwitz C., Cheng K., Bian H. (2016), Experimental study of helix-finned surface for nucleate pool boiling, Proceedings of the 24th International Conference on Nuclear Engineering. Volume 5: Student Paper Competition. Charlotte, North Carolina, USA, V005T15A003.

[31] Webb R.L., Pais C. (1992), Nucleate pool boiling data for five

refrigerants on plain, integral-fin and enhanced tube geometries, Int. J. of Heat and Mass Transfer, 35(8), 1893-1904.

[32] Memory S.B., Sugiyama D.C., Marto P.J. (1995), Nucleate pool boiling of r-114 and r-114-oil mixtures from smooth and enhanced surfaces I-Single tubes, Int. J. of Heat and Mass Transfer, 38(8), 1347-61.

[33] Huebner P., Kuenstler W. (1997), Pool boiling heat transfer at finned tubes: influence of surface roughness and shape of the fins, Int. J. Refrig., 20(8), 575-582.

[34] Tatara R.A., Payvar P. (2000), Pool boiling of pure R134a from a single turbo-BII-HP tube, Int. J. Heat Mass Transfer, 43(12), 2233-2236.

[35] Jung D., Kwangyong A., Jinseok P. (2004), Nucleate boiling heat transfer coefficients of Hcfc22, Hfc134a, Hfc125, and Hfc32 on various enhanced tubes, Int. J. Refrig., 27(2), 202-206.

[36] Jung D., Lee H., Bae D., Ha J. (2005), Nucleate boiling heat transfer coefficients of flammable refrigerants on various enhanced tubes, Int. J. Refrig., 28(3), 451-455.

[37] Thome J.R., Ribatski G. (2006), Nucleate boiling heat transfer of R134a on enhanced tubes, Appl. Therm. Eng., 26(10), 1018-1031.

[38] Wen-Tao J., Ding-Cai Z., Nan F., Jian-Fei G., Numata M., Guannan X., Wen-QuanT. (2010), Nucleate pool boiling heat transfer of r134a and r134a-pve lubricant mixtures on smooth and five enhanced tubes, J. of Heat Transfer, 132(11), 111502.

[39] Kim N.H., Choi K.K. (2001), Nucleate pool boiling on structured enhanced tubes having pores with connecting gaps, Int. J. of Heat and Mass Transfer, 44, 17-28.

[40] Chien L.H., Webb R.L. (1998), Visualization of pool boiling on enhanced surfaces, Exp. Therm. Fluid Sci., 16, 332–341.

[41] Rajulu K.G., Kumar R., Mohanty B., Varma H.K. (2004), Enhancement of nucleate pool boiling heat transfer coefficient by

reentrant cavity surfaces, Heat Mass Transfer, 41,127–132.

[42] Pastuszko R. (2008), Boiling heat transfer enhancement in subsurface horizontal and vertical tunnels, Exp. Thermal Fluid Sci., 32, 1564–1577.

[43] Das A.K., Das P.K., Saha P. (2009), Performance of different structured surfaces in nucleate pool boiling, Appl. Therm. Eng., 29, 3643–3653.

[44] Guglielmini G., Misale M., Schenone C., Boiling of saturated FC-72 on square pin fin arrays, Int. J. Therm. Sci. 41 (2002) 599–608.

[45] Xuenong G., Huibin Y., Yuyou H., Yutang F., Zhengguo Z. (2009), Nucleate pool boiling enhancement outside a horizontal bank of twisted tubes with machined porous surface, Appl. Therm. Eng., 29, 3212–3217.

[46] Forrest E., Williamson E., Buongiorno J., Hu L.W., Rubner M., Cohen R. (2010), Augmentation of nucleate boiling heat transfer and critical heat flux using nanoparticle thin-film coatings, Int. J. of Heat and Mass Transfer, 53, 58–67.

[47] Hsieh S.S., Weng C.J. (1997), Nucleate pool boiling from coated surfaces in saturated R-134a and R-407c, Int. J. Heat Mass Transfer, 40 (3), 519–532.

[48] Ahn H.S., Sinha N., Zhang M., Banerjee D., Fang S., Baughman R.H. (2006), Pool boiling experiments on multiwalled carbon nanotube (MWCNT) forests, J. Heat Transfer, 128, 1335–1342.

[49] Li C., Wang Z., Wang P.I., Peles Y., Koratkar N., Peterson G.P. (2008), Nanostructured copper interfaces for enhanced boiling, Small, 4(8), 1084–10188.

[50] Ramaswamy C., Joshi Y., Nakayama W., Johnson W.B. (2002), High-speed visualization of boiling from an enhanced structure, Int. J. Heat Mass Transfer, 45, 4761–4771.

[51] Chen R., Lu M.C., Srinivasan V., Wang Z., Cho H.H., Majumdar A. (2009), Nanowires for enhanced boiling heat transfer, Nano

Lett., 9, 548–553.

[52] Honda H., Takamastu H., Wei J.J. (2002), Enhanced boiling of FC-72 on silicon chips with micro-pin-fins and submicron-scale roughness, J. Heat Transfer, 124, 383–390.

[53] Zhang M, Lian K (2008), Using bulk micromachined structures to enhance pool boiling heat transfer, Microsyst. Technol., 14, 1499–1505.

[54] Coso D., Srinivasan V., Lu M.C., Chang J.Y., Majumdar A. (2012), Enhanced heat transfer in biporous wicks in the thin liquid film evaporation and boiling regimes, ASME J. Heat Transfer, 134, 101501.

[55] Kubo H., Takamatsu H., Honda H. (1999), Effects of size and number density of microreentrant cavities an bailing heat transfer from a silicon chip immersed in degassed and gas-dissolved FC-72, J. Enhanced Heat Transfer, 6, 155–160.

[56] Kotthoff S., Gorenflo D., Danger E., Luke A. (2006), Heat transfer and bubble formation in pool boiling: effect of basic surface modifications for heat transfer enhancement, Int. J. Therm. Sci., 45, 217–236.

[57] Li C., Peterson G.P. (2007), Parametric study of pool boiling on horizontal highly conductive microporous coated surfaces, J. Heat Transfer, 129(11), 1465–1475.

[58] Alam M.S., Prasad L., Gupta S.C., Agarwal V.K. (2008), Enhanced boiling of saturated water on copper coated heating tubes, Chemical Engineering and Processing, 47, 159–167.

[59] Wu W., Bostanci H., Chow L.C., Hong Y., Su M., Kizito J.P. (2010), Nucleate boiling heat transfer enhancement forwater and FC-72 on titanium oxide and silicon oxide surfaces, Int. J. of Heat and Mass Transfer, 53, 1773–1777.

[60] Sahu R.P., Sinha-Ray S., Sinha-Ray S., Yarin A.L. (2016), Pool boiling of Novec 7300 and self-rewetting fluids on electrically-

assisted supersonically solution-blown, copper-plated nanofibers, Int. J. Heat Mass Transf., 95, 83–93.

[61] Hendricks T.J., Krishnan S., Choi C., Chang C.H., Paul B. (2010), Enhancement of pool boiling heat transfer using nanostructured surfaces on aluminum and copper, Int. J. Heat Mass Transfer, 53, 3357–3365.

[62] Launaya S., Fedorova A.G., Joshia Y., Caob A., Ajayan P.M. (2006), Hybrid micro-nano structured thermal interfaces for pool boiling heat transfer enhancement, Microelectron. J., 37, 1158–1164.

[63] Feng B., Weaver K., Peterson G.P. (2012), Enhancement of critical heat flux in pool boiling using atomic layer deposition of alumina, Appl. Phys. Lett., 100, 053120.

[64] Yao Z., Lu Y.W., Kandlikar S.G. (2011), Direct growth of copper nanowires on a substrate for boiling applications, Micro Nano Lett., 6(7), 563–566.

[65] Kim S., Kim H.D., Kim H., Ahn H.S., Jo H., Kim J., Kim M.H. (2010), Effects of nano-fluid and surfaces with nano structure on the increase of CHF, Exp. Thermal Fuild Sci., 34, 487–495.

[66] Zou A., Maroo S.C. (2013), Critical height of micro/nano structures for pool boiling heat transfer enhancement, Appl. Phys. Lett., 103, 221602.

[67] Dong L., Quan X., Cheng P. (2014), An experimental investigation of enhanced pool boiling heat transfer from surfaces with micro/nano-structures, Int. J. Heat Mass Transfer, 71, 189–196.

[68] Lu S.M., Chang R.H (1987), Pool boiling from a surface with a porous layer, AIChE J., 33(11), 1813–1828.

[69] Li C., Peterson G.P. (2010), Experimental study of enhanced nucleate boiling heat transfer on uniform and modulated porous structures, Front. Heat Mass Transfer 1, 023007.

[70] Ali A., El-Genk M.S. (2012), Effect of inclination on saturation

boiling of PF-5060 dielectric liquid on 80- and 137-μm thick copper micro-porous surfaces, Int. J. of Thermal Sciences, 53, 42–48.

[71] Rioux R.P., Eric C.N., Calvin H.Li. (2014), A systematic study of pool boiling heat transfer on structured porous surfaces: From nanoscale through microscale to macroscale, AIP Advances., 4(11), 117133.

[72] Xu P., Li Q., Xuan Y. (2015), Enhanced boiling heat transfer on composite porous surface, Int. J. of Heat and Mass Transfer, 80, 107–114.

[73] Mori S., Aznam S.M., Okuyama K. (2015) , Enhancement of the critical heat flux in saturated pool boiling of water by nanoparticle-coating and a honeycomb porous plate, Int. J. Heat and Mass Transfer, 80, 1–6.

[74] Yang W.J., Takizawa H. (1991), Augmented boiling on copper–graphite composite surface, Int. J. Heat Mass Transfer, 34, 2751–2758.

[75] Vemuri S., Kim K.J. (2005), Pool boiling of saturated FC-72 on nano-porous surface, Int. Comm. Heat Mass Transfer, 32, 27–31.

[76] Lee C.Y., Bhuiya M., Kim K.J. (2010), Pool boiling heat transfer with nano-porous surface Int. J. of Heat and Mass Transfer, 53, 4274–4279.

[77] Lu M.C., Chen R., Srinivasan V., Carey V.P., Majumdar A. (2011), Critical heat flux of pool boiling on Si nanowire array-coated surfaces, Int. J. of Heat and Mass Transfer, 54, 5359–5367.

[78] Vassallo P., Kumar R., Amico S.D. (2004), Pool boiling heat transfer experiments in silica–water nano-fluids, Int. J. Heat Mass Transfer, 47, 407–411.

[79] Kim H., Kim J., Kim M.H. (2006), Effect of nanoparticles on CHF enhancement in pool boiling of nano-fluids, Int. J. Heat Mass Transfer, 49, 5070–5074.

[80] Bang I.C., Chang S.H. (2005), Boiling heat transfer performance and phenomena of Al_2O_3–water nano-fluids from a plain surface in a pool, Int. J. Heat Mass Transfer, 48, 2407–2419.

[82] Kim S.J., Bang I.C., Buongiorno J., Hu L.W. (2006), Effects of nanoparticle deposition on surface wettability influencing boiling heat transfer in nanofluids, Appl. Phys. Lett., 89, 153107.

[83] Kim H.D., Kim J., Kim M.H. (2007), Experimental studies on CHF characteristics of nano-fluids at pool boiling, Int. J. Multiphase Flow, 33, 691–706.

[84] Jeong Y.H., Chang W.J., Chang S.H. (2008), Wettability of heated surfaces under pool boiling using surfactant solutions and nano-fluids, Int. J. Heat Mass Transfer, 51, 3025–3031.

[85] Kim H., Kim M. (2009), Experimental study of the characteristics and mechanism of pool boiling CHF enhancement using nanofluids, Heat Mass Transfer, 45, 991–998.

[86] Kim H., Ahn H.S., Kim M.H. (2010), On the mechanism of pool boiling critical heat flux enhancement in nanofluids, ASME J. Heat Transfer, 132, 061501.

[88] White S.B., Shih A.J., Pipe K.P. (2010), Effects of nanoparticle layering on nanofluid and base fluid pool boiling heat transfer from a horizontal surface under atmospheric pressure, J. Appl. Phys., 107, 114302.

[89] Wen D., Corr M., Hua X., Lin G. (2011), Boiling heat transfer of nanofluids: the effect of heating surface modification, Int. J. Therm. Sci., 50, 480–485.

[90] White S.B., Shih A.J., Pipe K.P. (2011), Boiling surface enhancement by electrophoretic deposition of particles from a nanofluid, Int. J. Heat Mass Transfer, 54, 4370–4375.

[91] Vilhena L.M., Sedlacek M., Podgornik B., Vizintin J., Babnik A., Mozina J. (2009), Surface texturing by pulsed Nd:YAG laser, Tribol Int, 42, 1496-1504.

[92] Zuhlke C.A., Anderson T.P., Alexander D.R. (2013), Comparison of the structural and chemical composition of two unique micro/nanostructures produced by femtosecond laser interactions on nickel, Appl. Phys. Lett., 103 (12), 121603.

[93] Voronov V.V., Dolgaev S.I., Lavrishchev S.V., Lyalin A.A., Simakin A.V., Shafeev G.A. (2000), Formation of conic microstructures upon pulsed laser evaporation of solids, Quantum Electronics, 30(8), 710-714.

[94] Nayak B.K., Gupta M.C. (2010), Ultrafast laser-induced self-organized conical micro/nano surface structures and their origin, Opt. Lasers Eng., 48(10), 966–973.

[95] Deininger C. 2011, Copper machining with lasers, Laser Technik J., 8(3), 28-31.

[96] Vorobyev A.Y,. Guo C. (2013), Direct femtosecond laser surface nano/microstructuring and its applications, Laser Photonics Rev., 7 (3), 385–407

[97] Ulieru D., Ciuciumis A. (2005), The novel process of microstructures production by laser direct patterning, ICALEO P558.

[98] Kruse C.M., Anderson T., Wilson C., Zuhlke C., Alexander D., Gogos G., Ndao S. (2015), Enhanced pool-boiling heat transfer and critical heat flux on femtosecond laser processed stainless steel surfaces, Int. J. Heat and Mass Transfer, 82, 109–116.

[99] Zupancic M., Moze M., Gregorcic P., Golobic I. (2017), Nanosecond laser texturing of uniformly and non-uniformly wettable micro structured metal surfaces for enhanced boiling heat transfer, Appl. Surf. Sci., 399, 480–490.

[100] Gregorcic P., Zupancic M., Golobic I. (2018), scalable surface microstructuring by a fiber laser for controlled nucleate boiling performance of high- and low-surface-tension fluids, Sci. Rep., 8, 7461.

[101] Ham J., Kim H., Shin Y., Cho H. (2017), Experimental investigation of pool boiling characteristics in Al2O3 nanofluid according to surface roughness and concentration, Int. J. Therm. Sci., 114, 86–97.

[102] Rohsenow W.M. (1952), A method of correlating heat transfer data for surface boiling of liquids, Trans. ASME, 74, 969–976.

[103] Coleman H.W., Steele W.G. (1989), Experimental and uncertainty analysis for engineers, New York: Wiley,

[104] Kim J.H., Gurung A., Amaya M., Kwark S.M., You S.M. (2015), Microporous coatings to maximize pool boiling heat transfer of saturated R-123 and water, J. Heat Transfer, 137(8), 081501.

[105] O'Connor J.P., You S.M. (1995), A Painting technique to enhance pool boiling heat transfer in FC-72, ASME J. Heat Transfer, 117(2), 387–393.

[106] You S.M., O'Connor J.P. (1998), Boiling Enhancement Paint, U. S. Patent No. 5814392.

[107] Dehghani-Ashkezari E., Salimpour M.R. (2018), Effect of groove geometry on pool boiling heat transfer of water-titanium oxide nanofluid, Heat and Mass Transfer, 54, 11, 3473–3481.

[108] Kathiravan R., Kumar R., Gupta A., Chandra R. (2012), Preparation and pool boiling characteristics of silver nanofluids over a flat plate heater, Heat Transfer Engineering, 33, 2, 69–78.

Appendix I

Uncertainty analysis

The test facility developed for present investigation consists of different systems namely, heater assembly, test section, the instrumentation scheme and a power supply scheme. The present experimental investigation involves the measurement of various physical quantities such as the temperature of the test section, a diameter of the test section, supply voltage and current. The deviation in measured quantities initiates error in test results. Hence, in the present experimental investigation, the calibrated instruments are used to minimize errors in measurements.

An error analysis is made to estimate the errors associated in various parameters following the procedure suggested by Cole-man and steele [1.1] this is elaborated below.

If *R* is a dependent variable and is a function of n independent variables, it can be expressed as:

$$R = f(v1, v2, v3, \dots\dots.., v_n) \quad (I.1)$$

Let the uncertainties associated with independent variable be e_1, e_2, e_3,……, e_n and resulting uncertainty of *R* be Δ and expressed as:

$$\Delta = \left[\left(\frac{\partial R}{\partial v_1} e_1\right)^2 + \left(\frac{\partial R}{\partial v_2} e_2\right)^2 + \left(\frac{\partial R}{\partial v_3} e_3\right)^2 + \dots\dots\dots + \left(\frac{\partial R}{\partial v_n} e_n\right)^2\right]^{\frac{1}{2}} \quad (I.2)$$

Error in basic quantity

The errors involved in the measurement of basic quantity are listed in Table I.1. In the present experimental investigation, a voltmeter and ammeter is used to measure voltage and current supplied to the heaters, respectively. A Vernier caliper is used to measure dimensions of the test section and K-type thermocouples are used to measure the temperature of the test section.

The voltage and current readings recorded across main heater terminals are used to estimate the input heat flux (q'') to the test section by using the following equation.

$$q'' = \frac{V \times I}{\frac{\pi}{4} \times d_{cyl}^2} \tag{I.3}$$

Where, V is the voltage measured across heater terminals in volts, I is the current measured across heater terminals in amps, and d_{cyl} is the dimeter of the copper heater block. The copper block of 40 mm diameter is used as heater block in this study.

The heat transfer coefficient (h) is calculated by using the estimated heat flux and wall superheat expressed as below.

$$h = \frac{q''}{\Delta T} \tag{I.4}$$

The wall superheat ΔT can be obtained as the difference of surface temperature (T_s) and saturation temperature (T_{sat}).

Table I.1: Errors in measurement

Parameters	**Error**
Voltage, (V)	1 V
Current, (I)	0.01 A
Diameter, (d_{cyl})	0.02 mm
Distance, (Δx)	0.02 mm
Temperature, (T_{sat}, T_w)	± 0.2 ℃

The surface temperature (T_s) was calculated using the temperature of test section (T_w). A single thermocouple is inserted in the test section at a distance Δx (Δx =1.5 mm) from the top surface of the test section to measure the test section temperature (T_w). The surface temperature (T_s) is calculated by using following equation.

$$T_s = T_w - \frac{q'' \times \Delta x}{k} \tag{I.5}$$

Here, k denotes the thermal conductivity of copper block and the value of k is considered as 385 W/mK.

The individual uncertainties involved in various measuring parameters such as V, I, d, Δx and T are shown in Table I.1. The uncertainty in the estimated results for various parameters such as heat flux (q″), wall superheat (ΔT) and heat transfer coefficient (h) is given below. For V = 25 volts, I = 0.401 amp, the uncertainty in various parameters are calculated as below.

(a) Uncertainty in supplied heat flux (q")

Uncertainty in estimated results for supplied heat flux is given below:

$$q = f(V, I, d_{cyl})$$

The errors involved in V, I and d_{cyl} are e_V, e_I and e_{dcyl}, respectively. The uncertainty ($e_{q''}$) supplied heat flux is calculated by using Eq. (I.2) as:

$$\frac{e_{q"}}{q"} = \frac{1}{q"}\left[\left\{\left(\frac{\partial q}{\partial V} e_v\right)^2 + \left(\frac{\partial q}{\partial I} e_I\right)^2 + \left(\frac{\partial q}{\partial (d_{cyl})} e_{d_{cyl}}\right)^2\right\}\right]^{1/2} \qquad (I.6)$$

$$\frac{e_{q"}}{q"} = \sqrt{\left(\frac{e_v}{V}\right)^2 + \left(\frac{e_I}{I}\right)^2 + \left(\frac{2 \times e_{d_{cyl}}}{d_{cyl}}\right)^2} \qquad (I.7)$$

$$\frac{e_{q"}}{q"} = \sqrt{\left(\frac{1}{25}\right)^2 + \left(\frac{0.01}{0.401}\right)^2 + \left(\frac{2 \times 0.02}{40}\right)^2} \qquad (I.8)$$

$$\frac{e_{q"}}{q"} = 0.0471 \qquad (I.9)$$

$$e_{q"}\,\% = 4.71\,\% \qquad (I.10)$$

(b) Uncertainty in surface temperature (T_s)

Uncertainty in estimated results for supplied heat flux is given below:

$$T_s = f(T_w, q", \Delta x)$$

The errors involved in T_w, q'' and Δx are e_{Tw}, $e_{q''}$ and $e_{\Delta x}$, respectively. The uncertainty (e_{Ts}) is calculated by using Eq. (I.2) as:

$$e_{T_s} = \left[\left\{\left(\frac{\partial T_s}{\partial T_w} e_{T_w}\right)^2 + \left(\frac{\partial T_s}{\partial q"} e_{q"}\right)^2 + \left(\frac{\partial T_s}{\partial \Delta x} e_{\Delta x}\right)^2\right\}\right]^{1/2} \qquad (I.11)$$

$$e_{T_s} = \sqrt{\left(e_{T_w}\right)^2 + \left(-\frac{\Delta x \times e_{q"}}{k}\right)^2 + \left(-\frac{q" \times e_{\Delta x}}{k}\right)^2} \quad (I.12)$$

$$e_{T_s} = \sqrt{(0.2)^2 + \left(-\frac{0.0015 \times 0.0471}{385}\right)^2 + \left(-\frac{7977 \times .00002}{385}\right)^2} \quad (I.13)$$

$$e_{T_s} = \pm 0.2 \quad (I.14)$$

(c) Uncertainty in wall superheat ($\Delta T = T_s - T_{sat}$)

Uncertainty in estimated results for wall superheat is given below:

$$\Delta T = f(T_s, T_{sat})$$

The errors involved in T_s and T_{sat} are e_{Ts} and e_{Tsat}, respectively. The uncertainty ($e_{\Delta T}$) supplied heat flux is calculated by using Eq. (I.2) as:

$$e_{\Delta T} = \left[\left\{\left(\frac{\partial \Delta T}{\partial T_s} e_{T_s}\right)^2 + \left(\frac{\partial \Delta T}{\partial T_{sat}} e_{T_{sat}}\right)^2\right\}\right]^{1/2} \quad (I.15)$$

$$e_{\Delta T} = \sqrt{\left(e_{T_s}\right)^2 + \left(e_{T_{sat}}\right)^2} \quad (I.16)$$

$$e_{\Delta T} = \sqrt{(0.2)^2 + (0.2)^2} \quad (I.17)$$

$$e_{\Delta T} = \pm 0.28 \quad (I.18)$$

(d) Uncertainty in heat transfer coefficient (h)

Uncertainty in estimated results for wall superheat is given below:

$$h = f(q", \Delta T)$$

The errors involved in q″ and ΔT are $e_{q''}$ and $e_{\Delta T}$, respectively. The uncertainty (e_h) supplied heat flux is calculated by using Eq. (I.2) as:

$$\frac{e_h}{h} = \frac{1}{h}\left[\left\{\left(\frac{\partial h}{\partial q"} e_{q"}\right)^2 + \left(\frac{\partial h}{\partial \Delta T} e_{\Delta T}\right)^2\right\}\right]^{1/2} \quad (I.19)$$

$$\frac{e_h}{h} = \sqrt{\left(\frac{e_{q"}}{q"}\right)^2 + \left(\frac{e_T}{T}\right)^2} \quad (I.20)$$

$$\frac{e_h}{h} = \sqrt{\left(\frac{0.0471 \times 7977}{7977}\right)^2 + \left(\frac{0.28}{4}\right)^2} \quad (I.21)$$

$$\frac{e_h}{h} = 0.0843 \quad (I.22)$$

$$e_h \% = 8.43 \% \quad (I.23)$$

The error in various parameters such as surface heat flux and heat transfer coefficient is found to be 4.71 % and 8.43 %, respectively (as shown in Eq. I.10, I.23)

Additional Reference

[A.1] Coleman H.W. and Steele W.G. (1989), Experimental and uncertainty analysis for engineers, New York: Wiley.

Apendix II

Specifications of equipments

Items	Details	Pictorial View
Scanning Electron Microscope (SEM)	Make: Carl ZEISS; Model: Supra 55 Resolution: 1.0 nm @ 15 kV, 1.7 nm @ 1 kV, 4.0 nm @ 0.1 kV; Operating voltage range: 0.02-30 kV	
Wire-EDM	Make: Electronica; Model: Ecocut; Travel X × Y : 250 × 350 mm; Max.work-piece height : 150 mm	
Pulsed laser system	Make:Spectra Physics; Laser: Nd:YAG pulsed laser; Wavelengths: 1064 nm, 532 nm, 355 nm; Pulse Width: 5–8 ns	

Continuous wave laser marking machine	Make: Scantech; Laser type: Yb doped Fiber laser (IPG Photonics); Wavelength: 1064 nm	
Microscope	Make: Dewinter; Model: DMI Prime; Mechanical stage: 210mm X 140mm	
Contour and surface measuring station	Make: Mahr GmbH; Model: MarSurf LD130; Resolution: 0.8 nm	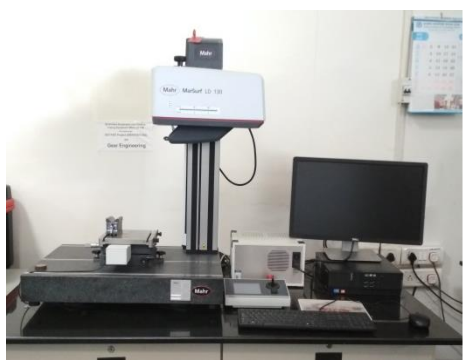

LIST OF PUBLICATIONS

(Part of the present dissertation)

International journals

1. **Nirgude V.V.** and Sahu S.K., Enhancement of nucleate boiling heat transfer using structured surfaces, *Chem. Eng. Process. Process Intensif.*, 122 (2017) 222-234. (IF: 3.0)
2. **Nirgude V.V.** and Sahu S.K., Enhancement in nucleate pool boiling heat transfer on nano-second laser processed copper surfaces, *Exp. Heat Transfer*, 32(6) (2018) 566-583. (IF: 2.0)
3. **Nirgude V.V.** and Sahu S.K., Nucleate boiling heat transfer performance of laser textured copper surfaces, *J. Enhanc. Heat Transf.*, 26(6) (2019) 597-618. (IF: 0.5)
4. **Nirgude V.V.** and Sahu S.K., Nucleate boiling heat transfer performance of different laser processed copper surfaces, Int. J. Green Energy, 17 (2020) 38-47. (IF: 1.3)
5. **Nirgude V.V.** and Sahu S.K., Heat transfer enhancement in nucleate pool boiling using laser processed surfaces: Effect of laser wavelength and power variation, Manuscript ID: TCA_2020_328 (Under review) (Elsevier). (IF: 2.1)

International conferences

1. **Nirgude V.V.,** Modak M., Sharma A.K. and Sahu S.K., Experimental Study on Structured Surfaces for Nuclear Pool Boiling Enhancement, Proceedings of the ASME 2017 25th International Conference on Nuclear Engineering (ICONE25), Shanghai, China, July 2-6, 2017.
2. **Nirgude V.V.,** Modak M. and Sahu S.K., Experimental Investigation of Pool Boiling Characteristics of Isopropyl Alcohol on Smooth Copper and Aluminum Surface, Proceedings of the 6th International and 43rd National Conference on Fluid Mechanics and Fluid Power (FMFP2016), Allahabad, India, December 15-17, 2016.

LIST OF PUBLICATIONS

(Apart from the present dissertation)

International journals

1. Chougule S.S., **Nirgude V.V.** and Sahu S.K., Experimental Study on Laminar Forced Convection of Al_2O_3/Water and Multiwall Carbon Nanotubes/ Water Nanofluid of Varied Particle Concentration with Helical Twisted Tape Inserts in Pipe Flow, *Heat Transfer Eng.*, 39 (9) (2018) 806-818. (IF: 1.7)
2. Chougule S.S., **Nirgude V.V.**, Gharge P.D, Modak M. and Sahu S.K., Heat Transfer Enhancements of Low Volume Concentration CNT/Water Nanofluid and Wire Coil Inserts in a Circular Tube, *Energy Procedia*, 90 (2016) 552-558.
3. Chougule S.S., **Nirgude V.V.**, Shewale S.P., Pise A.T., Sahu S.K. and Shah H., Application of Paraffin Based Nanocomposite in Heat Pipe Module for Electronic Equipment Cooling, *Materials Today: Proceedings* 5(11) (2018) 23333-23338.

International conferences

1. Yadav A.K., Sharma P., Sharma A.K., Modak M., **Nirgude V.V.** and Sahu S.K., Heat transfer characteristics of downward facing hot horizontal surfaces using mist jet impingement, Proceedings of the ASME 2017 25th International Conference on Nuclear Engineering (ICONE 25), Shanghai, China, July 2-6, 2017.
2. Modak M., **Nirgude V.V.**, Sharma A.K. and Sahu S.K., Experimental Study ON HEAT Transfer Characteristics Circular Jet Impingement Boiling on The Variety of Structured Copper Surfaces in Stagnation Zone, Proceedings of the ASME 2016 24th International Conference on Nuclear Engineering (ICONE 24), Charlotte Convention Center, Charlotte, NC, USA, June 26-30, 2016.
3. Poris B. R., **Nirgude V.V.**, Junaid S. and Sahu S.K., Theoretical Model to Predict the Bubble Departure Diameter in Nucleate Pool Boiling, 6th

International and 43rd National Conference on Fluid Mechanics and Fluid Power MNIT, Allahabad, India, Dec 15-17, 2016.

4. Chougule S.S., Gharge P.D, **Nirgude V.V.**, Modak M. and Sahu S.K., Heat Transfer Enhancements of Low Volume Concentration CNT/water nanofluid and Wire Coil Inserts in a Circular Tube, 5th International Conference on Advances in Energy Research Indian Institute of Technology Bombay, Mumbai, India, Dec 15-17, 2015.
5. Chougule S.S., **Nirgude V.V.**, Shewale S.P., Pise A.T. and Sahu S.K., Application of Paraffin Based Nanocomposite in Heat Pipe Module for Electronic Equipment Cooling, 5th International Conference on Advances in Energy Research Indian Institute of Technology Bombay, Mumbai, Dec 15-17, 2015.

Curriculum vitae

Vishal Nirgude

Doctoral Research Scholar
Fluid Mechanics and Machinery Laboratory
Discipline of Mechanical Engineering
Indian Institute of Technology Indore
Scandium Building, Khandwa Road
Village: Simrol, Tehsil: Mhow,
Dist.: Indore, M.P., India
E-mail: vishalnirgude@gmail.com
phd1401203005@iiti.ac.in
Mob: +91-8982356952

Academic

- **B. Tech.** (Mechanical Engineering) (Per. 68.75 %) from M.I.T., Aurangabad, Maharashtra, India **2006-2010**
- **M. Des.** (Mechanical Systems) (CGPA 8.24) from IIITDM Kancheepuram, Chennai, Tamilnadu, India **2012-2014**

Research

- **Ph.D.** Research scholar at Discipline of Mechanical Engineering, IIT Indore, Madhya Pradesh, India **2014-2019**

PhD Thesis: POOL BOILING HEAT TRANSFER CHARACTERISTICS OF STRUCTURED SURFACES

- Development of pool boiling experimental test facility to conduct experiments on various enhanced surfaces
- Development of enhanced surfaces using novel laser processing method and wire-EDM method
- Study the heat transfer performance of the enhanced surfaces at a varied range of input heat flux values and different pool liquids
- Report test data involving pool boiling curves, comparison of heat transfer coefficient and possible boiling mechanism involved in heat transfer enhancement

Teaching Experience

- Teaching Assistant: ME 254 (Fluid Mechanics and Machinery Laboratory) for B.Tech. 2nd Year
- Teaching Assistant: IC211 (Experimental Engineering Laboratory) for B.Tech. 2nd Year

Software Skills

- Programming language/code: C, C++, MATLAB
- Modelling/Analysis: AutoCAD, Autodesk Inventor, ANSYS

Papers presented in conferences

- 25th International Conference on Nuclear Engineering (ICONE25), Shanghai, China, July 2-6, 2017
- 6th International and 43rd National Conference on Fluid Mechanics and Fluid Power (FMFP2016), Allahabad, India, December 15-17, 2016
- 5th International Conference on Advances in Energy Research Indian Institute of Technology Bombay, Mumbai, India, Dec 15-17, 2015

Awards and recognition

- Lead author in Qualified student award winner paper in 25th International conference in nuclear engineering (ICONE25)
- Co-author in Qualified student award winner paper in 24th International conference in nuclear engineering (ICONE24)
- Actively involved for the development of Fluid Mechanics and Machinery Laboratory at IIT Indore during 2014-2017

Personal Details

Date of Birth	26 Aug 1989
Nationality	Indian
Status	Single
Contact	+91-8982356952
E-mail	vishalnirgude@gmail.com, phd1401203005@iiti.ac.in